Structure and Function of the Murine Lymph Node

Structure and Function of the Murine Lymph Node

A dissertation presented

by

Matthew Charles Woodruff

to

The Division of Medical Sciences

in partial fulfillment of the requirements

for the degree of

Doctor of Philosophy

in the subject of

Immunology

Harvard University

Cambridge, Massachusetts

September, 2014

Dissertation Advisors: Professor Michael Carroll Matthew Charles Woodruff
Professor Shannon Turley

Structure and Function of the Murine Lymph Node

Lymph nodes (LNs) are dynamic organs responsible for providing a supportive and centralized environment for the generation of immune response. Utilizing a highly organized network of non-hematopoietic stromal cells, the LN serves as the context in which the immune system collects and presents antigen, promotes innate and adaptive immune interaction, and generates protective cell-mediated and humoral immunity. In this way, proper organization and function of the LN environment is a critical component of effective immunity, and understanding its complexity has direct impact on the ability to generate and modulate primary immune response to specific antigens. To this end, the LN architecture, underlying stromal networks, and environmental and cellular responses to influenza vaccination were investigated. Using novel approaches to conduit imaging, details of the collagen network that comprises the LN scaffolding have been integrated into current understandings of LN architecture. The cellular compartment responsible for the maintenance of that scaffolding, fibroblastic reticular cells (FRCs), have been studied using an induced diptheria toxin receptor model. By specifically ablating the FRC population in mice, their role in the maintenance of T cell homeostasis has been confirmed *in vivo*. More surprisingly, a disruption of the FRC network resulted in a loss of B cell follicle structure within LNs, and a reduction in humoral immunity to influenza vaccination. These findings led to the identification of a new subset of FRCs which reside in B cell follicles, and serve as a critical source of the B cell survival factor BAFF. Turning towards the hematopoietic response to influenza vaccination, a highly unexpected lymph node resident dendritic cell (LNDC) response has been identified following vaccine antigen deposition within specialized sites in the LN medulla. Rapid migration of LNDCs into these sites optimizes exposure of the population to viral antigen, and d*e novo* synthesis of a CXCL10 chemokine

gradient by activated LNDCs ensures efficient antigen specific $CD4^+$ T cell response, and protective humoral immunity – independent of migratory dendritic cell status. Altogether, these studies highlight a highly dynamic, responsive LN environment with direct influence on primary immune response – the understanding of which has broad implications in vaccine biology.

Acknowledgements

A doctorate, although formally an academic exercise, is a critical time of personal and intellectual growth. While it is often viewed as an individual undertaking, the magnitude of the task requires a steady stream of guidance, support, collaboration, and friendship for its successful completion. The transition from a consumer, to a producer of knowledge is one that cannot be made in isolation, and it is my belief that this dissertation serves as a reflection of the community, both within Harvard and outside, that served as its context.

I must start with my family, my largest supporters and constant advocates. Words could be wasted here recording sentiments that are already understood, but to my brothers and parents – I could not be here without you. You have truly taught me how to live, and I am eternally grateful for it. I love you all.

Scientifically, I wish to express my deepest gratitude to my mentor, Professor Michael Carroll. He has taught me not only the theory of science, but also its business and application. He has given me the intellectual freedom to explore, provided me resources, pushed me when needed, and been a strong advocate within the scientific community. He has carefully guided me to a place where a career in immunology, which both excites and intrigues me, seems utterly achievable. For that, I cannot thank him enough.

On a similar note, I must also thank my co-mentor, Professor Shannon Turley. Her advice and guidance have been critical to my scientific success, and her openness with both myself, and the rest of the Harvard Immunology community should be held in the highest regard. She will be deeply missed as she moves on to what I'm certain can only be a true step in a brilliant scientific career.

Of course, bench science does not succeed without struggle, and its pain is made bearable by those struggling alongside. My bay-mate, Balthasar Heesters, has become a close friend in commiseration, and I look forward to many years of both the lamentation, and hopefully the celebration of science that follows as we move forward. My friend, Dr. Caroline Herndon,

has been a constant source of support, and I thank her for her uncanny ability to impose a sense of reality and calm on even the most difficult times. Finally, Dr. Viviana Cremasco has been a critical component of my scientific training, and a close collaborator. I thank her for her extensive contributions to this work, and her unrelenting dedication.

The Harvard Immunology community, both students and faculty, have been outstanding. I would specifically acknowledge Dr. Florian Winau, Dr. Kai Wucherpfennig, and Dr. Shiv Pillai for their formal and informal scientific guidance, and Sue Perkins for her masterful organization of the Harvard Immunology experience.

I would also like to thank Dr. Elisabeth Carroll, Minghe Ma, and Dr. Harry Leung for their facilitation of the scientific work contained herein, as well as personal guidance along the way.

Finally, I have had the pleasure of spending time with a few true friends in my time in Boston, so to Kevin Bonham, Jon Sitrin, Marshall Thomas, Dmitriy Kolodin, Alex Salsberg, Emily Deschler, Mary Bovenzi, Jennifer Loomis, and Brandy Pappas, thank you for the conversation, support, and the occasional scotch.

To my grandmother and grandfather,

and the family that they created.

Table of Contents

List of figures

Chapter 1 – Introduction to the lymph node environment

Chapter 2 – B cell homeostasis and follicle confines are governed by fibroblastic reticular cells

Chapter 3 – Trans-nodal migration of resident DCs into medullary inter-follicular regions initiates immunity to influenza vaccine

Chapter 4 – The influence of context on vaccine immunity

Chapter 1

Introduction to the lymph node environment

Chapter 1.1 – Circulatory dynamics

On an average day, an adult human pumps roughly 5L of blood through almost 100,000km of vasculature at a rate of 5L/min. Although exact measurements are inherently difficult to obtain, it is likely that at any given moment the total blood volume is contained within 800 and 1000m^2 of capillary bed where it is responsible for oxygen and nutrient exchange with local tissue to maintain a homeostatic tissue environment. While it is likely that few cells in the body are separated from a feeding capillary by more than 50μm, the tissue remains physically separated from the vessel lumen due to the tight junctions carefully maintained by the blood endothelial cells (BECs) that make up the vessel wall(Cliff, 1976). Although this physical barrier is capable of retaining cells in the lumen, it is not entirely impermeable to small molecule exchange and the slow leakage of plasma driven into the surrounding tissue by positive intravascular pressure and osmotic gradients(Casley-Smith, 1985). This interstitial fluid bathes the surrounding tissue, and its constant flow through the extracellular space carries away processed metabolites while maintaining a constant pH and providing the raw materials required for cellular homeostasis.

Due to the nature of this interstitial fluid flow, a scavenging system is required to remove excess fluid and serum protein (such as albumen) as it builds in the tissue to maintain osmotic homeostasis across the vessel wall. This scavenging system, known as the lymphatic system, serves as an outlet for the constant pumping of interstitial fluid into the tissue, and is ultimately responsible for the recycling of blood volume and albumin lost from the cardiovascular system. This process of fluid and metabolite removal is carried out through a complementary lymphatic vascular system largely comprised of highly organized lymphatic endothelial cells(LECs) (Chen et al., 2014). Unlike BECs, LECs do not exclusively form tight junctions, but instead form lymphatic vessels with primary valve-like structures allowing unidirectional fluid flow from the interstitial space into lymphatic capillaries(Schmid-Schönbein, 2003; Trzewik et al., 2001; Mendoza and Schmid-Schönbein, 2003). This unique structure, along with unidirectional valves

within the lymphatic vessels themselves, ensures that excess interstitial fluid can be effectively sequestered from the extracellular space, and directionally carried away as lymph to make room for fresh fluid to bathe the tissue(Hudack and McMaster, 1932). From the lymphatic capillaries, collected lymph is transported to less permeable collecting vessels(Baluk et al., 2007), and eventually into the thoracic duct which merges with the left subclavian vein, returning lost blood volume back into circulation.

This system of nutrient distribution and fluid recycling poses a significant theoretical problem when addressing the threat of infectious disease. Supposing a barrier breach in peripheral tissue (say a cut on the hand), and subsequent bacterial infection, the extracellular bacteria is bathed in the same interstitial fluid which is designed to feed the tissue under homeostatic conditions. While many pathogens are highly tissue tropic, overwhelming infection and high infectious titers could easily lead to the collection of bacteria into the lymphatic system along with interstitial fluid to be eventually recycled. Unrestricted, this lymph-born bacteria would travel through the lymphatic system into the thoracic duct, where it would eventually merge into active circulation. In this way, a bacterial infection initially restricted to the hand could quickly turn into a much more serious blood-borne infection leading to septicemia, toxic shock syndrome, and multi-organ failure. To prevent this scenario, the lymph is filtered to remove infectious material at several critical points in its journey from the periphery to the thoracic duct. These filtration points are referred to as lymph nodes.

Chapter 1.2 – Lymphatic structures of the lymph node

Lymph nodes (LNs) are small organs which are scattered along the strings of lymphatic vessels, beginning in the periphery, and leading to the thoracic duct. Each lymph node functions independently along the string, although they are often found in series such that lymph flows

from one LN to the next before finally rejoining circulation. Lymph vessels carrying lymph into a LN are referred to as afferent lymphatics, whereas vessels leading away from the node are termed efferent. As lymph enters the node through the afferent lymphatics, it first arrives in the subcapsular sinus (SCS) – a flat sinus residing just under the collagen capsule which comprises the outer boundary between the LN and the surrounding environment(Heath et al., 1986; Fossum, 1980a). While the dense collagen capsule of the LN demarcates the upper boundary of the SCS, a finer, more reticular lateral network of collagen bundles can be identified as the structural scaffolding of the SCS floor. Both the capsule and lateral reticular network can be conveniently labeled and visualized through subcutaneous injection of soluble fluorescein isothiocyanate (FITC) upstream of the draining LN **(Fig 1)**.

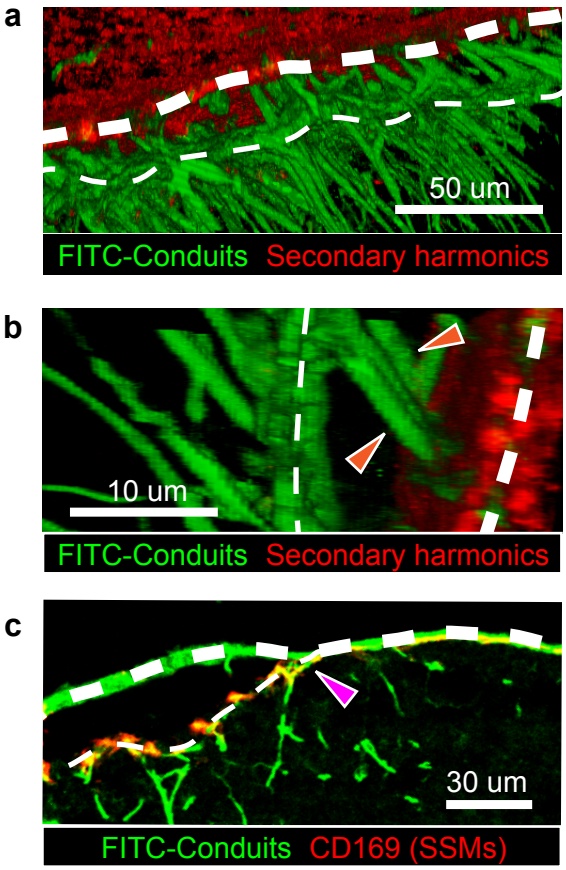

Figure 1 – Collagen structure of the subcapsular sinus floor. (a,b) C57BL/6 mice were *in vivo* labeled with PBS-FITC. PLNs were harvested, fixed, and optically cleared. LNs imaged by MPM, with second harmonics shown. Orange arrows – collagen spacers**(c)** Same as in [a,b], except mice were *in vivo* labeled with a-CD169. LN imaged by confocal microscopy following thin cryosectioning. Heavy dash - collagen capsule; light dash – lateral collagen matrix. Magenta arrow – capsule and lateral collagen network merging

The SCS is physically contiguous with the incoming afferent lymphatics, with the walls of the afferent lymphatics merging into the LN capsule. The luminal space is punctuated with collagen 'spacers' which span across the 0-20um lumen(Ohtani and Ohtani, 2008), and are directly attached to both the outer collagen capsule and lateral reticular floor **(Fig 1a,b)**. While the SCS is generally appreciated as a single lymph filled sheet draping the LN cortex, inconsistency of collagen spacer lengths, and the apparent periodic merging of the SCS floor

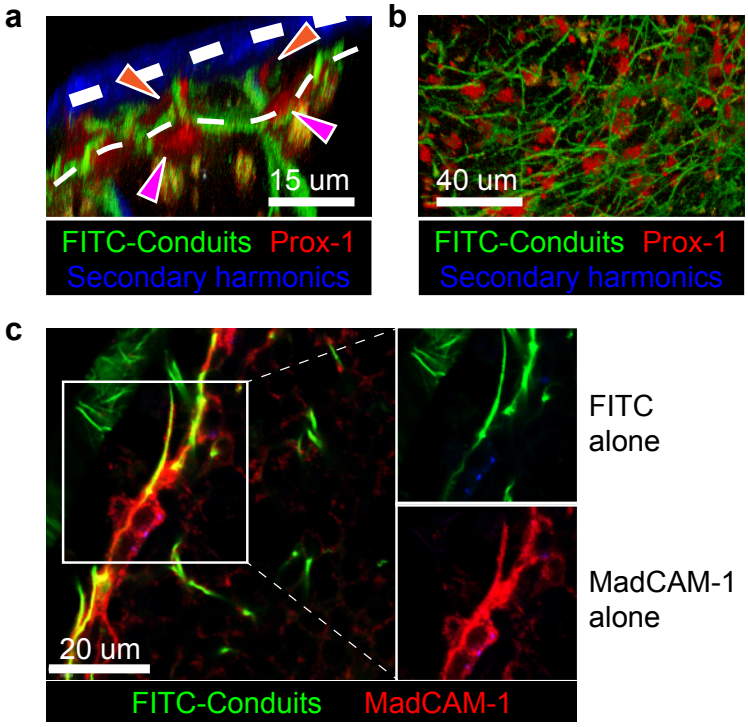

Figure 2 – Lymph node stroma in the subcapsular sinus. (a,b) *Prox1 x tdTomato* reporter mice were *in vivo* labeled with PBS-FITC. PLNs were harvested, fixed, and optically cleared. LNs imaged by MPM. Heavy dash - collagen capsule; light dash – lateral collagen matrix; Orange arrows– cLECs; Magenta arrows – fLECs **(c)** C57BL/6 mice were *in vivo* labeled with PBS-FITC. PLNs were harvested, fixed, and cryosectioned. Sections imaged by confocal microscopy.

with the outer collagen capsule as visualized by FITC painting suggests that this interpretation may be incorrect **(Fig 1c)**. Instead, an alternative model could be proposed where only specific sections of the SCS actually contain a luminal space contiguous with the upstream afferent lymphatics. More data is needed to confirm this view of the SCS structure, and understand the importance of this configuration in lymph node development, filtration, and immune response.

While the collagen structure provides the scaffolding for the SCS, CD31^{-}Podoplanin^{+}Lyve-1^{+} LECs are required to form the cellular barrier surrounding the luminal space(Chen et al., 2014). Recent studies have shown that there is a stratification of function in these LECs, currently typified by differential chemokine receptor expression (discussed later), which is dependent on their residence in the floor (paremchymal side, fLECs) or ceiling (capsular side, cLECs) of the SCS lumen (Ulvmar et al., 2014). Injection of soluble fluorescein isothiocyanate (FITC) into Prox-1-tdTomato fluorescent reporter mouse (a master regulator of lymphatic vessel development) reveals attachment of cLECs to the outer collagen capsule, while fLECs are seen embedded into the lateral collagen matrix in the SCS floor **(Fig 2a)**. Somewhat surprisingly, while Prox1^{+} LECs can be identified surrounding the SCS lumen,

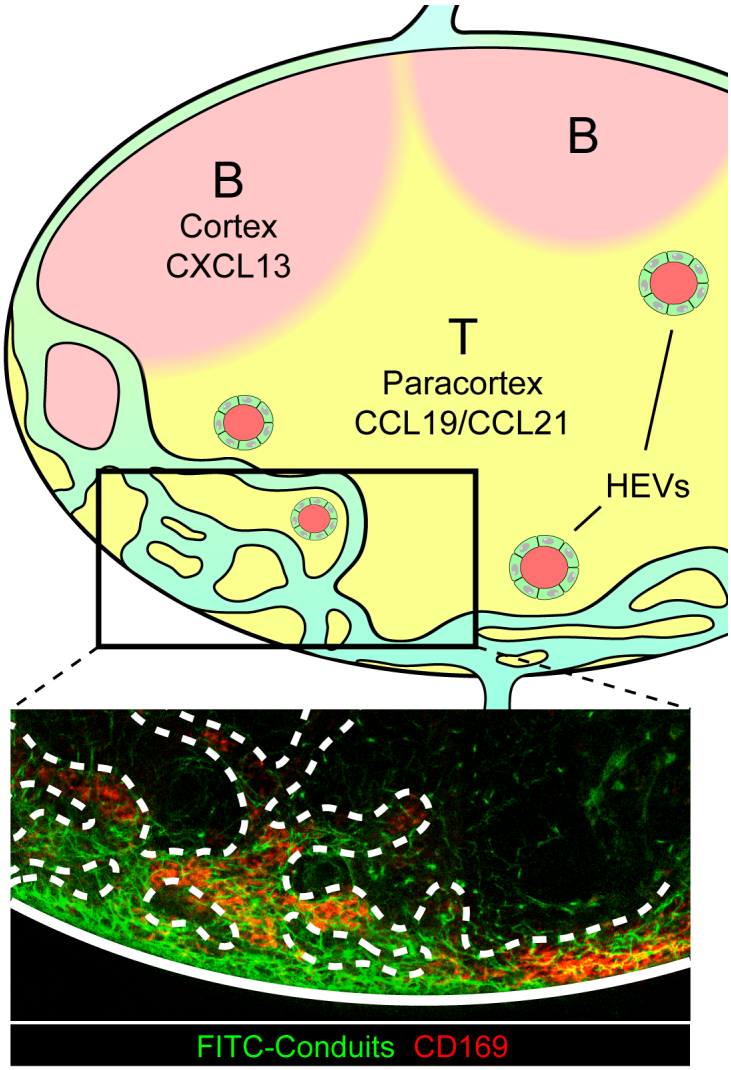

Figure 3 – Lymph node organization. Model of the lymph node highlighting the B cell cortex (pink), T cell paracortex (yellow), lymphatic structures (blue), and HEVs (green). Single plane illumination microscopy imaging (SPIM) displayed to emphasize medullary structure. C56BL/6 mice were in vivo labeled with PBS-FITC, and anti-CD169. PLNs were collected, fixed, and whole mount imaged. White line – LN capsule; White dashed line – medullary lymphatics.

they appear discontinuous on the sinus lining, raising interesting questions about the possibility of multiple populations responsible for SCS barrier integrity **(Fig 2b)**. Further, localization of MadCAM-1 positive cells wrapped around the collagen floor and spacers(Katakai, 2012) in the SCS further suggests that the exact identities of these stromal barrier cells may remain yet unclear **(Fig 2c)**

As the lymphatics that make up the SCS approach the efferent side of the LN, they begin to branch, and form a highly complex labrynth of lymphatic vessels known collectively as the medulla(Ohtani and Ohtani, 2008) **(Fig 3)**.Similar to the SCS, the lymphatic vessels that comprise the medulla are surrounded by a reticular collagen network, and contain collagen bundles that extend across the luminal space **(Fig 3)**. The cellular boundaries of the medullary lymphatic vessels are similarly maintained by Lyve-1^{+} LECs, although specialization within this population remains yet undocumented. As lymph flows from afferent to efferent, the medullary lymphatics merge together, and ultimately leave the node as a single vessel to form the efferent lymphatic.

Once in the efferent lymphatic, lymph will either travel to the next LN in the string, or return to circulation via the thoracic duct.

Chapter 1.3 – Filtration of lymph in the lymph node

Alternative to the physical and enzymatic means by which the kidneys and liver perform their filter functions, the filtration of pathogens and debris in the lymph node relies almost exclusively on phagocytosis and lysosomal degradation by lymph node resident macrophages. Although several populations of specialized macrophages exist within the LN, two appear to be particularly important in protection from infection, and active filtration of the lymph(Gray and Cyster, 2012).

The first population, resident in the SCS (termed subcapsular sinus macrophages [SSMs]), are exposed to the first wave of antigen that flows from the afferent lymphatics into the LN, and are characterized by their $CD11b^{hi}$ $F4/80^{-}$ $CD169^{+}$ expression pattern (Martinez-Pomares and Gordon, 2012). Electron microscopy and fluorescent imaging have identified SSM cell bodies on both the luminal, and parenchymal side of the SCS floor(Farr et al., 1980; Junt et al., 2007; Phan et al., 2007). In either case, SSMs have been shown to cast stable projections across the floor, so that they are directly exposed to the afferent lymph. Although these cells are proficient in the uptake of antigen, they are described as having low levels of phagocytic and degradative potential(CLARK, 1962; Nossal et al., 1965; Fossum, 1980a). Instead, SSMs are primarily implicated in transfer of intact-antigen hand off to underlying B cells in a process that will be described later. Interestingly, recent studies of this population have suggested that SSMs are highly susceptible to viral infection, but respond robustly to infection through the production of large quantities of type I interferons (Moseman et al., 2012; Iannacone et al., 2010). These data suggest that while SSMs may have little effect on overall lymph filtration due to low antigen

turnover, their specialized functions may be critical in responding to certain types of peripheral infection.

More relevant to the filtration of lymph in the LN, $CD11b^{hi}$ $F4/80^{+}$ $CD169^{+}$ $SIGNR\text{-}1^{+}$ medullary sinus macrophages (MMs) densely pack the labyrinth of lymphatic vessels that make up the medulla(Gray and Cyster, 2012). Anatomically, MMs are found attached to the lymphatic vessel wall or residing on the reticular fibers that cross the vessel lumen(Takahashi et al., 1998; Fossum, 1980b; Fossum and Vaaland, 1983). Unlike SSMs, MMs are highly phagocytic, and skewed towards non-specific degradation of antigen. This system of filtration is surprisingly efficient, and multiple studies have identified the medulla as the primary concentration point of antigen arriving through the lymphatics suggesting a broad spectrum of binding specificities(Fossum, 1980a; Steer and Foot, 1987; Gonzalez et al., 2010). Following MM disruption with cholodrinate loaded liposomes, injected antigen can be found in subsequent downstream LNs, highlighting their importance in maintaining a sterile lymph environment (Gonzalez et al., 2010). Interestingly, recent unpublished work has suggested that the human adjuvant, MF59, leads to a disruption of the MM population in mice, coinciding with humoral responses in non-draining LNs.

Due to their placement along the lymphatic vasculature, each individual LN is responsible for the filtration of a specific area of the organism. One example, the popliteal LN (a focus of this study), is situated directly behind the knee and serves as the first filtration point for every lymph-borne particle originating in the foot or lower leg. In the case of infection, any lymph-borne infectious material will accumulate in the local LN, but be absent from the downstream node. In this way, subcutaneous administration of infectious material in the foot will result in antigen accumulation *only* in the popliteal LN (PLN). The result of this configuration is that each individual lymph node will be bathed in cell debris, spent metabolites and any infectious antigen originating from the tissue which they drain. As the adaptive immune system requires exposure to foreign antigen in order to respond, the LN provides a convenient location for the adaptive immune system to effectively survey the upstream tissue for infection.

Chapter 1.4 – Organization of the lymph node

To accommodate adaptive immune surveillance, the parenchyma of the LN (which is compartmentally separated from the lymphatic lumen by lymphatic endothelial barriers) provides a range of functions to direct lymphocyte recruitment, support lymphocyte survival, and facilitate innate and adaptive immune interactions. Broadly, the parenchyma of the LN can be broken down into two compartments – the T cell zone (the paracortex) and the B cell zone (the cortex) **(Fig 3)**. These two compartments, although lacking a physical boundary between them, are nonetheless highly organized and independently controlled through the maintenance of chemokine gradients(Ansel et al., 2000).

Chemokines are a family of small cytokines between 8 and 10 kD primarily named for their ability to induce directional cell migration. Although 4 subfamilies exist with slightly different primary structures (CC, CXC, XC, and CX_3C), almost all have similar function in binding specific 7-transmembrane, G-coupled protein receptors often named for the type of chemokine that they bind (ie. CCR, CXCR, XCR and CX_3CR)(Rollins, 1997). These chemokine/chemokine receptor interactions result in leukocyte calcium flux, integrin activation and cellular migration towards increasing concentrations of the chemokine signal(Springer, 1994; 1995; Butcher, 1991). By establishing multiple, complex gradients, and restricting expression of specific chemokine receptors to different immune cell types, the immune system is organized within the lymph node without need of physical barriers(Ansel et al., 2000)**(Fig 3)**. This method of organization allows geographical flexibility in that a change of receptor expression on the surface of a lymphocyte can direct it to a different compartment within the node(Breitfeld et al., 2000; Kim et al., 2001). Alternatively, this study identifies the establishment of a new chemokine gradient within the lymph node to quickly and efficiently reorganize an immune response to promote interaction between specific cell types.

The paracortex of the LN, characterized by the expression of the chemokines CCL19 and CCL21(Gunn et al., 1998; Dieu et al., 1998; Luther et al., 2000), represents the more

efferent side of the LN parenchyma, although it is physically separated from the medullary lumen. CCR7, the receptor responsible for CCL19/21 recognition, is expressed at high levels on naïve T cells, resulting in high concentrations of T cells within the paracortex(Förster et al., 1999). Thus, the paracortex is often referred to as the 'T cell zone'. Importantly, the paracortex also serves as an entryway to incoming naïve lymphocytes looking to survey the node. High endothelial venules (HEVs), specialized blood vessels which are required for lymphocyte ingress, can be found punctuated throughout the compartment(Girard and Springer, 1995, **Fig. 3**). Decoration of the luminal side of HEVs with the paracortical chemokines CCL19/21 facilitates a critical step in the rolling adhesion cascade resulting in LN homing(Baekkevold et al., 2001; Andrian and Mempel, 2003).

Similarly to the paracortex, the cortex is physically separated from the lymphatic lumen by lymphatic endothelial barriers. The cortex, however, is characterized by expression of the chemokine CXCL13 rather than CCL19/21(Ansel et al., 2000), and is found on the afferent side of the node directly under the SCS. The receptor for CXCL13, CXCR5, is highly expressed on naïve B cells resulting in the demarcation of the 'B cell zone'. It is worth noting, however, that naïve B cells first entering the node express high levels of CCR7, and like T cells, utilize the HEV network in the paracortex for LN entry(Girard and Springer, 1995). Over the course of a normal humoral response, both lymphocyte populations are capable of altering their chemokine receptor expression (ie. B cells upregulating CCR7, and traveling to the cortical/paracortical junction) in order to facilitate cellular interactions important in the generation of immune response(Okada and Cyster, 2006; Pereira et al., 2010; Nurieva and Chung, 2010). In this way, organization of the immune system through chemokine gradients rather than physical barriers allows flexibility of cellular interaction, while maintaining separation and specialized function. This system of differential chemokine gradient expression is controlled largely by the specific stromal subsets that also inhabit the T and B cell zones.

The largest stromal component of the LN parenchyma is the fibroblastic reticular cell (FRC) network. Characterized as CD45- GP38+ CD31- (Malhotra et al., 2012a), FRCs form extensive networks which provide migratory traction to the more motile hematopoietic compartment (Bajénoff et al., 2007; Lämmermann and Sixt, 2008). Additionally, these cells are responsible for the structural maintenance of the LN environment through the production of the collagen conduit network (Gretz et al., 1997; Mueller and Germain, 2010; Turley et al., 2010; Katakai et al., 2004), and have been recently described to interact directly with the hematopoietic compartment to regulate T cell homeostasis and response (Link et al., 2007; Lukacs-Kornek et al., 2011; Saini et al., 2009; Pellegrini et al., 2011). As the major producers of CCL19 and 21 within the paracortex, FRCs are responsible for producing and maintaining the chemokine gradients required for the persistence of the T cell zone. FRC function in immune homeostasis and response is a critical component of this study, and will be discussed in detail later.

While FRCs have been identified in the B cell zone, their importance in the structure and maintenance of the cortex has remained unclear. Although this study attempts to clarify the role of FRCs in B cell follicles, the integrity of the B cell compartment has been attributed to an independent stromal compartment known as follicular dendritic cells (FDCs)(Heesters et al., 2014). These non-hematopoietic cells (CD45- CD35+ GP38+ CD31-) form dense dendrite networks which wrap the collagen reticular fibers throughout the cortex(Cyster et al., 2003), similarly to FRCs in the paracortex. In addition to producing the follicle specific chemokine CXCL13(Ansel et al., 2000), they have also been reported to express the B cell anti-apoptotic factor BAFF(Garin et al., 2010; Wu et al., 2009), highlighting their importance in both organization and survival of the B cell compartment within LNs. In addition to their function at steady state, FDCs are also highly specialized in the retention of large protein antigen(Mandel et al., 1980), and are critical for the formation of germinal centers in the establishment of humoral immune response(Kelsoe, 1996; MacLennan, 1994; Allen and Cyster, 2008).

Although FRCs and FDCs have been considered the major contributors to the establishment of chemokine gradients within the LN, cLECs have also been shown to help groom the chemokine gradient by sequestering excess CCL19 and 21 through the non-signalling receptor CCRL1, thereby serving as a chemokine 'sink' (Ulvmar et al., 2014). This finding, in accordance with previous reports identifying direct CCL21 expression by LECs in the afferent lymphatics as a mediator of lymphocyte homing suggests that these cells might also play an important role in lymph node organization and homeostasis (Stein et al., 2000). Altogether, these three stromal subsets (LECs, FRCs, and FDCs) work in concert to ensure the clear delineation of the cortical/paracortical junction through chemokine expression and regulation, and their proper function is critical in generating effective immune response(Malhotra et al., 2012a).

Chapter 1.5 – Antigen acquisition within the lymph node

While the parenchyma of the lymph node is contiguous, and allows for free travel between the B cell and T cell zones, so long as the correct chemokine receptors are expressed, the physical barrier between the parenchyma and the lumen of the lymphatics presents a unique challenge in generating protective humoral immune responses. As this barrier prevents direct encounter of lymphocytes with foreign antigen in the lymph environment, the antigen must find it's way into the LN parenchyma where the adaptive immune system can detect it and respond accordingly (Gonzalez et al., 2011). Especially in the case of B cells which must see intact antigen for effective response, it is critical for antigen at distal infected sites to find its way into the draining LN relatively intact. This challenge in antigen transport into the node is overcome through four independent mechanisms: 1. Dendritic cell (DC) transport from the

periphery; 2. Low molecular weight transport through conduits; 3. SSM antigen transport; 4. Direct antigen capture by lymph node resident dendritic cells (LNDCs).

Dendritic cells are highly specialized antigen presenting cells residing in almost all tissues in men and mice(Steinman, 1991). While in their resident tissue they are relatively sessile and inactive, they respond robustly to both pathogen associated molecular patterns (PAMPs) and danger associated molecular patterns (DAMPs) by quickly scanning the local environment for pathogens(Rescigno et al., 1997). By increasing phago- and pinocytosis, they rapidly uptake pathogens in the interstitial fluid, and effectively take a 'snapshot' of their local environment(Austyn, 1996; Alvarez et al., 2008). Having picked up potentially infectious material in their resident tissue, DCs become highly active and capable of performing their antigen presenting functions required for the establishment of adaptive immunity(Alvarez et al., 2008). By remodeling the local extracellular matrix(Yen et al., 2008), and following a CCL21 gradient via the chemokine receptor CCR7(Weber et al., 2013), activated DCs leave their resident tissue, migrate through the afferent lymphatics in integrin dependent or independent mechanisms(Platt and Randolph, 2013; Schmidt and Friedl, 2010; Lämmermann et al., 2008), and ultimately arrive in the SCS of the draining LN (Förster et al., 1999; Ohl et al., 2004; Förster et al., 2008; Braun et al., 2011). Once there, DCs cross the SCS floor utilizing a carefully groomed CCL19/21 gradient, and enter the paracortex where they then interact with antigen specific T cells to initiate adaptive immunity (Ulvmar et al., 2014). In this way, migratory DCs are capable of recognizing potentially pathogenic antigen in the periphery, and actively transporting it into the draining LN – thus bypassing the barrier problem.

In addition to the active transport of antigen to the LN by migratory DCs, any pathogen or small molecule which is released into the interstitial fluid of the periphery will be carried to the draining LN through normal lymphatic flow(Kissenpfennig et al., 2005). Leaving the tissue, antigen is collected into lymphatic capillaries, and eventually drains into the SCS as previously described. In the SCS, antigen flows through a luminal space spanning 0-20μm, packed with subcapsular sinus macrophages(Farr et al., 1980; Junt et al., 2007; Phan et al., 2007). While

the floor of the SCS is made of LECs which are largely impermeable to antigen escape, the floor is punctuated with collagen conduits which serve as a shortcut for fluid to flow into the parenchyma of the LN(Roozendaal et al., 2009).

Collagen is by far the most abundant protein in humans, accounting for one third of total protein, and three quarters of the dry weight of skin (Shoulders and Raines, 2009). While at least 28 independent types of collagen have been identified in vertebrates, all share a common repeating XaaYaaGly polypeptide sequence flanked by N and C terminal pro-peptides(Shoulders and Raines, 2009). Each individual polypeptide chain forms a tight left-handed helix mediated by the repeating glycine residues(Okuyama, 2008). Once secondary structure is established, the flanking pro-peptides allow for assembly of three parallel polypeptide strands into a right-handed triple helix(Berisio et al., 2002; Wess et al., 1998; Traub et al., 1969). The propeptides are then trimmed from the triple-helices, which then self assemble into larger collagen microfibrils. Finally, microfibrils are cross-linked to form dense collagen fibers up to 500nm in diameter (Shoulders and Raines, 2009). After assembly of these individual collagen fibers, multiple fibers can be packaged together into much larger bundles for increased strength. While individual fibers are dense and highly cross-linked, bundles of fibers are less tightly associated. This more loose configuration allows for fluid and small molecule penetration of the fibers, which can then travel the length of the bundle freely. In the lymph node environment, this interesting property allows collagen bundles to act as conduits of lymph flow directly through the cortical and paracortical regions which are otherwise largely impermeable(Roozendaal et al., 2009; Sixt et al., 2005; Gretz et al., 2000).

Conduits, which are reported to be secreted by FRCs, initiate at the SCS lateral collagen matrix floor, often as extensions of the SCS collagen spacers, and extend throughout the LN before emptying back into the efferent lymph or HEVs **(Fig 4)**. The dense, bundled collagen structure of conduits ensures that only small molecules under ~70kD (Gretz et al., 2000)have direct access to the B cell follicles underlying the SCS floor(Roozendaal et al., 2009). Once in conduits, antigen can be directly sampled by naïve B cells and FDCs in the LN leading to the

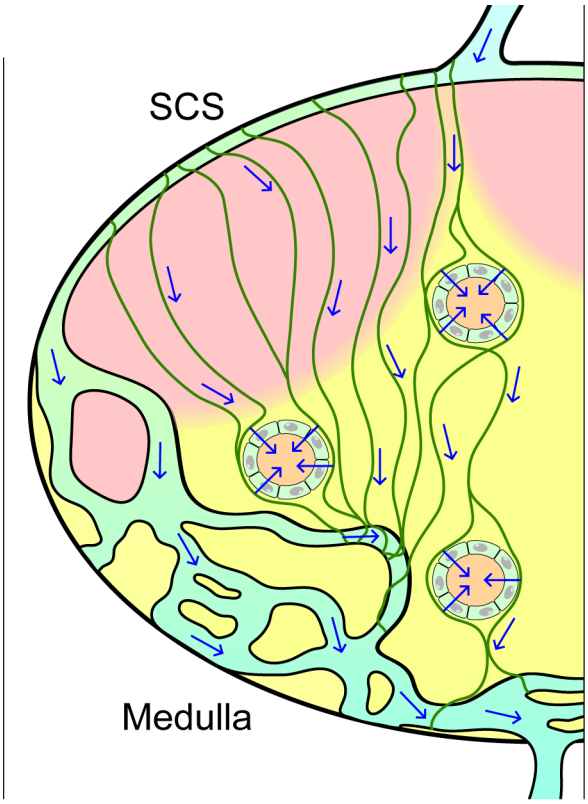

Figure 4 – Lymph node organization. Model of the lymph node highlighting Lymphatic flow through the lymphatic (blue) and conduit system (green). Blue arrows represent flow from afferent to efferent, and partial fluid deposition into HEVs is represented. Pink – B cell follicle; Yellow – T cell zone; Orange – HEVs.

initiation of humoral immunity. Although conduits are usually found wrapped by FRCs throughout the LN(Anderson and Anderson, 1975; Anderson and Shaw, 1993; Kaldjian et al., 2001), transmission electron microscopy has revealed fine dendrites of FDCs reaching through the FRC layer and directly into the collagen bundle(Roozendaal et al., 2009). Antigen specific B cells display rapid acquisition of cognate antigen via this conduit mechanism within minutes of antigen injection upstream of the draining LN, ultimately resulting in downstream humoral immunity(Roozendaal et al., 2009). In addition to serving as pathways for lymph flow, this dense collagen network also serves as a substrate for hematopoietic motility within the LN environment(Bajénoff et al., 2007; Lämmermann and Sixt, 2008).

Rather than entering the conduit system, antigen larger than 70kD is forced to flow through the SCS where it will eventually drain into the medulla, and ultimately, the efferent lymph. Due its dense nature, draining antigen is in direct contact with SSMs within the luminal space. Additionally, SSMs have been described to be situated underneath the SCS floor, sending projections into the lumen to ‘sample’ the lymph flowing past(Berney et al., 1999; Martinez-Pomares et al., 1996). While SSMs are not particularly phagocytic, they are highly specialized in capturing soluble antigen in the lymph, particularly opsonized antigen through complement receptor 3 (CD11b/CD18), and actively transporting it intact across the SCS floor(Phan et al., 2007; Junt et al., 2007; Carrasco and Batista, 2007). Once transported,

antigen can be handed off to underlying B cells in either a complement specific (via complement receptor 2 [CD21]), or BCR specific manner(Junt et al., 2007; Phan et al., 2007). B cells that have acquired antigen from SSMs can then transfer it to FDCs via complement receptors where it can be retained for the establishment of a germinal center response. This method of antigen transport is especially enticing due to its ability to protect the native epitopes present in complex antigen which could then be used for effective humoral immunity(Phan et al., 2007).

Despite the efficient capture of complement fixed antigen by SSMs, their low phagocytic potential and tendency to protect –rather than degrade – complex protein antigen renders them less useful in large scale filtration of the lymph. In cases where antigen is abundant, such as vaccination, large amounts of antigen rapidly flows through the SCS and is collected in the medulla(Fossum, 1980a; Steer and Foot, 1987; Gonzalez et al., 2010). Here, MMs quickly sequester and degrade macromolecules and pathogens. While these cells are critical for filter function in the LN, they are less well described in their contribution to antigen transport, or presentation to the adaptive immune compartment. These macrophages, however, are interspersed with small numbers of resident DCs which are more equipped to make use of antigen filtered in the medulla(Gonzalez et al., 2010).

As with most peripheral tissues, the LN environment is home to specific DC subsets referred to as lymph node resident DCs. The LNDC compartment is primarily comprised of 'conventional' DCs which can be broken down further into $CD8a^{+}$ ($CD11b^{int\text{-}neg}$ $CD11c^{hi}$ $CD8a^{+}CD4^{-}$), $CD11b^{hi}$ ($CD11b^{hi}$ $CD11c^{hi}$ $CD8a^{-}CD4^{+}$), and double negative ($CD11b^{hi}$ $CD11c^{hi}$ $CD8a^{-}CD4^{-}$) cDCs(Dudziak et al., 2007; Shortman and Heath, 2010; Villadangos and Schnorrer, 2007). In addition, migratory DCs (both dermal DCs and langerhaans cells) which constitutively migrate in from the periphery are present in the LN, and seem important for the maintenance of peripheral tolerance(Igyártó et al., 2011; Helft et al., 2010; Heath and Carbone, 2009; Hawiger et al., 2001). While the importance of LNDCs has been less well characterized in direct antigen capture from the lymph, at least one subset ($CD11b^{hi}$ $CD11c^{hi}$ $CD8a^{-}$ $SIGNR\text{-}1^{hi}$) have been shown to be directly involved in antigen capture and the ensuing humoral response in the case

of influenza vaccination(Gonzalez et al., 2010). This study supports this mechanism of direct dendritic cell acquisition and priming within the medulla as an important pathway in driving downstream adaptive immunity.

In light of these four mechanisms, the initiation of adaptive immunity in the LN can be viewed as series of steps whereby lymph flow carries antigen from its source in the periphery towards the draining LN, and independent populations of innate immune cells attempt to utilize it effectively throughout that journey. Especially in the case of vaccination, the high concentration of injected antigen ensures passive antigen delivery to the draining LN, and the engagement of antigen presentation mechanisms beyond traditional transport by migratory DCs. As a result, it may be critical to understand the influence that these pathways have in governing adaptive response to vaccination, and the underlying LN environment which serves as their context. This study attempts address some of these questions in the following steps:

1. Utilize novel imaging tools to clarify the collagen networking within the LN, which may play a critical role in lymph flow and immune response

2. Understand the role of the LN stroma, specifically fibroblastic reticular cells, in maintenance of both homeostatic and inflammatory immune function

3. Identify novel mechanisms by which LNDCs utilize LN architecture to optimize antigen exposure, and drive downstream protective immunity.

Chapter 2

B cell homeostasis and follicle confines are governed by fibroblastic reticular cells

Text and figures adapted from:

Cremasco, V., Woodruff, M.C., Onder, L. Cupovic, J, Neives-Bonilla, J.M., Schildberg, F.A., Chang, J., Cremasco, F., Harvey, C.J., Wucherpfennig, K., Ludewig, B., Carroll, M.C., Turley, S.J. 2014. B cell homeostasis and follicle confines are governed by fibroblastic reticular cells. *Nat. Immunol.* Accepted.

Chapter 2.1 – Introduction

Secondary lymphoid organs are essential sites for the induction of adaptive immune responses. One of their most remarkable features is the segregation of B and T cells into discrete domains comprising structural and functional units for optimal immune cell activation(Turley et al., 2010; Mueller and Germain, 2010). These specialized environments are inhabited by different subsets of mesenchymal stromal cells, which are commonly viewed as serving scaffolding function for T and B lymphocytes and dendritic cells. Current dogma holds that fibroblastic reticular cells (FRCs) within the paracortical region coordinate T cell responses whereas follicular dendritic cells (FDCs) within the cortex support B cell responses. However, a precise understanding of how the stromal network of lymphoid organs controls adaptive immunity has been beyond our reach due to limitations in the technology for targeting each of the mesenchymal cell populations.

The T cell paracortical region of the lymph node is delineated by FRCs, the most abundant population of non-hematopoietic or stromal cells in this organ. Typified by expression of the glycoprotein podoplanin (PDPN), and molecules such as CD140α and CD140β, FRCs construct an elaborate conduit network that allows small molecules to rapidly flow from upstream tissues deep into the parenchyma of lymph nodes(Gretz et al., 2000; Roozendaal et al., 2009; Sixt et al., 2005). Expression of CCL19 and CCL21 by FRCs, in addition to other adhesion molecules, facilitates chemokine receptor CCR7-dependent homing of naive T cells and provides essential guidance cues to dendritic cells that migrate from non-lymphoid tissues into the lymph node paracortex(Acton et al., 2012; Jillian L Astarita, 2012; Malhotra et al., 2012b). Additionally, interleukin 7 (IL-7) production by FRCs is thought to be essential for preservation of the peripheral T cell pool under homeostatic conditions(Link et al., 2007). More recently, FRCs have also been found to control the extent of proliferation of newly activated T

cells through regulated release of nitric oxide(Khan et al., 2011; Lukacs-Kornek et al., 2011; Siegert et al., 2011).

The two stromal cell populations commonly characterized within the lymph node cortex include FDCs and marginal reticular cells (MRCs). FDCs are characterized by localization within B cell follicles, expression of the complement receptors CR1 and CR2 (CD35 and CD21), the follicular dendritic cell marker 1 (FDCM1), and the ability to display opsonized antigens to B cells. Expression of B cell trophic factors, namely the chemokine CXCL13 and the pro-survival factor BAFF (also known as BlyS, TALL-1, TNFSF13B, TNFSF20), is often attributed to FDCs, implicating these cells in shepherding B cells to follicles, supporting B cell survival and coordinating the germinal center reaction(Cyster, 2010; Cyster et al., 2003; Roozendaal and Carroll, 2007; Tew et al., 1990). Previous work employing a system to ablate FDCs provided definitive evidence that, while this stromal subset is critical for germinal center responses, it plays only a minor role in B cell homeostasis within resting lymph nodes(Wang et al., 2011). Likewise, loss of FDCs was not mirrored by a decrease in *Tnfsf13b*, hereafter referred to as *Baff*, transcript abundance, pointing to the presence of an alternative source. These observations have led some investigators to postulate that MRCs, which reside in close juxtaposition to the subcapsular sinus (SCS) of lymph nodes(Katakai et al., 2008), serve these functions, but data supporting this hypothesis are not yet available. Thus, the cell population supporting B cell homeostasis within primary follicles has remained enigmatic.

We have developed and experimentally validated an inducible mouse model (*Ccl19*-Cre x *Rosa26*-diphtheria toxin receptor (iDTR) mice) for conditional ablation of FRCs *in vivo*. In these mice, administration of diphtheria toxin (DTxn) caused a rapid and extensive depletion of FRCs, while sparing other stromal cell populations. Our data demonstrate that FRC ablation led to marked alterations in T cell homeostasis and compartmentalization, with profound consequences in the activation, expansion and effector function of viral antigen-specific T lymphocytes. Unexpectedly, loss of FRCs also led to significantly reduced B cell viability and altered follicular organization, followed by marked impairment in humoral immunity to T-

dependent and T-independent viral antigens. Mechanistically, we determined that a subset of FRCs residing within lymphoid follicles establishes a favorable niche for B lymphocytes via production of BAFF. Collectively, these results demonstrate that FRCs are required for the generation of virus-specific T cell responses within lymphoid organs. Additionally, our study broadens the current paradigm of FRCs solely supporting T cell immunity, and highlights an essential role for FRCs in directly controlling B cell homeostasis, distribution and activation.

Chapter 2.2 – *In vivo* genetic targeting and selective ablation of FRCs

Manipulation of FRCs *in vivo* has been thus far limited by a lack of specific genetic models targeting this population of stromal cells. A transgenic Cre mouse line that permits targeting of FRCs, in which expression of Cre recombinase is directed by the *Ccl19* promoter(Chai et al., 2013), was only recently generated. By crossing the transgenic *Ccl19*-Cre line to *Rosa26*-enhnaced yellow fluorescent protein (EYFP) mice, we have generated *Ccl19*-Cre x *Rosa26*-EYFP reporter mice, in which EYFP expression is achieved following Cre-mediated excision of a *lox*P-flanked transcriptional "stop" sequence (**Fig. 5a**). Confocal laser scanning microscopy of lymph nodes from *Ccl19*-Cre x *Rosa26*-EYFP mice revealed expression of the transgene in the T cell zone, thereby supporting efficient excision of floxed loci in the expected location (**Fig. 6a,b**).

Flow cytometric analysis demonstrated EYFP expression in FRCs, identified as non-hematopoietic cells expressing the glycoprotein podoplanin (PDPN) and negative for the endothelial marker CD31 and the cell adhesion molecule MadCAM-1 ($CD45^-PDPN^+CD31^-MadCAM^-$) (**Fig. 6c** and **Fig. 5b**). EYFP expression was not detected in other lymph node stromal cells including lymphatic endothelial cells (LECs, $CD45^-PDPN^+CD31^+$), blood endothelial cells (BECs, $CD45^-PDPN^-CD31^+$) or integrin α_7-expressing pericytes (IAPs, $CD45^-PDPN^-CD31^-$) (**Fig. 6c**), thereby confirming specificity of the *Ccl19* promoter. Despite the recent

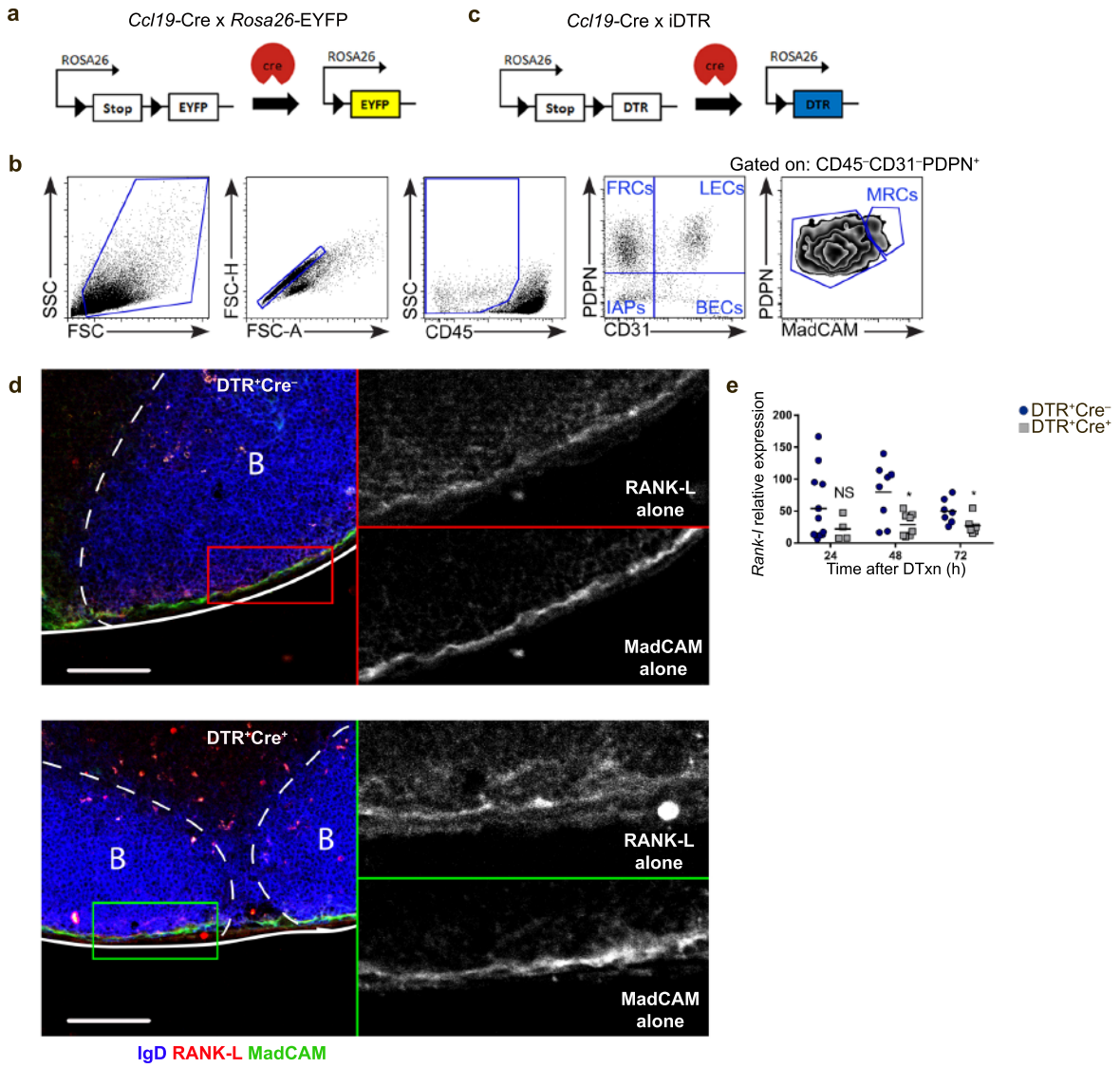

Figure 5. Generation and characterization of Ccl19-Cre x Rosa26-EYFP and Ccl19-Cre x iDTR mice. (a) EYFP expression is achieved in Ccl19-Cre x Rosa26-EYFP mice following Cre-mediated excision of a loxP-flanked transcriptional "stop" sequence. **(b)** Representative flow cytometric profile of freshly isolated stromal cells from skin draining lymph nodes (n>10 mice from 3 independent experiments). **(c)** In Ccl19-Cre x iDTR mice, the DTxn receptor gene is expressed following Cre-mediated recombination. **(d)** Confocal analysis of popliteal lymph nodes from DTR+Cre+ animals 24 h following DTxn administration stained for IgD, RANK-L and MadCAM. Scale bars 100 μm (n=3 mice from 3 independent experiments). **(e)** Lymph nodes from Ccl19-Cre x iDTR mice were collected, lysed in trizol and analyzed for the presence of Rank-l transcript. Lines indicate mean. Data are normalized to cyclophillin. Each data point represents one lymph node from individual mice (n=4-10 mice/group from 2-3 separate experiments). NS non significant, * $p<0.05$

reports suggesting a close developmental relationship between FRCs and MRCs(Katakai, 2012) ($CD45^{-}PDPN^{+}CD31^{-}MadCAM^{+}$), MRCs did not appear to be targeted with *Ccl19*-directed recombinase, as demonstrated by the absence of EYFP expression in MadCAM-1^{+} cells lining

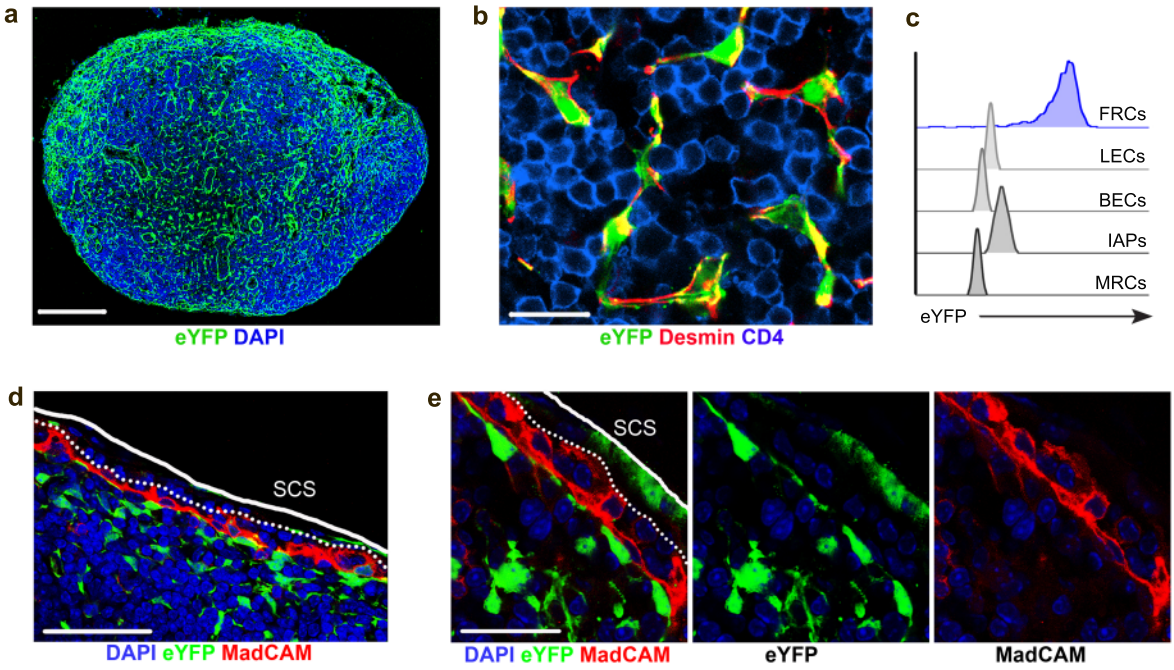

Figure 6. Specific Ccl19 promoter activity in FRCs. (a) Popliteal lymph node sections from Ccl19-Cre x Rosa26-EYFP reporter mice were sectioned and stained for GFP and DAPI. Scale bar 200 µm. **(b)** Figure shows higher magnification images of the paracortical area stained for GFP, Desmin and CD4 from mice as in a. Scale bar 25 µm (n>3mice from 3 independent experiments). **(c)** Flow cytometric analysis of freshly isolated stromal cells from Ccl19-Cre x Rosa26-EYFP mice showing Ccl19 promoter activity. FRCs, fibroblastic reticular cells; LECs, lymphatic endothelial cells; BECs, blood endothelial cells; IAPs, integrin α7-expressing pericytes; MRCS, marginal reticular cells (n=3mice from 2 independent experiments). **(d,e)** Confocal micro SCS, subcapsular sinus. Lines indicate the ceiling and the floor (dotted line) of the subcapsular sinus. Scale bars 50 µm (d) and 25 µm (e) (n>3mice from 3 independent experiments).

the subcapsular sinus expression by flow cytometry and confocal microscopic analysis (**Fig. 6c-e**).

To generate a mouse model that enables selective depletion of FRCs, mice harboring the gene encoding DTR downstream of a floxed transcriptional stop element in the ubiquitously expressed *Rosa26* locus(Buch et al., 2005) were crossed to *Ccl19*-Cre mice (**Fig. 5c**). In these mice, cells with an active *Ccl19* promoter (FRCs) express the simian DTR, and are selectively vulnerable to toxin-induced apoptosis when exposed to DTxn. A single injection of DTxn into these mice was sufficient to achieve rapid and extensive ablation of FRCs from lymph nodes. FRCs were lost as early as 24 h following DTxn administration (**Fig. 7a-c**) and deletion was specific, as we did not measure changes in cellularity of other lymph node stromal populations, including LECs, BECs and IAPs (**Fig. 7d**). Consistent with FRCs being the predominant source

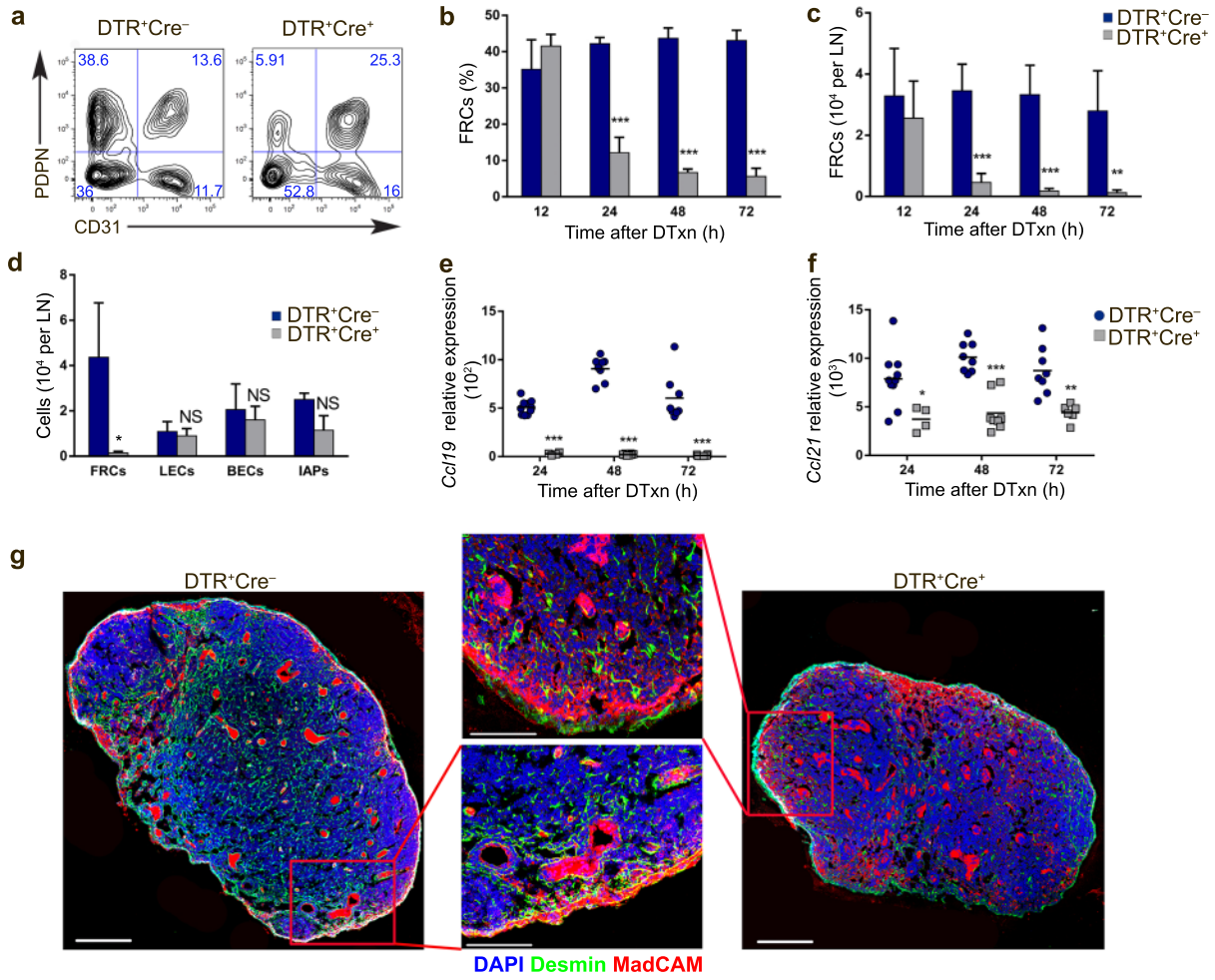

Figure 7. Conditional ablation of FRCs. (a) The FRC (PDPN+CD31–) compartment was analyzed 24 h after DTxn administration in DTR+Cre+ mice that express DTR in Ccl19+ cells, and in DTR+Cre– control mice. Numbers shown in quadrants depict percents. **(b,c)** The effect of DTxn-induced FRC ablation is shown as percent among stromal cells (CD45–) and total number per lymph node. Data are representative of at least three independent experiments (mean+/-sd, n=4 mice/group per experiment). **(d)** Ccl19-Cre x iDTR mice were injected with DTxn and, 72 h later, lymph nodes were collected, digested and stromal cells enumerated by flow cytometry (FRCs, CD45–PDPN+CD31–, LECs, CD45–PDPN+CD31+, BECs, CD45–PDPN–CD31+, IAPs, CD45–PDPN–CD31-). Data are representative of at least three independent experiments (mean+/-sd, n=3 mice/group per experiment). **(e,f) F**ollowing DTxn administration, lymph nodes were collected, lysed in trizol and analyzed for the presence of Ccl19 or Ccl21 transcripts. Lines indicate mean. Data are normalized to cyclophillin. Each data point represents one lymph node from an individual mouse (n=4-10 mice/group from 2-3 separate experiments). (**g) M**RCs were identified in lymph nodes from Ccl19-Cre x iDTR mice by staining with a MadCAM antibody together with DAPI and anti-Desmin. Scale bars 200 μm and 100 μm for the insets. (n>3mice from 3 independent experiments). NSnon significant, *p<0.05, **p<0.01, ***p<0.001

of the chemokine CCL19 (Malhotra et al., 2012b; Link et al., 2007), its expression in lymph nodes was abrogated after FRC ablation, whereas expression of genes shared with other cells, such as *Ccl21* (Malhotra et al., 2012b), was only partially reduced (**Fig. 7e,f**). As such, we were able to detect MadCAM-1^{+}RANK-L^{+} cells along the lymph node subcapsular sinus of FRC-

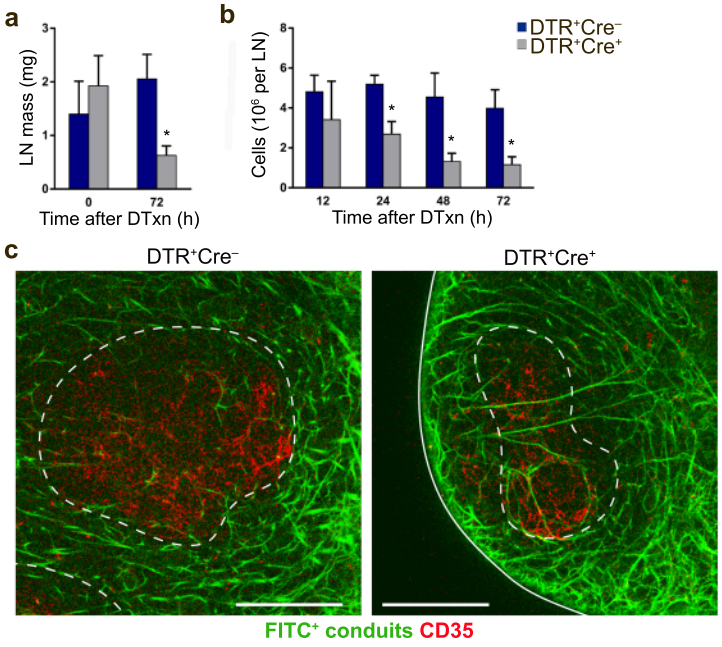

Figure 8. FRC ablation has profound consequences on lymph node cellularity despite preserving conduit functionality. (a,b) Lymph node mass and total cellularity after DTxn administration were determined. Data are representative of at least two independent experiments (mean+/-sd, n=3 mice/group per experiment). **(c)** Representative multiphoton microscopic images of popliteal nodes from Ccl19-Cre x iDTR mice depicting FITC-tracer transported into conduits. Scale bars 100 µm (n>3mice from 2 independent experiments). * p<0.001

ablated mice (**Fig. 7g** and **Fig. 5d**), confirming a lack of *Ccl19* promoter activity in MRCs. In line with this finding, *Rank-l* transcript encoded by *Tnfsf11*, which is shared by MRCs and FRCs (Malhotra et al., 2012b; Katakai et al., 2008), was only partially reduced in total lymph node mRNA preparation after FRC ablation (**Fig. 5e**), despite complete abrogation of *Ccl19* (**Fig. 7e**).

Despite FRCs comprising a minute cellular compartment (~0.5% of total lymph node cells) (Fletcher et al., 2011), their ablation resulted in marked alterations in lymph nodes, with significant reductions in organ size, weight and cellularity (**Fig. 8a,b** and data not shown). However, these effects were not symptomatic of a global collapse of lymph node architecture, as FRC ablation perturbed neither the integrity nor the permeability of the conduit network (**Fig. 8c**). DTxn administration was not associated with systemic toxicity, and it did not lead to weight loss or extra-nodal pathology (**Fig. 9a** and data not shown). Furthermore, we did not observe accumulation of either neutrophils ($CD11b^{+}Gr1^{hi}$) or monocytes ($CD11b^{+}Gr1^{neg/lo}$), or increased expression of inflammatory cytokines, ruling out extraneous inflammation secondary to FRC ablation (**Fig. 9b,c**). Collectively, these data suggest that the *Ccl19*-Cre mouse system allows for specific ablation of FRCs *in vivo*.

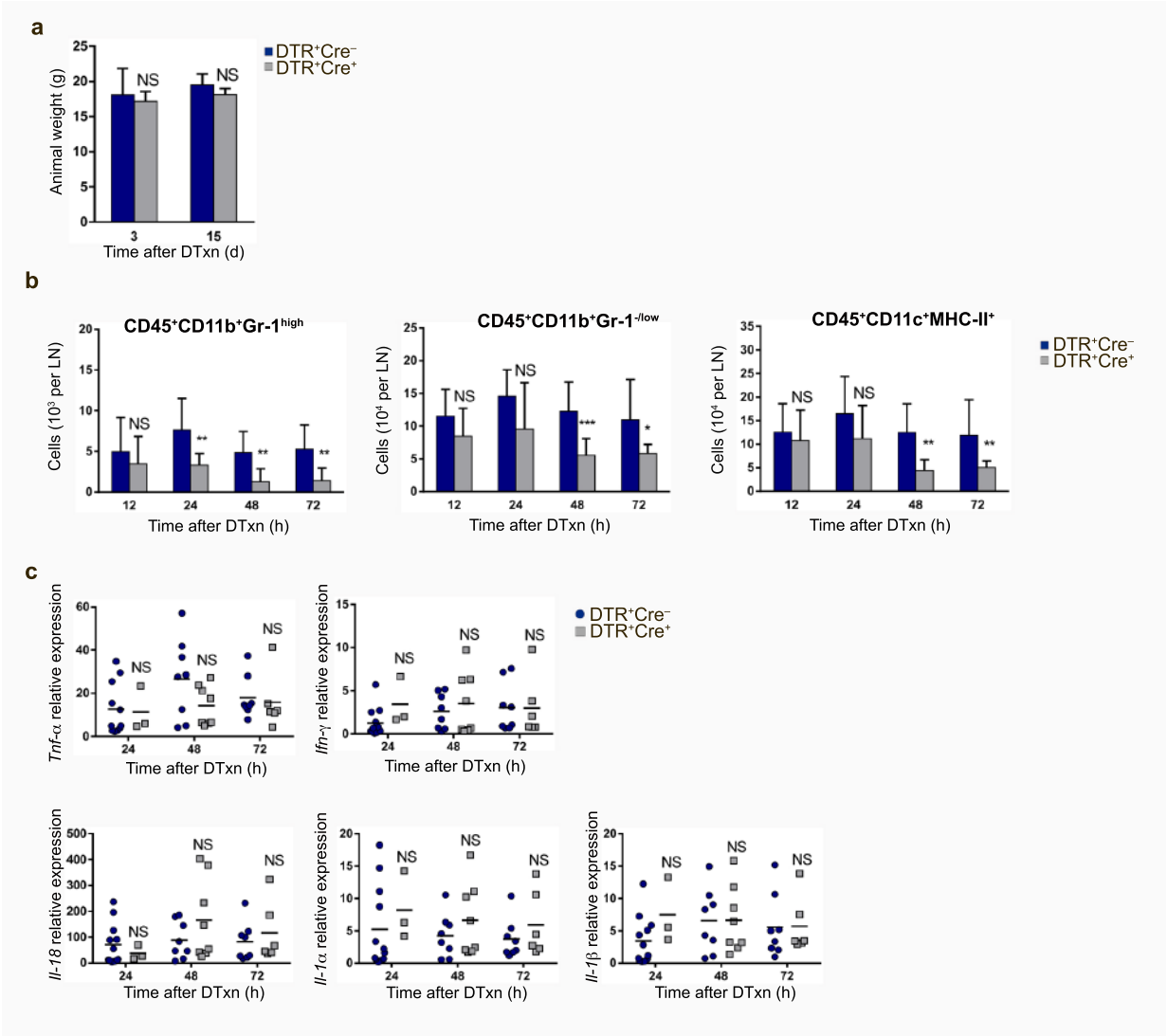

Figure 9. DTxn injection does not result in systemic toxicity or inflammation. (a) Animal weight was determined following DTxn administration (n=3-4 mice/group per experiment from two independent experiments). **(b)** Lymph nodes from Ccl19-Cre x iDTR mice were collected and processed into single cell suspensions. Neutrophils (CD45+CD11b+Gr1high), monocytes (CD45+CD11b+Gr1–/low) and dendritic cells (CD45+CD11c+MHCII+) were enumerated using flow cytometric analysis. Data are representative of at least three independent experiments (mean+/-sd, n=3 mice/group per experiment). **(c)** Lymph nodes from Ccl19-Cre x iDTR mice were collected, lysed in trizol and analyzed for expression of inflammatory mediator genes. Lines indicate mean. Data are normalized to cyclophillin. Each data point represents one lymph node from individual mice (n=4-10 mice/group from 2-3 separate experiments). NS non significant, *p<0.05, **p<0.01, ***p<0.001

Chapter 2.3 – Ablation of FRCs impairs anti-viral T cell responses

Confocal laser scanning microscopy of DTxn-treated mice confirmed disappearance of FRCs from the T cell zone parenchyma, and revealed aberrant localization of T lymphocytes

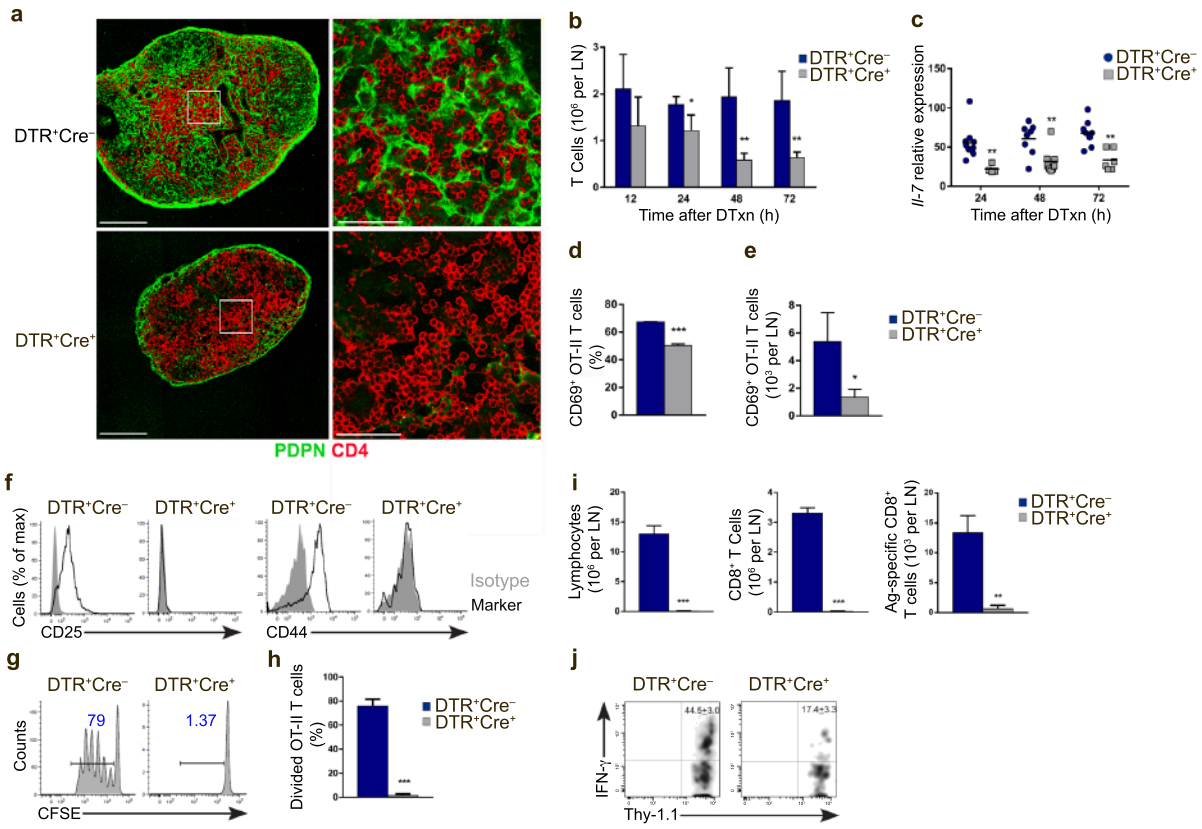

Figure 10. FRC ablation impairs T cell immunity. (a) Confocal microscopy of lymph node sections from Ccl19-Cre x iDTR mice stained for CD4 (T cells) and PDPN (FRCs) to depict FRCs in paracortical areas 3 days after DTxn treatment. Scale bars 200 µm (left) and 50 µm (right). (n>3mice from 3 independent experiments). **(b)** Skin-draining lymph nodes from Ccl19-Cre x iDTR mice were collected, and T cells were enumerated using flow cytometric analysis (CD45+B220–CD3+). Data are representative of at least three independent experiments (mean+/-sd, n=4 mice/group per experiment). **(c)** Lymph nodes from Ccl19-Cre x iDTR mice were collected, lysed in trizol and analyzed for the presence of Il-7 transcript. Lines indicate mean. Data are normalized to cyclophillin. Each data point represents one lymph node from individual mice (n=4-10 mice/group from 2-3 separate experiments). **(d,e)** Following DTxn treatment, mice were adoptively transferred with CFSE-labeled OT-II T cells. Recipients were immunized with UV-inactivated OVA-expressing influenza virus in the footpad, popliteal nodes were collected 24 h after immunization, and the presence of antigen-specific activated T cells was determined by flow cytometry (CFSE+CD3+CD4+Vα5+CD69+) (n=3mice/group). **(f)** Flow cytometric analysis of CD25 and CD44 expression by antigen specific T cells 60 h following immunization. **(g,h)** Proliferation of OT-II T cells from mice as in (f) was determined as CFSE dye-dilution (n=3 mice/group). **(i)** DTxn-treated mice received CD8+T cells specific for the viral spike protein prior to immunization with non-replicating coronaviral particles. Numbers of lymphocytes, CD8+T cells and antigen-specific T cells was assessed 72h after virus injection (n=3 mice/group). **(j)** IFNγ production was determined by intracellular staining (n=3 mice/group). *p<0.05, **p<0.01, ***p<0.00

within cortical regions (**Fig. 10a**). Notably, we also observed a global reduction of T cell numbers in lymph nodes (**Fig. 10b**) with both $CD4^+$ and $CD8^+$ T cells equally affected by loss of FRCs (**Fig. 11a,b**). Moreover, expression of the T cell survival factor *Il-7* was also reduced in lymph

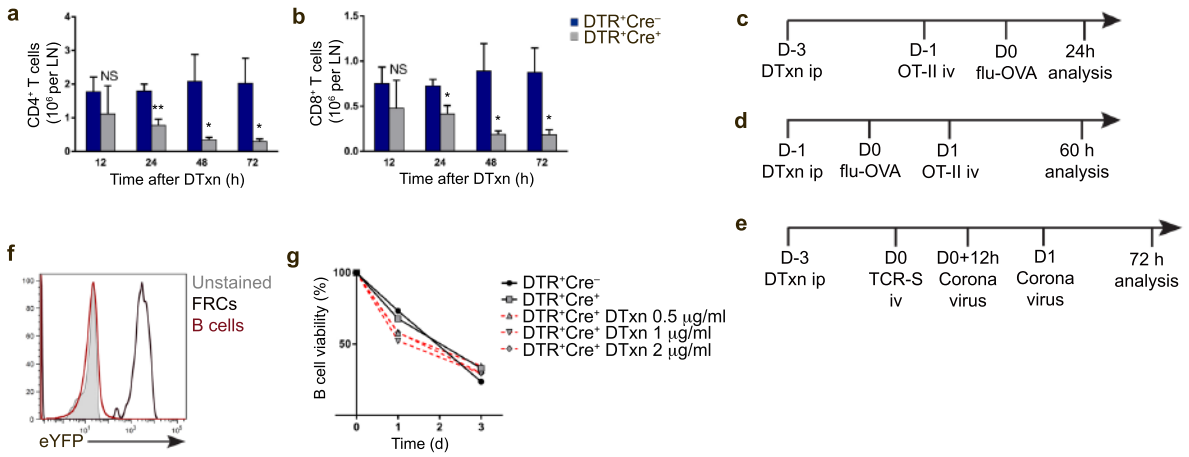

Figure 11. Effects of FRC ablation on T and B cells. (a,b) Lymph nodes from Ccl19-Cre x iDTR mice were collected and processed into single cell suspensions. CD4+ and CD8+ T cells were enumerated using flow cytometric analysis (CD45+B220–CD3+CD4+/–CD8+/–). Data are representative of at least three independent experiments (mean+/-sd, n=4 mice/group per experiment). **(c-e)** Schematic representation of the experimental protocols utilized to assess T cell immunity. **(f)** Ccl19 promoter activity was evaluated in B cells from Ccl19-Cre x Rosa26-EYFP mice. **(g)** B cells from DTR+Cre+ mice were cultured in vitro in the presence of DTxn and viability was determined over the course of 72 h (n=3 wells/group). NS non significant, * p<0.01, **p<0.001

nodes from FRC-ablated mice, suggesting that diminished T cell viability may compound the reduction in T cell numbers (**Fig. 10c**).

To assess the impact of FRC ablation in adaptive T cell responses, *Ccl19*-Cre x iDTR mice were immunized with a replication-incompetent influenza A virus expressing the OT-II ovalbumen peptide, and the generation of antigen-specific T effector cells was monitored (**Fig. 11c,d**). Loss of FRCs resulted in diminished priming of antigen-specific T cells (**Fig. 10d,e**), as well as reduced activation and proliferation (**Fig. 10f-h**). Furthermore, deterioration of anti-viral T cell responses was observed in a coronavirus-based vector system(Perez-Shibayama et al., 2013), in which generation and effector function of exogenously transferred TCR transgenic $CD8^+$ T cells specific for the viral spike protein prior to immunization (**Fig 11e**) was monitored. Strikingly, generation of the virus-specific T cell response was also profoundly disrupted with reduced numbers of antigen-specific $CD8^+$ T cells and defective interferon-γ production in FRC-ablated mice (**Fig. 10i,j**). Altogether, our data demonstrate a critical role for FRCs in T cell homeostasis, positioning and activation.

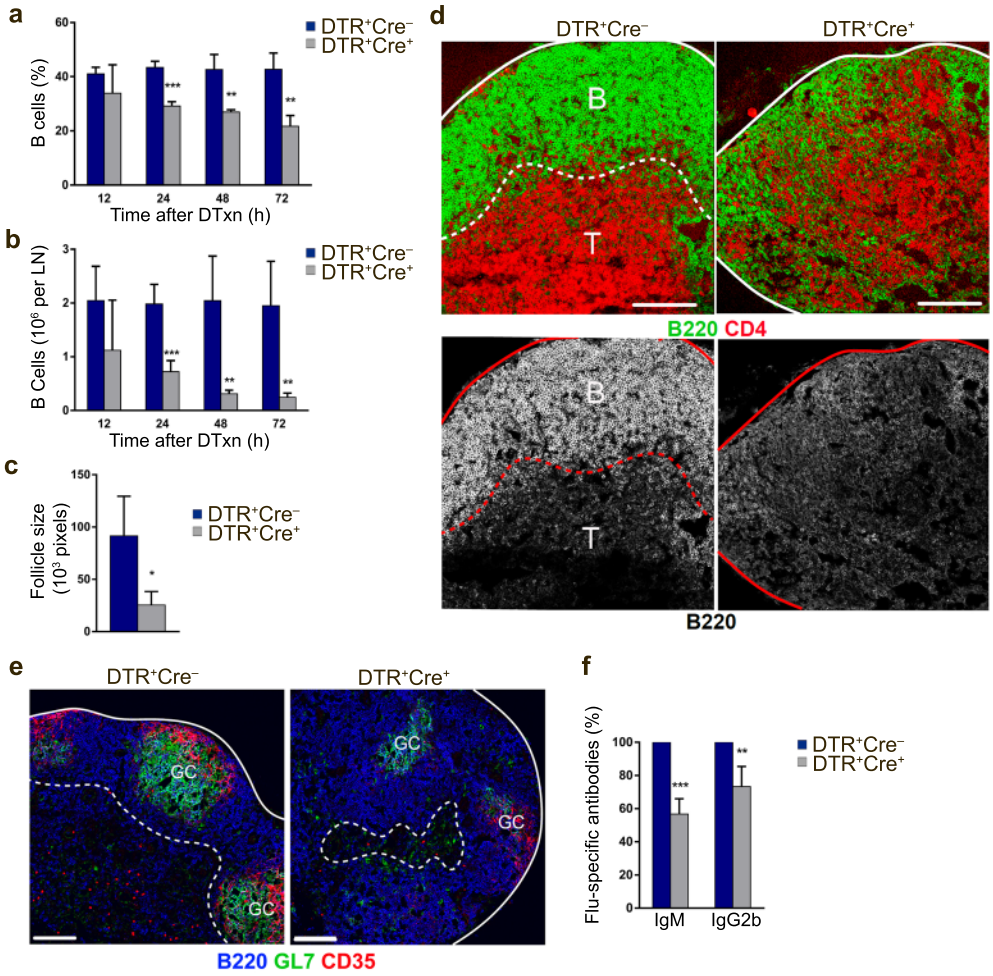

Figure 12. FRC ablation is detrimental to B cells. (a,b) Skin-draining lymph nodes from Ccl19-Cre x iDTR mice were collected, processed into a single cell suspension and B cells numbers were determined by flow cytometric analysis (CD45+B220+CD3–). B cell numbers are shown as percent among hematopoietic (CD45+) cells and total numbers per lymph node. Data are representative of at least three independent experiments (mean+/-sd, n=4 mice/group per experiment). **(c,d)** Follicle size (n=3mice) and architecture (n>3mice from 3 independent experiments) in lymph node sections from Ccl19-Cre x iDTR mice was determined 3 days after DTxn injection by staining with B220 (B cells) and CD4 (T cells). Scale bars 100 μm. **(e)** Popliteal nodes were collected 14 days after influenza immunization and analyzed for the presence of germinal centers. (B220, B cells; GL7, activated B cells; CD35, FDCs. Scale bars 100 μm. **(f)** T-independent (IgM) and T-dependent (IgG2b) humoral responses were determined by ELISA for the presence of flu-specific serum antibodies. Data are representative of two independent experiments (n=3-5 mice/group per experiment). *p<0.05, **p<0.01, ***p<0.001

Chapter 2.4 – FRC ablation is detrimental to B cells

Unexpectedly, a substantial reduction in lymph node B cells was identified following DTxn administration (**Fig. 12a,b**). Structural alterations in the lymph node cortex were also

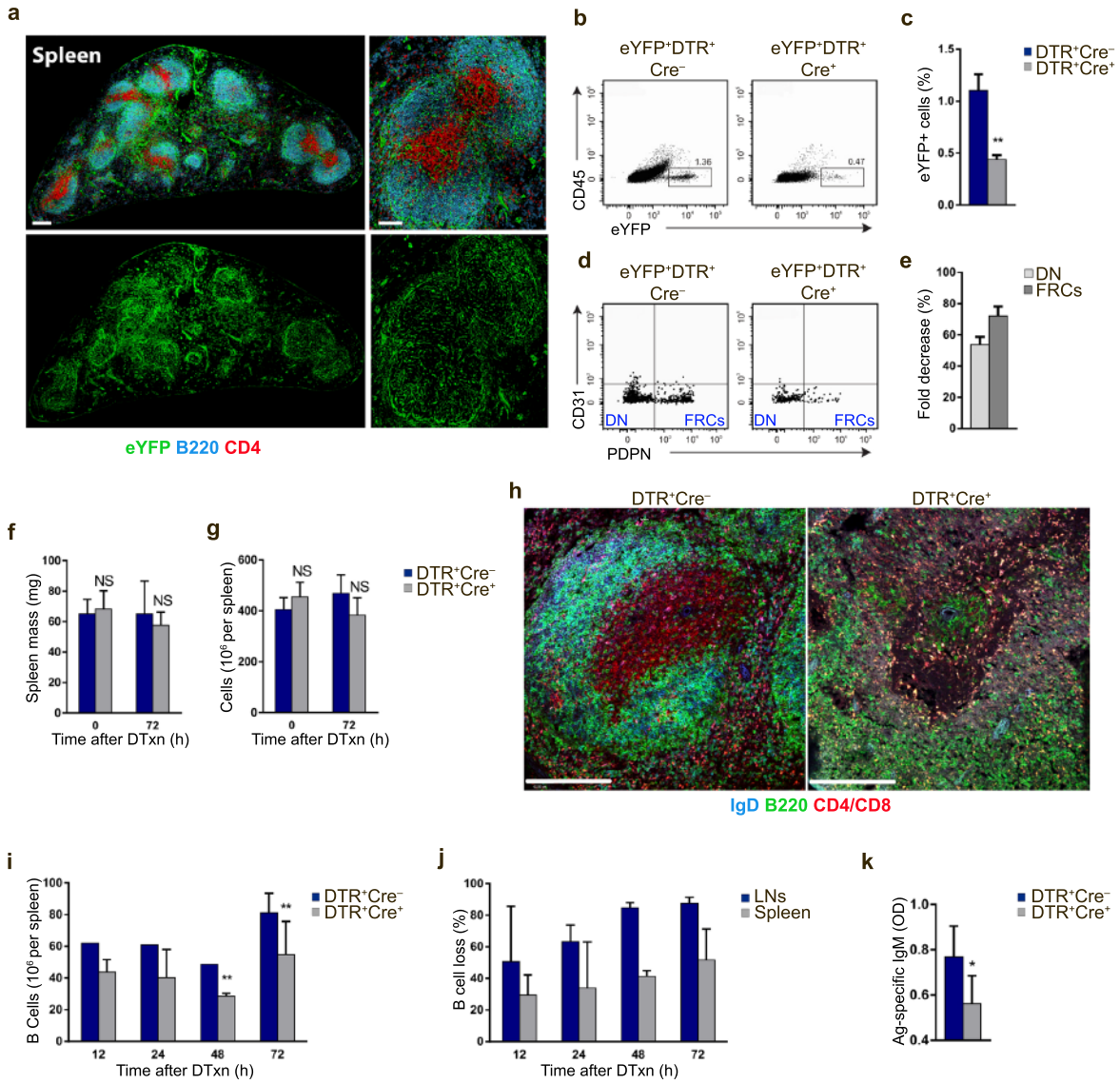

Figure 13. FRC ablation disrupts splenic white pulp organization and marginal zone humoral responses. **(a)** Confocal analysis of spleen sections from Ccl19-Cre x Rosa26-EYFP mice stained for GFP, B220 and CD4. Scale bars 200 μm (left) and 50 μm (right) (n=3 mice from two separate experiments). **(b-e)** Spleens from Ccl19-Cre x Rosa26-EYFP-iDTR mice were processed into single cell suspensions and EYFP+cells were enumerated using flow cytometry. (mean+/-sd, n=3 mice). **(f,g)** Weight and total cell numbers for spleens of Ccl19-Cre x iDTR mice are indicated. Data are representative of at least two independent experiments (mean+/-sd, n=3 mice/group per experiment). **(h)** Confocal analysis of splenic white pulp from Ccl19-Cre x iDTR animals 24 h following DTxn administration. Scale bars 200 μm (n=3 mice from two independent experiments). **(i)** B cells in the spleen were enumerated using flow cytometric analysis (CD45+B220+CD3–). Data are representative of at least three independent experiments (mean+/-sd, n=3 mice/group per experiment). **(j)** Flow cytometric analysis of lymph nodes and spleen in DTR+Cre– and DTR+Cre+ animals. Fold decrease in FRC numbers at indicated time points is shown. **(k)** Marginal zone humoral responses were assessed by determining antigen-specific IgM production via ELISA following TNP-ficoll immunization. NS non significant, *p<0.05, **p<0.0

observed, with reduced follicle size (**Fig. 12c**) and a loss of follicle boundaries (**Fig. 12d**).

Ultimately, this resulted in an unfurling of the B cell zone with mixing of B and T lymphocytes

throughout the cortex (**Fig. 12d**). Notably, no *Ccl19* promoter activity or intrinsic toxicity of DTxn in B lymphocytes was detected, suggesting a physiologic relationship between B cell homeostasis and the presence of FRCs (**Fig. 11f,g**).

To determine the functional consequences of the aberrant follicular architecture and decreased B cell numbers, the ability of FRC-ablated mice to mount a humoral response to influenza A virus was assessed. Immunization with UV-inactivated influenza virus resulted in a disorganized accumulation of B cells in the ensuing germinal center response (**Fig. 12e**), as well as a significant reduction in influenza-specific IgM (T-independent(Gonzalez et al., 2010)) and IgG2b (T-dependent) antibody production (**Fig. 12f**).

The detrimental effect of FRC ablation on B cells was not restricted to lymph nodes. In splenic white pulp, where the *Ccl19* promoter is active in both FRCs and $CD31^{-}PDPN^{-}$ (DN) cells ((Chai et al., 2013) and **Fig. 13a**), DTxn administration efficiently targeted $EYFP^{+}$ stroma (**Fig. 13b,c**), with a significant decrease in FRCs and DN cells (**Fig. 13d,e**). FRC ablation had no effect on splenic weight or cellularity (**Fig. 13f,g**) but markedly altered white pulp architecture (**Fig. 13h**). B cell numbers were also reduced in the spleen (**Fig. 13i**), although to a lesser extent than in lymph nodes (**Fig. 13j**). Functionally, the effects observed in the spleen impinged on marginal zone humoral responses, with a significant decrease in IgM production upon TNP-ficoll immunization (**Fig. 13k**).

As *Ccl19* promoter activity was also reported in Peyer's patches (**Fig. 14a**), we investigated the fate of Peyer's patches following FRC ablation. Systemic DTxn administration evoked less severe effects in Peyer's patches, with milder reductions in FRC and B cell numbers (**Fig. 14b,c**). Similarly, no major anatomical alterations were observed, with the exception of a paucity of T cell clusters in interfollicular regions (**Fig. 14d**). Together, these observations pointed to an unanticipated regulation of B cell homeostasis by FRCs, and suggest that damage to the FRC network has deleterious consequences on the cellular circuitries that underpin humoral responses.

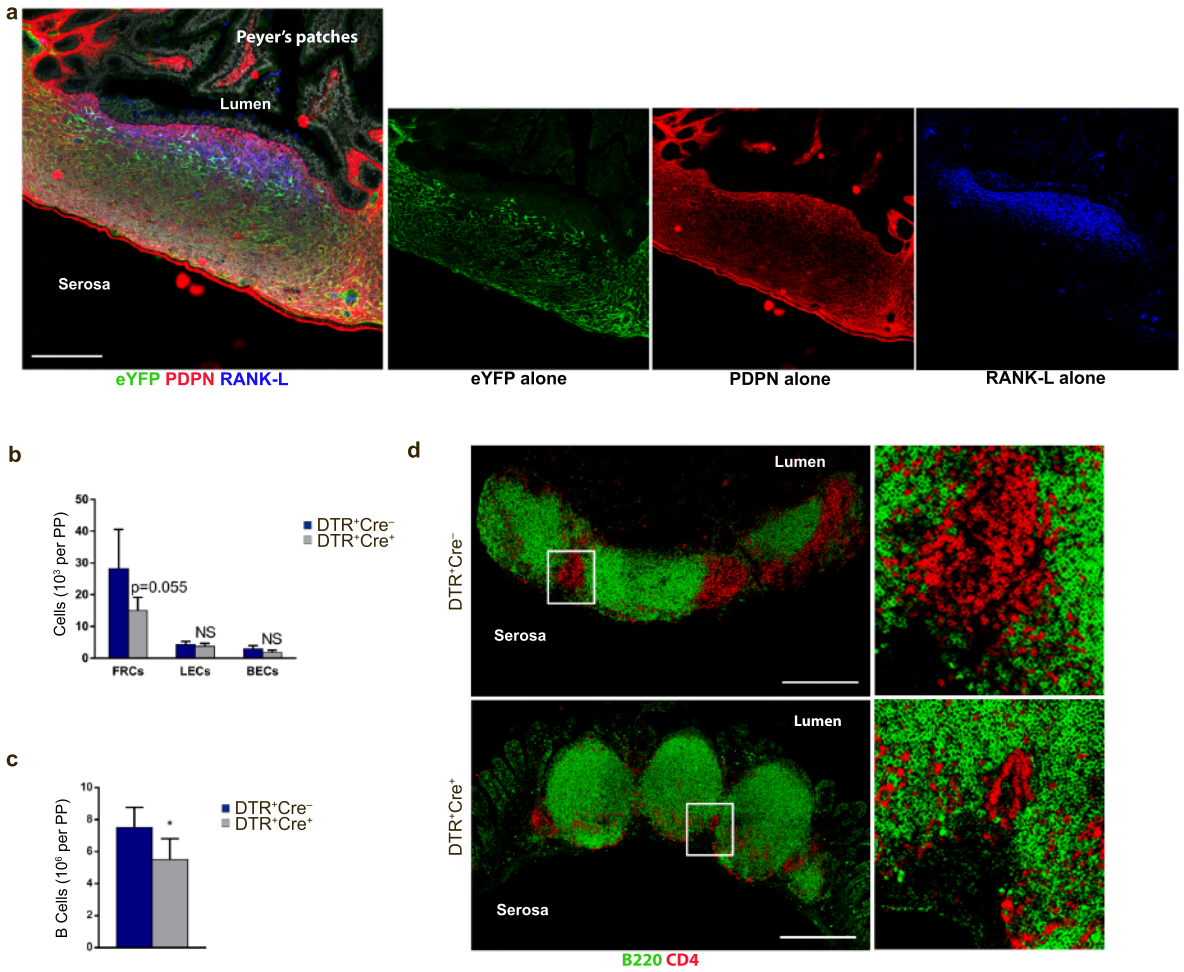

Figure 14. Peyer's patches are only marginally affected by FRC ablation. (a) Confocal analysis of Peyer's patches sections from Ccl19-Cre x Rosa26-EYFP mice stained for GFP, PDPN and RANK-L. Scale bar 150 µm (n=3 mice from two independent experiments). **(b,c)** Peyer's patches from Ccl19-Cre x iDTR mice were processed into single cell suspensions and stromal and B cells were enumerated using flow cytometry 72 h after DTxn administration. The figure shows two combined experiments (mean+/-sd, n=3 mice/group per experiment). **(d) C**onfocal analysis of Peyer's patches from Ccl19-Cre x iDTR animals 72 h following DTxn administration. Scale bars 400 µm (n=3 mice from two independent experiments). NS non significant, *p<0.05

Chapter 2.5 – Lymph node FRCs support homing and survival of B cells

Given the reported role for FRCs in regulating immune cell trafficking(Acton et al., 2012; Jillian L Astarita, 2012; Link et al., 2007; Chyou et al., 2008), we hypothesized that the decrease in B cell numbers after FRC ablation could stem from impaired lymphocyte homing to

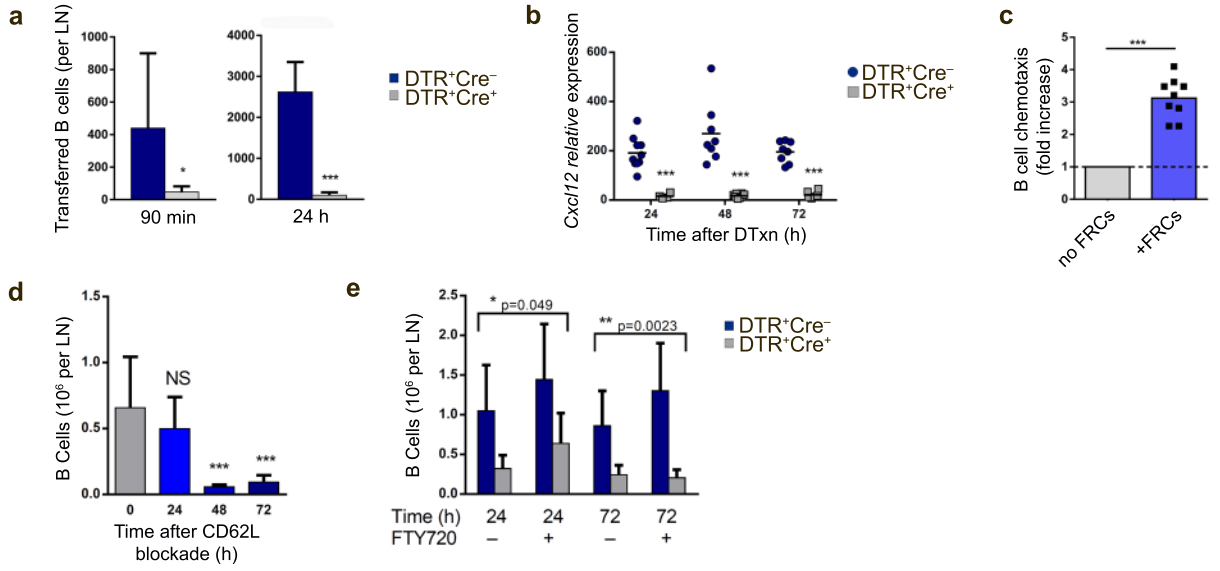

Figure 15. FRCs promotes B cell migration. (a) Ccl19-Cre x iDTR mice were injected with CFSE-labeled, CD45.1+ congenic B cells 24 h after DTxn administration. Homing of B cells to lymph nodes was evaluated 90 min or 24 h later. Data are representative of three independent experiments (mean+/-sd, n=3 mice/group per experiment). **(b)** Lymph nodes from Ccl19-Cre x iDTR mice were collected, lysed in trizol and analyzed for the presence of Cxcl12 transcript. Lines indicate mean. Data are normalized to cyclophillin. Each data point represents one lymph node from individual mice (n=4-10 mice/group from 2-3 separate experiments). **(c)** Purified FRCs were cultured in a 24 well plate. CFSE-labeled B cells were seeded on top of a transwell insert and allowed to migrate towards the FRCs for 2 h. After that time, cells were recovered and B cells enumerated by flow cytometry. The figure shows three combined experiments (mean+/-sd, n= 3 wells/condition per experiment). **(d) W**T mice received one single dose of CD62L-specific antibody i.p. and B cell numbers were determined in lymph nodes at different time points. The figure shows two combined experiments (mean+/-sd, n=3 mice/group per experiment). (**e) C**cl19-Cre x iDTR mice were injected with 1 mg/kg FTY720 i.p. and, 4 h later, with DTxn. B cell numbers were determined 24 or 72 h after DTxn administration. **F**or analysis at 72 h, mice received an additional dose of FTY720. The figure shows two combined experiments (mean+/- sd, n= 3-4 mice/group per experiment). NS non significant, *p<0.05, **p<0.01, ***p<0.001

lymph nodes. To test this hypothesis, congenic CFSE-labeled B cells were adoptively transferred into DTxn-treated *Ccl19*-Cre x iDTR mice, and enumerated within lymph nodes 90 min and 24 h later by flow cytometry. Donor B cell numbers were markedly reduced in lymph nodes of FRC-ablated mice at both time points (**Fig. 15a**). B cell homing to lymph nodes depends on CCL19 and CXCL12 (Okada et al., 2002)), and *Cxcl12* expression in FRCs has been previously documented(Malhotra et al., 2012b). Indeed, *Cxcl12* expression was significantly reduced in FRC-ablated mice (**Fig. 15b**), and FRCs were sufficient to evoke B cell chemotaxis *in vitro* (**Fig. 15c**), suggesting that FRCs recruit B cells, possibly via CXCL12 and CCL19. Importantly, blockade of lymphocyte ingress (via treatment with a CD62L blocking antibody) was not sufficient to significantly perturb B cell numbers in the first 24 h after

treatment (**Fig. 15d**), in contrast to the rapid B cell loss observed in FRC-ablated mice (**Fig. 12a,b**). Additionally, preventing lymphocyte egress from lymph nodes with a sphingosine 1-phosphate receptor antagonist, FTY720, did not completely restore B cell numbers following FRC ablation (**Fig. 15e**).

Altogether, these data suggest that while B cell entry requires an intact FRC network, impaired B cell trafficking can only account for part of the reduction in B cell numbers following FRC ablation. This consideration prompted investigation of the possibility that FRCs may regulate additional aspects of B cell homeostasis. Consistent with this hypothesis, B cell loss in FRC-ablated mice coincided with a significant increase in propidium iodide-positive B cells (**Fig. 16a,b**) implicating FRCs in promoting B cell survival.

Figure 16. FRC ablation impairs B cell survival. (a,b) B cell viability was assessed by flow cytometric analysis of lymph node single cell suspensions (CD45+B220+PI+). Representative dot plots of PI+ stain in B cells at 72 h are depicted. Data are representative of two independent experiments (n=3-5 mice/group per experiment). **(c)** Confocal images of lymph nodes from Ccl19-Cre x Rosa26-EYFP mice to depict FRCs in follicular regions. Insets show higher magnifications of the boxed regions. Scale bar 50 μm (n>3mice from 3 independent experiments). (**d)** Confocal analysis of popliteal lymph nodes from Ccl19-Cre x Rosa26-EYFP reporter mice stained for FDCM1, CXCL13, GFP and CCL21. Left, chemokine expression is shown; middle, FDCs are identified; right, single channels of the follicle area are provided. Scale bar 100 μm (n>3mice from 2 independent experiments). (**e) C**onfocal analysis of popliteal lymph nodes from Ccl19-Cre x iDTR animals 24, 48, or 72 h following DTxn administration. FDCs are identified by FDCM1 stain. Scale bar 200 μm (n>3mice per group). **(f) Q**uantitation of cumulative FDCM1 expression within the follicles of images as in (e). Each point represents a single lymph node from an individual mouse. (**g,h) C**hanges in Baff expression and B cell numbers were compared between FRC-ablated mice (Ccl19-Cre x iDTR) and FDC-ablated mice (Cd21-Cre x iDTR, lethally irradiated and reconstituted with WT bone marrow) 24 h after DTxn administration (n=2-4 mice/group). (**i,j) T**hree days after DTxn administration, lymph nodes from Ccl19-Cre x iDTR were collected, lysed in trizol and analyzed for the presence of Baff and April transcripts. Lines indicate mean. Data are normalized to cyclophillin. Each data point represents one lymph node from individual mice (n=6-8 mice/group from 3 separate experiments). (**k)** BAFF protein production in FRC-ablated mice was determined by confocal microscopy in lymph nodes from Ccl19-Cre x iDTR stained with an antibody against BAFF together with DAPI. Scale bars 50 μm (n=2 mice from two separate experiments). NS non significant, *p<0.05, **p<0.01, ***p<0.001

Fig 16, continued

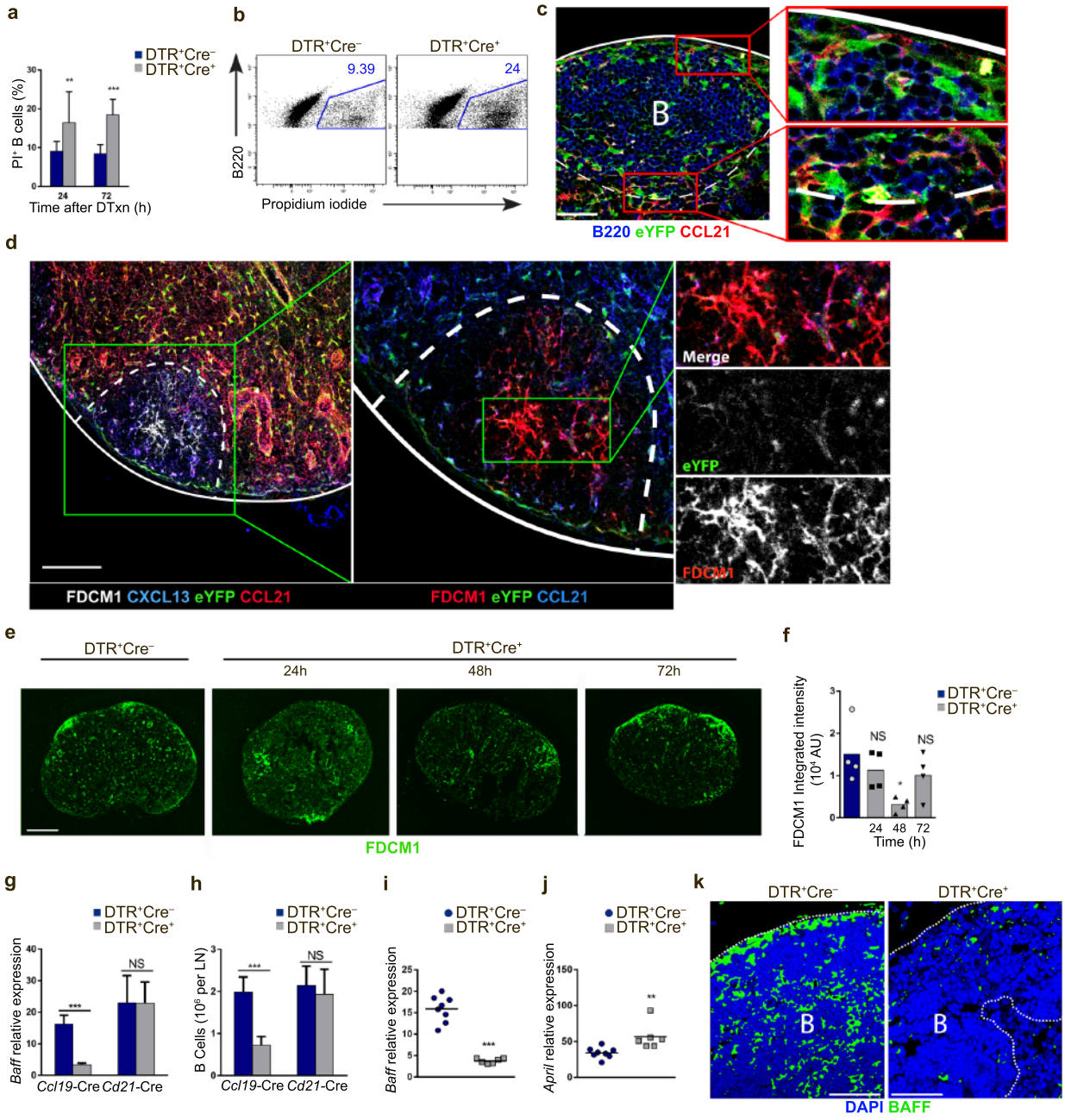

Chapter 2.6 – FRC ablation impairs BAFF production *in vivo*

Most efforts to characterize FRCs have thus far focused on their roles in supporting T cell homeostasis, migration and activation. However, a discrete population of FRCs is also found in and around follicles (B cell zone FRCs, **Fig. 16c**), and it was reasoned that such a locale could position FRCs to directly interact with and influence B cells. This observation, together with the decreased B cell survival observed in FRC-ablated mice, led to the hypothesis that FRCs may provide critical survival factors for naive B cells. In this context, BAFF plays a critical role in survival of mature B cells(Mackay and Browning, 2002; Gorelik et al., 2003). The key source of BAFF in secondary lymphoid organs was previously identified as a radiation resistant cell(Gorelik et al., 2003), with FDCs often considered the sole BAFF-producing stromal cell(Garin et al., 2010). Thus, it was possible that the phenotypes observed in FRC-ablated mice may be secondary to a reduction in FDCs.

To test if FDCs were directly targeted in our system, we ascertained whether the *Ccl19* promoter was active in follicular dendritic cells (FDCs) *in situ* by fluorescence imaging in *Ccl19*-Cre x *Rosa26*-EYFP mice. As depicted by FDCM1 and CXCL13 staining, EYFP was absent in the majority of FDCs in steady state lymph nodes (**Fig. 16d**). Less EYFP staining was detected in a small number of FDCM1$^+$ processes (**Fig. 16d**), possibly due to the tight interconnections that exist between FRCs and FDCs in follicles(Roozendaal et al., 2009; Gonzalez et al., 2011). Additionally, to assess the status of FDCs in FRC-ablated mice, we performed quantitative microscopic analysis of lymph nodes at different time points after DTxn administration. Our data demonstrated that FDCs are present 24 h after DTxn administration (**Fig. 6e** and quantified in **Fig. 16f**), despite profound loss of FRCs (**Fig. 2c**). Furthermore, FDCs remained functionally competent at this time point, as demonstrated by their ability to correctly display exogenous immune complexes (**Fig. 17a**). Prolonged DTxn exposure led to a progressive reduction in FDC volume, as depicted by a decrease in FDCM1 integrated intensity (**Fig. 16e,f**) and decreased CD35 staining as well (data not shown). Notably, contraction of the FDC network appeared to be transient and was followed by reappearance of FDCM1$^+$ cells 3 days after FRC ablation (**Fig.**

16e,f). Furthermore, direct comparison of FRC and FDC ablation revealed that loss of FRCs rapidly abrogated *Baff* expression *in vivo* while depletion of FDCs did not (**Fig. 16g**).

Together these results point to a previously unrecognized regulatory role for FRCs in maintaining BAFF amounts and B cell viability. Accordingly, the large decrease in B cell numbers was only observed in FRC-ablated mice but not in FDC-ablated animals (**Fig. 16h**). Notably, FRC ablation perturbed *Baff* expression without perturbing expression of the closely related factor April encoded by *Tnfsf13* (**Fig. 16i,j**). Moreover, impaired *Baff* mRNA expression in FRC-ablated mice was mirrored by a similar abrogation in BAFF protein abundance, as assessed by confocal microscopic analysis of lymph node sections (**Fig. 16k**). Interestingly, concentrations of BAFF protein in serum were unperturbed in FRC-ablated mice (**Fig. 17b**), indicating that FRC loss influences local BAFF production rather than perturbing a systemic reservoir. Furthermore, by injecting carefully titrated DTxn in the footpad, we were able to achieve anatomically restricted FRC ablation, and consequently B cell loss, only in the draining popliteal lymph nodes, without disrupting distal lymph nodes (**Fig. 17c,d**). Thus, the functional consequences of FRC depletion on B cell homeostasis are primarily mediated by a local effect in the organ where the ablation occurs.

Chapter 2.7 – B cell zone FRCs constitute a chief source of BAFF

The data shown so far suggest that FRCs may directly promote B cell survival by serving as a non-redundant source of BAFF, in agreement with previous studies demonstrating *Baff* mRNA expression in highly purified FRCs(Malhotra et al., 2012b). Confocal microscopic *in situ* analysis of B cell zone FRCs revealed that these cells are indeed capable of producing BAFF protein (**Fig. 18a**). In line with this finding, BAFF production was also observed by flow cytometry in a discrete fraction of freshly isolated FRCs (**Fig. 18b**). Notably, BAFF was rapidly

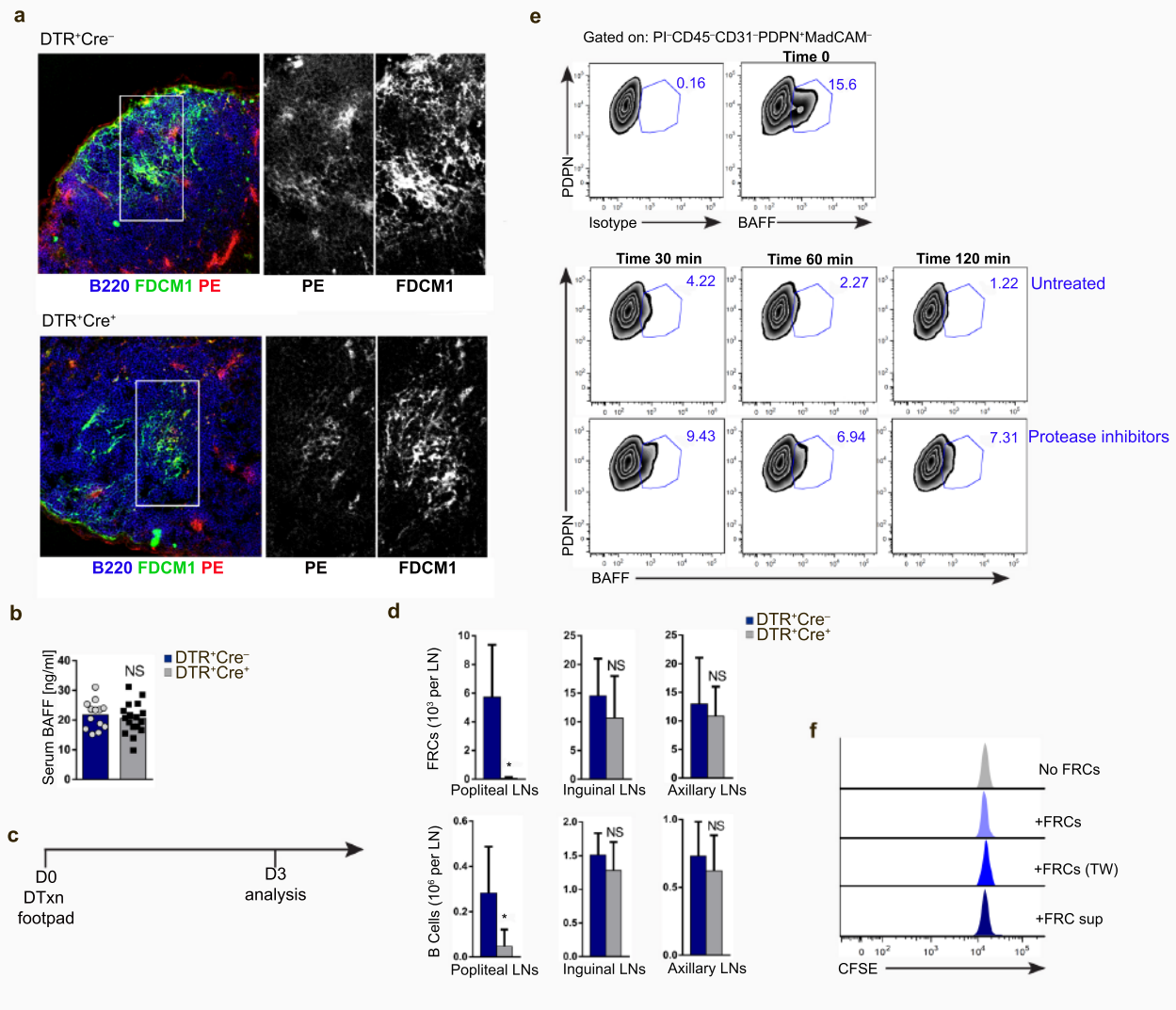

Figure 17. Functional consequences of FRC-ablation. (a) Ccl19-Cre x iDTR mice were injected with DTxn, followed by passive immunization with rabbit anti-phycoerythrin. 18 h later, mice received phycoerythrin (PE) in the footpad and the popliteal node was imaged 6 h later for B220, FDCM1 and PE. (n=3 mice). **(b)** Serum was collected from Ccl19-Cre x iDTR mice 3 days after DTxn administration and levels of circulating BAFF were determined by flow cytometry-based bead assay. Each dot represents a mouse. **(c,d)** Ccl19-Cre x iDTR mice were injected in the footpad with 0.5 ng/g DTxn and numbers of FRCs and B cells were determined by flow cytometry 72 h later. Data are representative of two independent experiments (mean+/-sd, n=3 mice/group per experiment). **(e)** After enzymatic digestion of lymph nodes, cell suspensions were left untreated in complete medium or treated with protease inhibitors at room temperature. BAFF staining was evaluated by flow cytometry at different time points. Data are representative of three independent experiments. **(f)** CFSE-labeled purified B cells were cultured in vitro for 5 days in contact with FRCs, separated from FRCs by a transwell filter (TW), or with FRC-conditioned culture supernatant. B cell proliferation was determined as CFSE dilution in B220+ cells. NS non significant, * p<0.001

cleaved from the cell surface in a protease-dependent manner, similar to other molecules belonging to the TNF superfamily (**Fig. 17e**). Importantly, BAFF$^+$ cells were characterized by expression of several FRC canonical genes encoding PDPN, α-smooth muscle actin (αSMA),

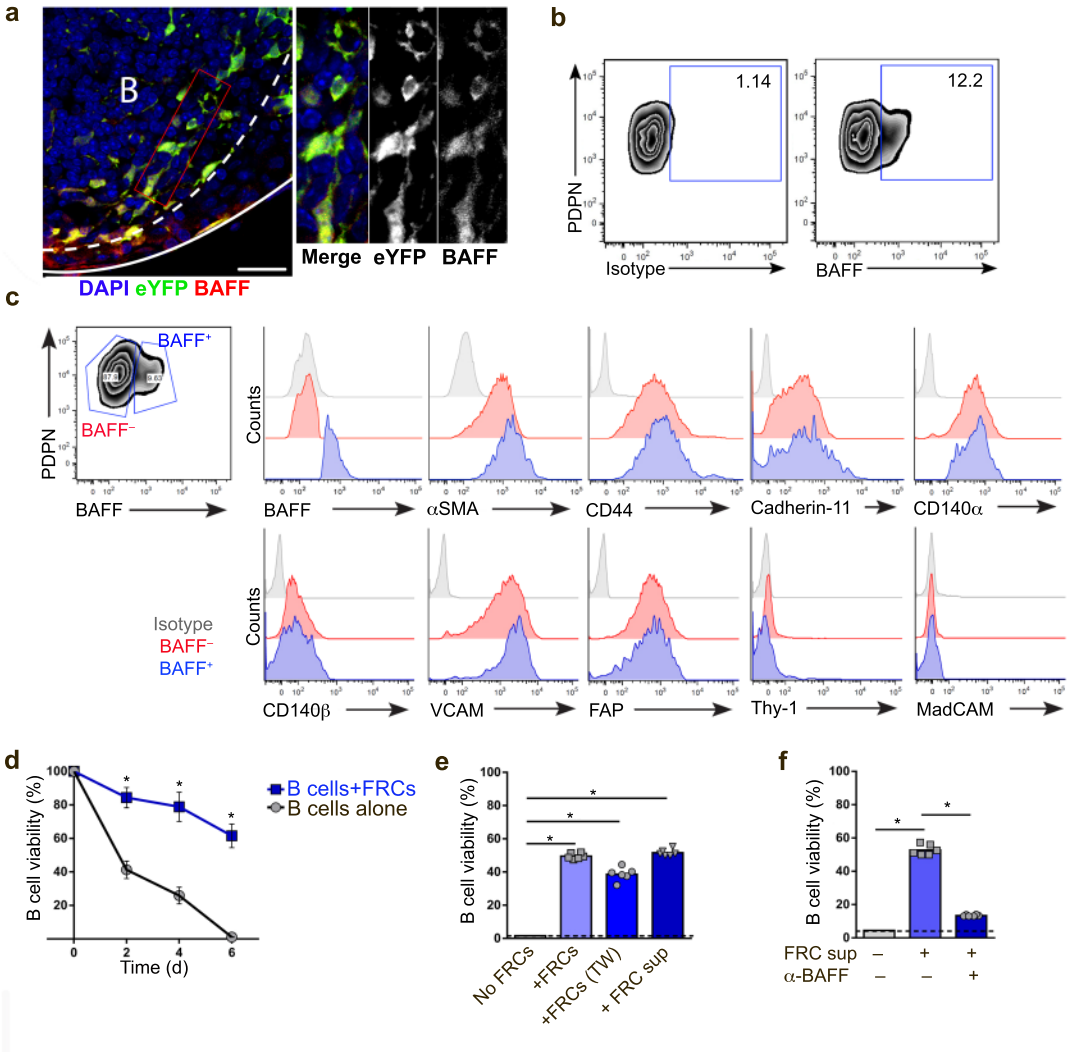

Figure 18. FRCs support the survival of B cells through the production of BAFF. (a) BAFF production by FRCs (EYFP+ cells) was determined in Ccl19-Cre x Rosa26-EYFP mice by staining lymph nodes with a BAFF-specific antibody together with anti-GFP and DAPI. Line depicts lymph node capsule while dotted line delineates B cell follicle. Scale bar 20 μm (n=3 mice from two separate experiments). **(b)** BAFF production by FRCs (CD45–PDPN+CD31–MadCAM– cells) was determined by flow cytometry in freshly isolated lymph node stromal cells. Numbers indicate percent (n>6 mice from 3 separate experiments). **(c)** Flow cytometric analysis of canonical FRC marker expression in BAFF+ or BAFF– FRCs. **(d)** Purified B cells were cultured alone or in the presence of FRCs and cell viability was determined daily by enumerating the numbers of PI–B220+ cells in each well. Data represent three independent experiments (mean+/-sem, n=2-4 wells/group per experiment). **(e)** B cell viability was determined at day 5 in B cells cultured alone, in contact with FRCs, separated from FRCs by a transwell filter (TW), or with FRC-conditioned culture supernatant (FRC sup). Data represent three independent experiments (mean, n=2-4 wells/group per experiment). **(f)** B cells were cultured alone or with FRC-conditioned supernatant (FRC sup). BAFF-specific neutralizing antibody was added to some of the wells and B cell viability was determined by flow cytometry. Data represent three independent experiments (mean, n=2-4 wells/group per experiment). * p<0.001

CD44, Cadherin-11, CD140α and CD140β, VCAM, and fibroblast-activation protein (FAP) **(Fig. 18c**), supporting that these cells are nearly identical to FRCs. Thus, our data suggest that FRCs positioned in follicular regions contribute to B cell homeostasis by providing the pro-survival factor BAFF.

To directly test the aforementioned hypothesis, we cultured B cells in the presence or absence of FRCs and measured B cell viability using propidium iodide staining by flow cytometry. Remarkably, B cells exhibited significantly enhanced viability when cultured in the presence of FRCs compared with B cells cultured alone (**Fig. 18d**). The elevated number of propidium iodide-negative $B220^{+}$ cells in cultures with FRCs could not be accounted for by proliferation (**Fig. 17f**). To ascertain whether the survival advantage conferred by FRCs was due to a soluble factor, B cells were cultured with stromal cells in separate compartments of a

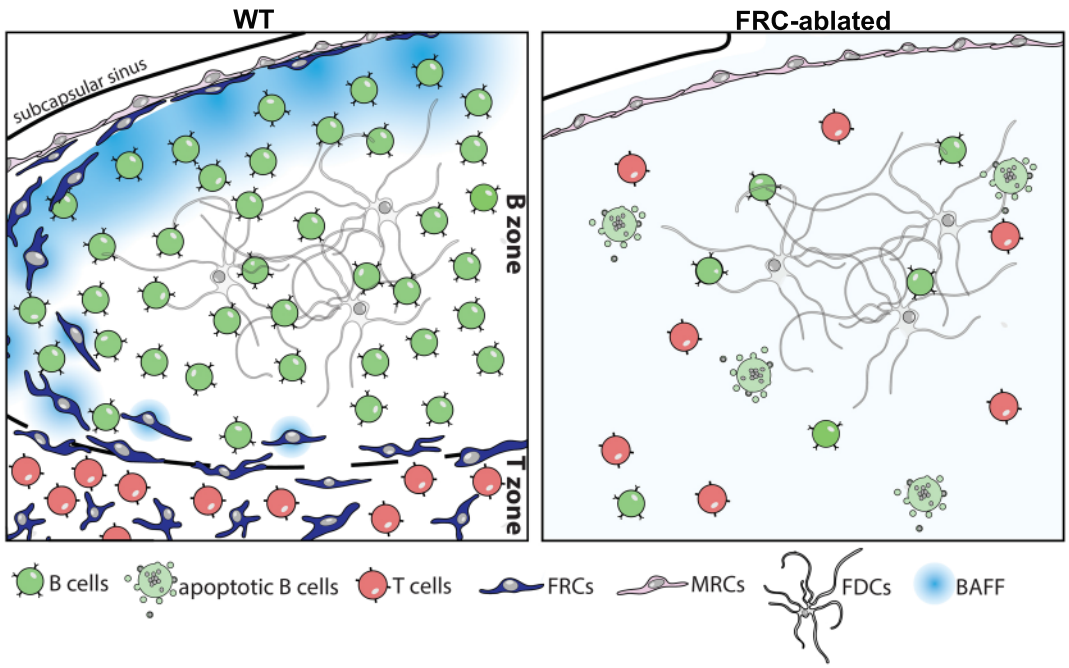

Figure 19. FRC model. Juxtaposed to marginal reticular cells (MRCs) underneath the subcapsular sinus and at the boundary between T and B cell zones, FRCs nurture B cells by producing BAFF. Ablation of FRCs has detrimental effects on B cell homeostasis: the architectural integrity of primary follicles is lost and B cell viability is profoundly decreased, leading to a significant loss of B lymphocytes.

transwell chamber or with FRC-conditioned medium. In both conditions, B cells exhibited enhanced viability indicating the presence of a soluble pro-survival factor derived from FRCs

(**Fig. 18e**). Next we sought to determine whether the pro-survival factor contributed by FRCs was BAFF. To this end, FRC-conditioned medium was pre-incubated with a BAFF-specific blocking antibody prior to addition to B cells. Strikingly, the enhancement of B cell survival was largely abrogated following BAFF neutralization (**Fig. 18f**). In sum, our data describe a subset of FRCs delineating the borders of B cell follicles in lymph nodes (B cell zone FRCs) that nurture B cells through the production of BAFF (**Fig. 19**).

Chapter 2.8 – Discussion

The absence of genetic tools for targeting FRCs has limited systematic, *in vivo* assessment of their precise function in lymphoid organs. Recent generation of *Ccl19*-Cre mice provided a solution to this technological limitation. In particular, DTR cell type--specific expression of DTR allowed us to test the functional outcomes of disrupting the FRC network in physiological settings. FRC ablation caused a severe reduction in T cell numbers in resting lymph nodes, and marked impairment in antigen-specific T cell responses. Unexpectedly, FRC ablation was not immediately accompanied by a collapse of the structured conduit system, suggesting that lymph node infrastructure can persist and function for longer periods following damage to stromal cells. Rather, the absence of the cellular source of the reticular network (that is, the FRCs) impinged on T cell dynamics and function. Thus, our study demonstrates that FRCs are essential for optimal T cell immunity but not short-term maintenance of the conduit system.

Using this genetic approach we made the unexpected observation that FRCs direct B cell homeostasis. While most lymph node FRCs reside within the T cell-rich paracortex, some localize in the vicinity of follicular conduits near the subcapsular sinus (Roozendaal et al., 2009; Gonzalez et al., 2011). Our identification of *Ccl19*-Cre^{+} cells in B cell follicles (B cell zone

FRCs) confirmed that FRCs span both the inner and outer regions of the lymph node (Bajénoff and Germain, 2009). Unexpectedly, we found that B cell zone FRCs constitute a non-redundant source of BAFF. The source of BAFF in secondary lymphoid organs was previously identified as a radio-resistant cell (Gorelik et al., 2003), often attributed to FDCs. This concept was confounded however by reports that abrogation of LTβR signaling, critical for FDC development and maintenance, did not affect BAFF expression or B cell numbers(Alimzhanov et al., 1997; Boulianne et al., 2013; Browning et al., 2005; Koni et al., 1997). Further, *Cd21*-Cre conditional ablation systems provided evidence that FDCs are dispensable for BAFF expression and naive B cell survival(Wang et al., 2011). Although it cannot be excluded that FDCs contribute to BAFF production and their ablation induces a compensatory up-regulation by other cells, these data pointed to an alternate source of BAFF in resting lymph nodes. Based on our data, we propose that B cell zone FRCs represent this source of BAFF and thereby directly support B cell homeostasis. Disrupted follicular organization in FRC-ablated mice may also contribute to decreased B cell survival, as FRCs in intact lymphoid organs would coordinate migration of naive B cells from high endothelial venules to BAFF-rich follicles.

As a functional consequence of impaired B cell homeostasis in *Ccl19*-Cre x iDTR mice, generation of humoral responses was severely compromised. We cannot exclude that FRC ablation affects the ability of dendritic cells to capture and deliver antigens, thus contributing to the diminished antibody production observed following FRC loss. However, our findings indicate that alterations in lymph node stromal composition can have catastrophic consequences on immunological competency, with decreased lymphocyte viability and disorganized spatial coordination of T and B cell responses.

Having demonstrated a central role for FRCs in B cell homeostasis and humoral immunity, our findings highlight the pleiotropic nature of FRCs and indicate functional heterogeneity, raising the intriguing concept of distinct FRC subsets within defined lymph node regions. In this context, stromal cells are thought to arise from a primordial mesenchyme in the lymph node anlagen, which initially develops into lymphoid tissue organizer (LTo) cells(Mebius,

2003). B and T lymphocyte colonization after birth then promotes the development of conventional stromal subsets. Similar expression patterns of cellular markers between MRCs and LTo cells suggested that MRCs may differentiate into FRCs and FDCs and continuously supply additional stromal subsets (Katakai et al., 2008). If indeed FRCs arise from MRCs in adult lymph nodes, then the *Ccl19* promoter must be silenced in MRCs. Furthermore, our studies indicated that most FDCs were devoid of promoter activity, and should thus be refractory to DTxn-induced apoptosis. A few cell processes from FDCM1$^+$ cells displayed weak positivity for EYFP. However, given the tight association between FRCs and FDCs in follicles (Roozendaal et al., 2009; Gonzalez et al., 2011), it remains difficult to discern between promoter activity in these FDCs, or proximity to EYFP$^+$ FRCs in follicular regions. In this regard, we observed functionally competent FDCs early after DTxn administration, when profound loss of FRCs has already occurred, suggesting that FDCs are not directly targeted in this system. Consequently, reduction of FDCM1 staining at later time points, likely mediated by a contraction or de-differentiation of the FDC network , may arise from a yet unrecognized crosstalk between FRCs and FDCs. Our finding that contraction of the FDC network was transient and rapidly followed by a regeneration phase is of particular interest. One potential explanation is that damage to the FDC network, secondary to FRC loss, may induce MRCs to generate new FDCM1$^+$ cells(Jarjour et al., 2014).

As complexity of the cellular constituents of lymph node stroma continues to grow, our understanding of their developmental origins and functional interactions remains incompletely understood. Our results demonstrate heterogeneity within the FRC network and indicate functional specialization of T cell zone FRCs versus B cell zone FRCs. BAFF$^+$ FRCs in follicles share common signatures with canonical FRCs, suggesting that there is some relationship between them. However, they differ in their localization, and BAFF-producing cells are not found in T cell areas. As mesenchymal cells are typically highly flexible in nature depending on the surrounding environment it is possible that BAFF production by B cell zone FRCs is maintained by microanatomic cues. Several functions associated with T cell immunity have been assigned

to FRCs(Gretz et al., 2000; Roozendaal et al., 2009; Link et al., 2007; Chai et al., 2013; Chyou et al., 2008; Yang et al., 2014), yet the requirement for these cells in humoral responses has not been addressed. Our finding that B and T cell homeostasis is governed by a common stromal cell expands our understanding of the stromal network and underscores its central role in immunity.

Stromal cells have long been recognized as key structural components of secondary lymphoid organs(Junt et al., 2008). More recently, we have come to understand how stromal cells interact with hematopoietic cell populations and influence adaptive immunity(Koning and Mebius, 2012; Malhotra et al., 2012a). A number of pathogens have been reported to affect the stromal network in mammalian lymphoid organs and such alterations can be deleterious to host defense and vaccine responsiveness(Scandella et al., 2008; Mueller and Germain, 2010). Here, we uncovered the existence of a mesenchymal cell population with FRC characteristics that supports follicle identity and B cell survival through localized production of BAFF. We anticipate that these findings may inform new approaches to boost natural and vaccine-induced humoral immunity and protect against potentially devastating infections.

Chapter 2.9 – Methods

Mice. *Ccl19*-Cre mice were previously described(Chai et al., 2013). *Rosa26*-EYFP (stock number 006148), *Rosa26*-DTR (iDTR, stock number 007900) *Cd21*-Cre (stock number 006368) and OT-II (stock number 004194) were purchased from Jackson Laboratory. Mice were maintained under specific pathogen-free conditions in accordance with institutional and National Institute of Health guidelines and used at 5-7 weeks of age. Experiments were conducted without blinding using sex and age matched mice for all *in vivo* experiments. For multiple time-point experiments, mice were randomly assigned to each group. Animal studies were approved by the Research Animal Care committee of Dana-Farber Cancer Institute.

Antibodies. The following antibodies were used: αCD45 (30-F11), αCD31 (390), αPDPN (8.1.1), αMadCAM (MECA-367), , αB220 (RA3-6B2), αAlphaSMA (1A4), αThy1 (53-2.1), αCD140α (APA5), αCD140b (APB5), αCD106 (429), αCD11b (M1/70), αCD11c (N418), αGr1 (RB6-8C5), αMHC class II (M5/114.15.2), αCD4 (RM4.5) and αCD8 (RM2206) from Biolegend, αBAFF (121808 from R&D), anti-GFP (A10263 from Life Technologies).

Systemic FRC ablation *in vivo*. *Ccl19*-Cre mice were bred to *Rosa26*-iDTR to generate *Ccl19*-Cre x iDTR animals. DTR^+Cre^+ mice that express DTR in *Ccl19*+ cells and DTR^+Cre^- control mice were injected i.p. with 8 ng/g DTxn and sacrificed at 12, 24, 48 or 72 h as indicated in figure legends. Ablation efficiency was assessed by flow cytometry at various time points with 80–90% reduction in FRCs ($CD45^-PDPN^+CD31^-$) commonly seen by 72 h. *Ccl19*-Cre^+iDTR^+ (DTR^+Cre^+) and *Ccl19*-Cre^-iDTR^+ (DTR^+Cre^-)

Local FRC ablation *in vivo*. DTR^+Cre^+ mice that express DTR in *Ccl19*+ cells and DTR^+Cre^- control mice were injected in the footpad with 0.5 ng/g DTxn and sacrificed 72 h later. Local ablation was assessed by comparing FRC ablation in draining (popliteal) and non-draining lymph nodes.

FDC ablation *in vivo*. *Cd21*-Cre mice were bred to *Rosa26*-iDTR to generate *Cd21*-Cre x iDTR animals. For FDC ablation experiments, 6 week-old, male recipients were irradiated and adoptively transferred with bone marrow from WT C57BL/6 mice. 6 weeks after reconstitution, mice were injected i.p. with 8 ng/g DTxn and sacrificed 24 h later.

Anti-viral T cell-dependent responses. Influenza propagation and isolation was carried out as previously described(Gonzalez et al., 2010). 3 days after DTxn administration, mice were adoptively transferred with 5×10^6 CFSE-labeled, purified OT-II transgenic $CD4^+$T cells by tail

vein. 24 h later, mice received 20 μl virus suspension (1×10^6 p.f.u.) S.C. into the footpad. Mice were sacrificed 24 h later and flow cytometric analysis was performed on popliteal lymph nodes. Activation and CFSE dilution were determined 60 h after T cell transfer. For the coronavirus experiments, DTxn injection was performed 72 h before adoptive T cell transfer[23]. A total of 2×10^6 TCR-S transgenic $CD8^+$T cells were transferred by intravenous injection and, 12 h after transfer, the mice were subcutaneously injected with 3×10^6 of non-replicating coronaviral particles in both flanks[23]. A second injection of non-replicating coronaviral particles was performed 12 h following the first one. Lymph nodes were analyzed 72 h after the first viral particle injection.

Anti-viral humoral responses. 2 days after DTxn administration, mice received 20 μl influenza virus suspension (1×10^6 p.f.u.) subcutaneously into the footpad. 14 days later, popliteal draining lymph nodes were collected, cryopreserved and imaged to determine formation of germinal centers. Additionally, serum was collected to determine the presence of influenza-specific antibodies. ELISA analysis of serum was carried out through immobilization of UV-PR8 on a high binding plate, addition of collected serum, and probing for specific binding of IgM or IgG2b (Sigma) using standard alkaline phosphatase development. For TNP-Ficoll immunization experiments, mice were injected with DTxn and, 2 days later, with TNP-ficoll i.p. (250 μg/mouse). IgM antibody titers were determined at day 8 in the blood.

Anti-CD62L and FTY720 treatments. For CD62L blockade, mice received one single dose of MEL-14 CD62L antibody i.p. (200 μg/mouse, BioXcell). To prevent cell egress, mice were injected with 1 mg/kg FTY720 Fingolimod, R&D) i.p. and, 4 h later, with DTxn. Mice received an additional dose of FTY720 at 48 h and were sacrificed for analysis at 72 h.

BAFF Serum. Serum was collected from mice 3 days after DTxn administration and stored at -80 °C until processing. Soluble BAFF was measured in the serum samples at a 1:2 dilution using a modified cytometric bead array. BD CBA Functional Beads (BD Biosciences) were activated and coated with immunopure streptavidin (Thermo Scientific) per manufacturer's instructions. For array development, a commercial anti-BAFF ELISA kit (R&D systems, catalog #DY2106-05) was used in an inverted manner. Biotinylated detection antibody was incubated with 30 μl of streptavidin-conjugated bead slurry at 3 μg/ml and subsequently washed three times with PBS containing 3% FBS. Following overnight blocking, serum samples were incubated with anti-BAFF beads in Multiscreen plates (Millipore) for 2 h. Beads were then washed three times with 3% FBS in PBS. ELISA capture antibody was used to detect BAFF bound to beads at a concentration of 4 μg/ml. Following 1 h incubation, beads were washed, followed by incubation with goat anti-rat Alexa 546 antibody (Molecular Probes) for 1 h. Beads were washed three times with 3% FBS in PBS followed by an additional four washes in PBS alone. Fluorescence was detected on a BD FACSAriaIIIu, and data were analyzed using FlowJo software.

Enzymatic digestion of lymphoid organs. For flow cytometric analysis or cell culture of lymph node stromal cells, skin-draining lymph nodes from individual mice were dissected and incubated at 37 °C in RPMI containing 0.1 mg/ml Dnase I (Invitrogen), 0.2 mg/ml Collagenase P (Roche) and 0.8 mg/ml Dispase (Roche) for 50–60 min[22]. Cells were collected in PBS containing 2% FBS and 5 mM EDTA every 15–20 min, replacing the digestion medium with new one. Digestion of spleens was performed similarly, and red blood cells were lysed with ACK buffer before analysis by flow cytometry. Peyer's patches were collected and washed in 2 mM EDTA and 1 mM DTT in PBS to remove the epithelium before enzymatic digestion.

FRC culture *in vitro*. Single cell suspensions from pooled skin-draining lymph nodes were enriched for MadCAM-1$^-$ cells using a biotinylated MadCAM-1-specific antibody and anti-biotin microbeads (Miltenyi). Cells were counted and plated at a density of 5×10^5 cells/cm^2 in αMEM supplemented with 10% FBS, 1% penicillin/streptomycin and 1% glutamine. Non-adherent cells were removed after 24 h. After 5 days, primary cultures (FRCs and LECs primarily) were harvested and MACS-purified for CD45$^-$CD31$^-$ cells (FRCs).

FRC-B cell cocultures. FRCs were purified from primary lymph node cultures (see above) and seeded at a concentration of 2.5×10^5 cells/ml in complete αMEM medium. Freshly purified lymph node B cells (B220 negative selection kit, Miltenyi) were overlaid on top of the FRC layer, at a ratio of 1 FRC : 5 B cells. In some experiments, FRCs were grown on the bottom of a transwell system chamber and B cells were added to the top of the insert. Alternatively, B cells were cultured in FRC-conditioned medium (supernatant from purified FRCs collected 5 days after seeding).

BAFF flow cytometry and protease inhibition. Lymph nodes were enzymatically digested and single cell suspensions were stained in flow cytometry buffer. FRCs were identified as negative for staining with propidium iodide and CD45$^-$CD31$^-$PDPN$^+$MadCAM$^-$. ABAFF monoclonal antibody or isotype control (both from R&D, BAFF clone 121808) were used. For protease inhibition, cells were treated with Batimastat (25 μM in DMSO, abcam) and Decanoyl-Arg-Val-Lys-Arg-Chloromethylketone (25 μM in DMSO, Bachem).

Immunohistochemistry and confocal microscopy. Isolated tissues were fixed in 4% paraformaldhehyde (PFA) for 2–4 h, and placed in 30% sucrose until saturation. Tissue was

embedded in OCT medium (*Optimal Cutting Temperature*), frozen, and cut into 10–20 μm sections. Sections were immunostained, and imaged using a Leica SP5X laser-scanning confocal microscope. All of the images with EYFP signal were counterstained with a chicken GFP-specific antibody (Life Technologies), followed by FITC-conjugated anti-chicken antibody.

PE immune complexes deposition. PE-IC uptake by FDCs was assessed by standard confocal microscopy. 18 h following FRC ablation, mice were passively immunized with 100 μg rabbit PE monoclonal antibody, followed 6 h later by S.C. footpad injection of 1 μg PE. Popliteal draining lymph nodes were fixed in 4% PFA, cryopreserved, sectioned, and imaged as described above.

Conduit analysis. Mice were injected i.v. with 3 μg CD35 (clone 8C12) antibody conjugated to alexa-568 6-18 h prior to lymph node harvest. Conduit staining was achieved through s.c. injection of FITC-saturated PBS solution (10 μl) into the footpad 4-6 h prior to popliteal lymph node harvest.

FDC quantitation. Popliteal lymph nodes from DTxn-treated mice were isolated and fixed in 4% PFA. Lymph nodes were equilibrated in 30% sucrose and serially sectioned. 4 sections from each individual lymph node were taken at 100 μm increments through the lymph node, and stained for confocal microscopic analysis. Resulting images were analyzed using CellProfiler to identify individual B cell follicles within each section. Fluorescence data was assessed for each follicle, and then integrated such that each lymph node data point represents at least 3 combined sections.

Statistical analysis. Two-tailed, unpaired student's *t*-tests were performed, assuming equal sample variance, using GraphPad Prism. Differences were considered to be statistically

significant when $P < 0.05$. For graphs, data are shown as mean +/- SD, unless otherwise indicated. Sample size was not specifically predetermined, but the number of mice used was consistent with prior experience with similar experiments

Chapter 2.10 – Author contributions

V.C. and M.C.W. designed and performed experiments and analyzed results; J.M.N.-B., F.A.S., F.C., J.Cu., L.O., J.Ch. and C.J.H. performed experiments; B.L. provided *Ccl19*-Cre *mice* and critical input on the manuscript; K.W. provided reagents and critical input on the manuscript; M.C.C. and S.J.T. designed and supervised the study. V.C., M.C.W., and S.J.T. wrote the manuscript.

Chapter 3

Trans-nodal migration of resident DCs into medullary inter-follicular regions initiates immunity to influenza vaccine

Text and figures adapted from:

Woodruff, M.C., Heesters, B.A., Herndon, C.N., Groom, J.R., Thomas, P.G., Luster, A.D., Turley, S.J., Carroll, M.C. 2014. Trans-nodeal migration of resident dendritic cells into medullary interfollicular regions initiates immunity to influenza vaccine. *J. Exp. Med.* 211 (8) 1611-1621. doi:10.1084/jem.20132327

Chapter 3.1 – Introduction

Since early descriptions of dendritic cells (DCs) as primary stimulators of adaptive immunity(Steinman, 1991), their role in establishing and regulating immune responses has been central to diverse immunological fields such as transplantation(Larsen et al., 1990; Hill et al., 2011), autoimmunity(Llanos et al., 2011), infectious disease(Poudrier et al., 2012), and vaccinology(Arnason and Avigan, 2012). As critical mediators of antigen presentation, significant effort has been spent describing activation of conventional DCs (cDCs) in peripheral tissue(Moodycliffe et al., 1994; Austyn, 1996; Rescigno et al., 1997), and characterization of their subsequent migration to secondary lymphoid organs(Itano et al., 2003; Randolph et al., 2005; Alvarez et al., 2008; Tal et al., 2011; Braun et al., 2011). Once in peripheral LNs, migrating DC populations (mDCs) from the injection site present antigen to cognate T and B cells and stimulate adaptive immunity(Qi et al., 2006).

The activation and maturation of mDCs is thought to follow a three-stage process. First, immature DCs encounter antigen in the periphery leading to upregulation of MHC class II and costimulatory molecules with a concomitant reduction in phagocytic capacity(Rescigno et al., 1997). Second, antigen loaded DCs acquire migratory capacity through the expression of matrix metalloproteases(Yen et al., 2008), migratory adhesion molecules(Acton et al., 2012), and rapid actin treadmilling in order to enter and migrate along lymphatic vessels(Lämmermann et al., 2008). Finally, lymph node (LN) bound mDCs cross the subcapsular sinus floor into the paracortical region and interact with cognate T cells and lymph node resident DCs (LNDCs) within the draining LN (Braun et al., 2011; Allan et al., 2006) to establish protective downstream immunity.

Following antigen capture in peripheral tissues, the activation and migration of mDCs into draining LNs is delayed for up to 18-24h to allow for transcriptional and translational modification, and a crawling migration sometimes representing distances of thousands of cell body lengths of the mDC. In the case of vaccination, however, arrival of injected antigen is

rapid, with detectable antigen arriving in the draining LN via the afferent lymphatics within minutes(Roozendaal et al., 2009; Gonzalez et al., 2010). This timing discrepancy between antigen arrival in the LN, and the migration of DCs from the periphery leaves open a potential window whereby targeting a vaccine to a non-degradative, immunostimulatory compartment within the LN could have important humoral immune ramifications.

Several studies have focused on the drainage of lymph-borne antigen from the afferent lymph into the subcapsular sinus of the draining LN(Szakal et al., 1983; Phan et al., 2007; Carrasco and Batista, 2007; Junt et al., 2007; Roozendaal et al., 2009; Gonzalez et al., 2010). A current view is that subcapsular sinus macrophages (SSMs) rapidly capture antigen from the lymph, and participate in its active transport to the B cell follicle. Less well described is the downstream filtration of the lymph within the medulla by medullary sinus-lining macrophages(Gray and Cyster, 2012) and LNDCs (Gonzalez et al., 2010). Historically, DC residing in the LN (LNDC) have been described as relatively sessile at steady state, (Steinman et al., 1997; Lindquist et al., 2004) and insufficient to drive effective immunity following direct antigen acquisition (Itano et al., 2003; Allenspach et al., 2008). The recent observation of direct viral capture in the medulla by the LNDC population, however, suggested they may have a more active role in the establishment of downstream immune response in the case of influenza vaccination(Gonzalez et al., 2010).

To extend our understanding of the role of LNDCs in establishing immune response to influenza vaccination, resident DCs were characterized at a whole-LN level. Unexpectedly, a major trans-nodal repositioning of LNDCs from the T cell cortex to the afferent medulla was observed within minutes of viral antigen arrival from the afferent lymphatics – areas recently shown to be important in vaccine efficacy(Liu et al., 2014). This migration leads to rapid viral acquisition by LNDCs and stimulation of viral specific naïve CD4+ T cells. Further, total elimination of skin mDCs had a negligible effect on the generation of a protective humoral response in mice vaccinated with UV-inactive virus. Taken together, the results suggest a

model where LNDCs are fully competent in establishing robust, long term viral immunity, even in the absence of mDCs from the injection site.

Chapter 3.2 – Activation of LNDCs following influenza vaccination

To characterize LNDC response following vaccination, CD11c-eYFP C57BL/6 mice (Gerner et al., 2012; Hickman et al., 2008; Lindquist et al., 2004; Kastenmuller et al., 2013; Sung et al., 2012) were immunized subcutaneoulsy (S.C.) in the footpad with UV-inactivated Influenza-A virus strain PR8 (UV-PR8). DCs were tracked by multi-photon intravital microscopy (MP-IVM) of the popliteal lymph node (PLN) by surgically exposing the node in live, anesthetized mice(Kastenmuller et al., 2013; Gonzalez et al., 2010; Sung et al., 2012). Continuous imaging for 40 min following UV-PR8 vaccination revealed an influx of LNDC proximal to the collagen capsule (<150 um) (**Fig 20a**). Quantitation of cellular trafficking over this period identified a 3-4 fold increase in the number of YFP+ DCs within this region (3.23 ± 0.24; $p<0.001$), suggesting a rapid repositioning to the periphery of the PLN .

In addition to increased cell number within the LN periphery, LNDCs exhibited extensive morphological changes over the 40 min imaging period (**Fig 20a, inset**). Measured in bulk, DCs within these regions increased in surface area by almost 50 percent following vaccination and experienced a concomitant increase in volume, and decrease in spherical index – a measure of the spherical nature of an object (**Fig 20c**), and data not shown). Importantly, the fluorescence intensity of individual DCs did not change over this time period, indicating that the observed phenotypic changes were not due to changes in YFP expression. Together, these data suggest an unexpected accumulation and activation of resident DCs in the PLN periphery immediately following vaccination.

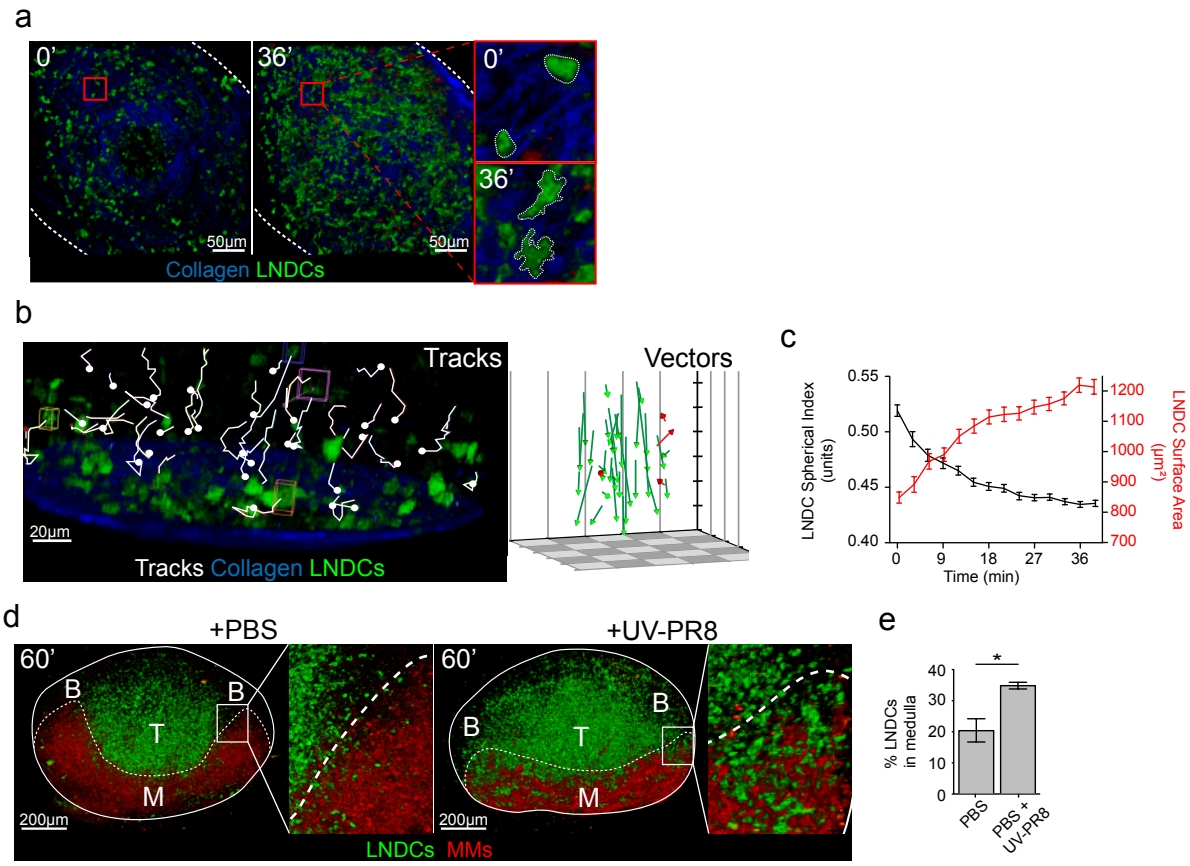

Figure 20. LNDCs migrate to the medulla following influenza vaccination
(a) MP-IVM of DC arrival in the PLN periphery following UV-PR8 vaccination. Snapshots taken at 0 and 36min post injection, and representative of 3 independent surgeries (3 mice) from different imaging sessions. Scale bars – 50μm. Inset: high magnification of two individual LNDCs **(b)** (left) Real time tracking of LNDCs from Fig1a. LNDC tracks highlighted (white) and final destinations marked (closed circle). Vector representation of complete tracks (right). Green and red vectors represent LNDCs with migration paths towards or away from the PLN capsule, respectively. Representative of 3 independent surgeries (3 mice) from different imaging sessions. Scale bar – 20μm **(c)** Quantitation of bulk DCs from live imaging in Fig 1a. DC spherical index (red) and surface area (black) displayed. ANOVA (black) $p<0.005$ ANOVA (red) $p<0.005$ **(d)** Fluorescent reconstructions of in vivo labeled CD11c-eYFP reporter PLNs. PLNs collected at 60 min following PBS or UV-PR8 vaccination. Representative of reconstructed 3 PLNs. Scale bars – 200μm **(e)** Quantitation of the percentage of LNDCs inside or outside of the medulla as in (d) (n=3 PLNs).

Chapter 3.3 – Repositioning of LNDCs to the medulla

In order to address the origin of the accumulating DCs, *in vivo* cellular tracking was applied to the live imaging model. By tracking individual DCs, it was observed that rather than infiltrating from an outside source, the cells originated from the interior of the PLN (>150μm from

the collagen capsule), which is beyond the imaging depth threshold for our imaging system (**Fig. 20b**). Pretreatment of mice with CD62L blocking antibody, or local administration of Pertussis toxin, two approaches that limit influx of leukocytes from the vasculature or lymphatics, had negligible effect on DC accumulation (data not shown). These results provide additional evidence that the activated DCs originated within the PLN prior to vaccination and confirmed their identity as lymph node resident DCs (LNDCs).

To assess the overall movement of LNDCs following vaccination, 50 μm serial cryosections of PLNs were imaged by multi-photon microscopy (MPM), and serially reconstructed for analysis of whole PLNs. Similar approaches were reported by Cyster and colleagues using confocal microscopy for partial PLN imaging(Groom et al., 2012; Grigorova et al., 2010). By *in vivo* labeling medullary macrophages (MMs) through pre-injection of an α-F4/80 monoclonal antibody (mAb) into the footpad of CD11c-eYFP reporter mice, the medulla could be outlined and shown to include relatively sparse populations of LNDCs in resting naïve LNs (**Fig 20d**). In agreement with the live imaging data, injection of UV-PR8 into the footpad of CD11c-eYFP mice stimulated a visible shift of the LNDC population into the medullary compartment by 60min post vaccination (**Fig 20d**). Flow cytometric analysis of single cell suspensions of PLN indicated no appreciable increase of LNDCs at these time points. This global repositioning of the LNDCs can be quantified through a shift in the ratio of medulla-occupying versus total LNDCs (**Fig 20e**). Migration data were further verified through MP-IVM, where the rapid arrival of LNDCs into the medulla could be observed. Surprisingly, this change in both LNDC morphology and localization could not be identified following the injection of traditional adjuvants such as Alum and MF59 despite extensive inflammation of the PLN, suggesting that this response may be specific towards viral antigen or endosomal TLR signaling.

Chapter 3.4 – Capture of viral antigen by LNDCs within inter-follicular regions

Recent studies have identified interactions of DCs and T cells outside of the T cell area within inter-follicular regions (IFRs) in the stimulation of memory CD8+ T cell responses(Groom et al., 2012; León et al., 2012; Hickman et al., 2008; Sung et al., 2012). In these studies, central memory T cells were generated following viral infection with the purpose of tracking those cells in the LN after secondary challenge. Although there is debate on the resting location within the LN, it is clear that following secondary challenge, central memory CD8+ T cells are rapidly recruited to the IFRs where they undergo activation by antigen-loaded APCs. Further, a study by Hickman et. al. suggested a primary role for these sites in priming CD8 T cell immunity(Groom et al., 2012; Hickman et al., 2008).

We hypothesized that these sites may serve as destinations for migrating LNDCs. To characterize the architectural identity of the IFRs, PLNs were *in vivo* labeled with antibodies against the lymphatic endothelium (a-Lyve-1) and subcapsular sinus macrophages (a-CD169), and then optically cleared for MP imaging. Projections of whole nodes following optical clearing(Ertürk et al., 2012) identified long extensions of the medulla that protrude extensively between B cell follicles and merge with the subcapsular sinus. This observation identified two different types of IFR structure – cortical IFRs (cIFRs), which represent chemokine boundaries between the paracortex and B cell follicles, and medullary IFRs (mIFRs), which represent the most afferent connection points between the medulla and the subcapsular sinus (**Fig 21a**). Interestingly, these regions have recently been targeted by Liu et. al. (Nature 2014) in vaccination attempts, resulting in greatly enhanced T cell priming(Liu et al., 2014). Confocal imaging of mIFRs in PBS, or UV-PR8 vaccinated PLN identified YFP+ clusters similar to those identified in reconstruction analysis, identifying these sites as destinations for migrating LNDCs (**Fig 21b**). Histological staining confirmed that both $CD11b^{hi}$, and $CD8a^{pos}$ LNDC populations

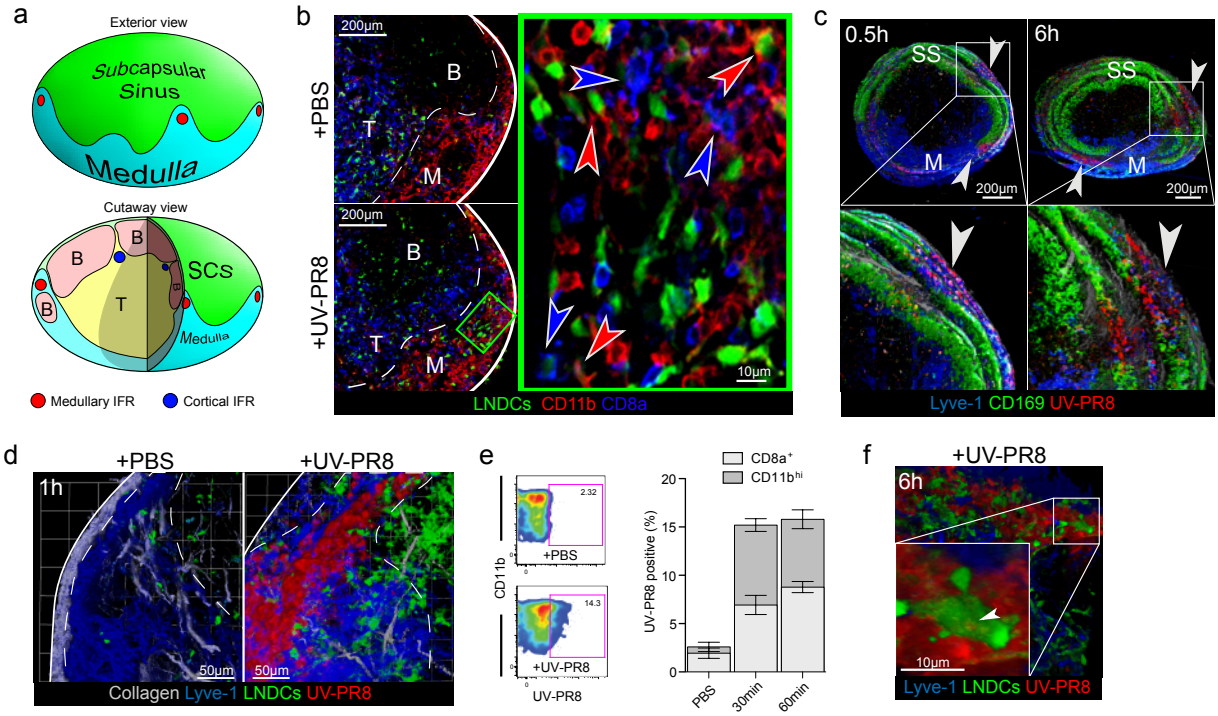

Figure 21. LNDCs infiltrate mIFRs and acquire viral antigen
(a) Schematic diagram of the architecture of a PLN. Medullary and cortical IFRs (mIFR and cIFR) are highlighted in red and blue respectively **(b)** Confocal imaging of mIFRs in CD11c_eYFP PLNs 40min following vaccination with PBS or UV-PR8. Blue arrows: CD8apos DC; Red arrows: CD11bhi DC. Scale bars – 125μm. Representative of 3 independent trials; 3 mice/trial **(c)** Reconstructions of in vivo labeled C57BL/6 PLNs vaccinated with A633-UV-PR8 and collected at 0.5, or 6h post-injection. White arrows: IFRs. Scale bars – 200μm. Images representative of 3 independent experiments; 2 mice per time point per experiment. **(d)** MPM of in vivo labeled CD11c-eYFP PLNs 60 min following PBS or A633-UV-PR8 vaccination. Dashed line: IFRs. Scale bars – 40μm. Representative of 4 independent experiments, 2 mice per experiment **(e)** **L**NDC capture of A488-UV-PR8 by flow cytometry 60min post-injection. (left) Cells displayed are pre-gated to be CD11chi. (n=4 PLNs) (**f)** **M**PM of in vivo labeled CD11c-eYFP PLNs, 6hr post A633-UV-PR8 vaccination. Scale bar – 10μm. Representative of 4 independent experiments; 2 mice per experiment.v

had accumulated in mIFRs within 60min of vaccination suggesting a multi-subset responsiveness to inactivated influenza (**Fig 21b**).

Afferent lymph flowing through the medullary sinus is constitutively filtered by sinus lining macrophages(Gray and Cyster, 2012), and this process predicts a natural gradient of viral antigen following vaccination. Thus, it is proposed that the highest antigen concentrations would reside at the tips of these mIFRs. To test this possibility, mice were injected S.C. with UV-PR8 labeled with Alexa 633. Fluorescent PLN reconstructions at various time points identify accumulation of viral antigen within mIFRs over 6h following vaccination (**Fig 21c**). By contrast,

lower levels of virus were retained in the subcapsular sinus and the deeper medullary compartments connecting with the efferent lymphatics. It was hypothesized that these antigen-rich regions might serve as a destination for migrating LNDCs. High-resolution imaging of IFRs bearing dense deposits of viral antigen showed large numbers of infiltrating LNDCs within 60 min of viral arrival at the node. Analysis of LNDCs by flow cytometry confirmed viral capture by both $CD11b^{hi}$ and $CD8a^{pos}$ LNDCs within 30min post-injection (**Fig 21e**), which was verified by MPM identifying viral patches on the surface of LNDCs at later time points (**Fig 21f, inset**).

Chapter 3.5 – LNDCs present viral antigen to CD4+ T cells near IFRs

Previous work by Itano et. al. interrogated the role of migratory versus LN resident DCs in CD4+ T cell stimulation. In that study, soluble peptide designed for presentation on MHC II was injected subcutaneously, and downstream T cell responses were tracked in the draining LN. The authors observed two waves of peptide presentation – one at 6 hrs which resulted in only transitory activation, and one at 18 which stimulated a more robust, long term T cell response. The authors concluded that while resident DCs can activate T cells, the resident cells induce only a limited response with mDCs from the injection site required for robust immunity(Itano et al., 2003). To determine if LNDC participate in activation of viral specific CD4+ T cells within this study, CD11c-eYFP mice were adoptively transferred with labeled, ova-specific CD4+ OT-II T cells 24h prior to vaccination with a UV-inactive recombinant strain of PR8 (UV-PR8-OTII), which was engineered to express the OT-II epitope(Thomas et al., 2006).

As predicted, vaccination with UV-PR8-OTII stimulated activation of cognate T cells within 6h, as evidenced by CD69 up-regulation (**Fig 22a**). While individual DC-T cell contacts could be observed as early as 6h, extensive interaction between LNDCs and CD4+ OT-II T cells

Figure 22. Cognate CD4+ T cells relocate to mIFRs following vaccination

(a) C57BL/6 mice received naïve OT-II T cells and were vaccinated with UV-PR8-OT2. OT-II T cell activation in PLNs was analyzed by flow cytometry. (n=4 mice) **(b)** CD11c-eYFP mice received labeled naïve OT-II T cells, and were vaccinated with UV-PR8-OT2. MPM of PLN 12h following vaccination. White arrows: LNDC/OT-II contacts. Scale bars – 50, 10μm. Representative of 3 PLNs; 2 independent trials **(c)** OT-II neighbor analysis of PLNs as shown in (b). Each symbol type represents an individual PLN, with 4 XY planes shown. **(d)** Heat map of OT-II neighbor counts as shown in (c). OT-II cells identified from images (left), and displayed with color indicative of the number of corresponding OT-II neighbors (right). Scale bars – 200μm **(e)** CD11c-eYFP recipients received labeled naive OT-II T cells and were vaccinated with UV-PR8-OT2. Fluorescent reconstruction of PLN, 24h following vaccination. T: T cell cortex, Per: PLN "periphery" . Scale bar – 100μm. Representative of 3 independent trials; 2mice/trial (**f)** C57BL/6 mice received OT-II T cells and were vaccinated with UV-PR8-OT2. PLNs were collected at 24hr following vaccination, optically cleared and imaged. Data represented with medulla isosurfacing to aid visual interpretation. White arrows: mIFR/T cell cluster colocalization. Scale bar – 100μm. Representative 2 trials; 2mice/trial.

Fig 22, continued

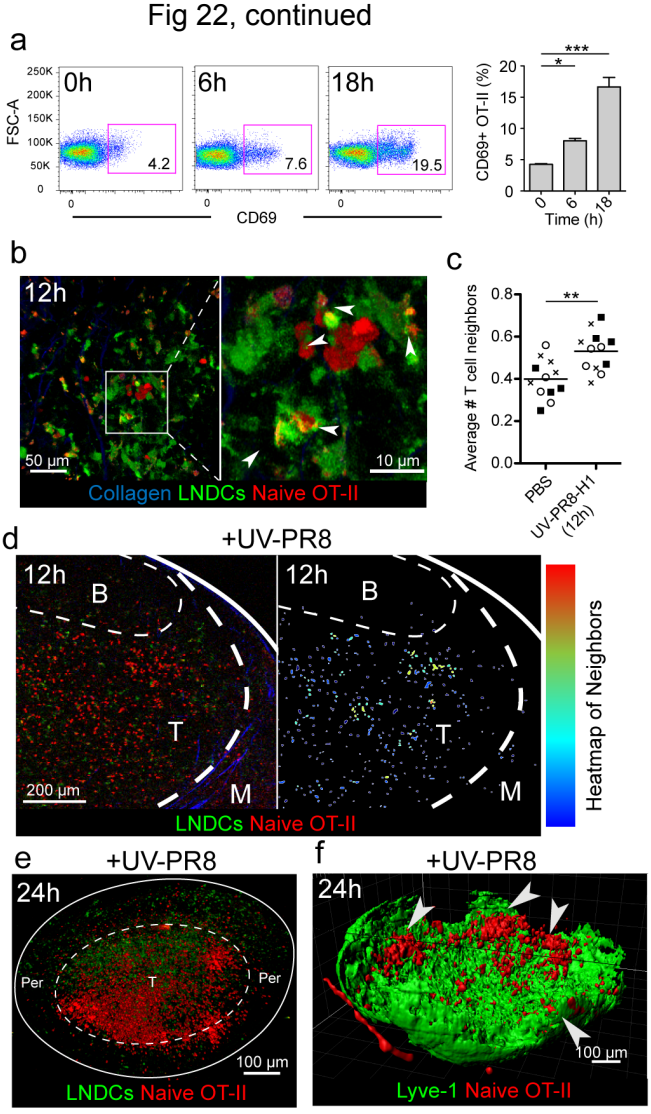

was observed near IFRs by 12h following vaccination (**Fig 22b**). Additionally, small clusters of viral-specific T cells could be identified surrounding LNDCs in these regions. To quantitate clustering, labeled, naive OT-II T cells were transferred into CD11c-eYFP recipients, which were subsequently vaccinated with UV-PR8-OTII 12h prior to LN harvesting. The LNs were serially imaged for reconstruction, and single plane images were captured from each reconstruction, representing 400μm of vaccinated vs. control LNs. Using histocytometric analysis(Gerner et al., 2012), OT-II T cells were identified within each plane, and each T cell was assessed for the number of T cell “neighbors” present in the image within one T cell diameter. The resulting measure of T cell clustering revealed significant increases in the average number of T cell neighbors and increases in the absolute number of T cells with multiple neighbors within vaccinated vs. non-vaccinated LNs (**Fig 22c**). Significantly, heat mapping the number of T cell neighbors onto the original images identified the border between the paracortex and IFRs as the most densely populated by clustered T cells (**Fig 22d**). Analysis of T cell migration at 24h post-immunization identified

discreet clusters at the extremes of the paracortex, with specific co-localization of T cell clusters at the medullary IFR-cortical junctions (**Fig 22e,f**).

Chapter 3.6 – Clustering of viral-specific CD4 T cells is chemokine dependent

Previously mentioned studies describing central memory CD8 T cell responses within cIFRs have suggested the chemokine CXCR3 as a critical mediator of cellular retention in these regions. The ligands for CXCR3, CXCL9 and CXCL10, are produced by both hematopoietic and stromal cells in response to viral challenge, and are critical to CD8 T cell recruitment to these sites. (Kastenmuller et al., 2013; Sung et al., 2012). Additionally, Groom et. al. has recently described the upregulation of CXCR3 as an early first step in the generation of robust Th1 CD4 T cell responses(Groom et al., 2012). Thus, we hypothesized that the clustering of CD4+ OT-II T cells with LNDC and virus in the IFR following immunization with UV-PR8 OTII could be CXCR3-dependent. To examine whether CD4+ OT-II T cells become activated and differentiate to CXCR3+ T cells, LNs were harvested immunized mice and CD4+ T cells analyzed by flow cytometry for expression of cell surface markers of activation. Notably, an increase in CD69 expression on CD4+ OT-II T cells was observed, followed by a corresponding increase in CD44 (**Fig 23a**, and data not shown). By gating on newly activated CD69+ cells, increases in CXCR3 expression could be identified as early as 12h post-vaccination, and continued to increase over several days (**Fig 23a,b**).

As recent reporting has shown that activated DCs arriving from the periphery express CXCL10, and that direct injection of LPS/Poly I:C can induce CXCL10 expression within 12h in the draining LN(Groom et al., 2012), it was predicted that LNDCs might express this chemokine following immunization with UV-PR8 OTII. Thus, the release of CXCL10 by activated LNDCs

Figure 23. CXCR3-dependent clustering of viral specific CD4+ T cells in mIFR

M: medulla, B: Follicles **(a)** Flow cytometry of OT-II T cell activation following UV-PR8-OT2 vaccination at indicated time points. (n=4) **(b)** Expression of CD69 (black) and CXCR3 (red) by OT-II T cells at indicated time points as in (a) CD69+ OT-II cells gated for CXCR3 expression analysis. Symbols represent individual mice. ANOVA (CD69) $p<0.0005$, ANOVA (CXCR3) $p<0.005$ (n=4) **(c)** CXCL10 expression in vaccinated REX3 mice or unvaccinated REX3 controls by flow cytometry. (left) displayed cells gated on CD11chi cDCs, followed by CD11bhi or CD8apos as indicated. (right) Percent CXCL10 positive DCs by subset (red: CD8apos; black: CD11bhi) following vaccination. (n=4) **(d)** MP imaging of REX3 PLN 24h following UV-PR8 vaccination. Dotted line: medulla. Representative of 4 PLNs from 2 independent trials. Scale bars – 100μm. **(e)** Confocal imaging of REX3 PLN 24h following UV-PR8 vaccination. Arrows: CXCL10 positive DCs. Representative of 4 PLNs; 2 independent trials. Scale bar – 32μm **(f)** C57BL/6 recipients received differentially labeled Wt, or CXCR3 deficient naïve OT-II T cells. Recipients were vaccinated with UV-PR8-OT2, and PLNs were collected at 24h. Quantitation of clustering efficiency of wt, or CXCR3 deficient OT-II T cells shown. (n=5). **(g,h)** Adoptive transfers were carried out as in (f). Recipients were vaccinated, and PLN suspensions were collected 60h post-vaccination for flow analysis. Individual T cell populations compared to the same population in unvaccinated contralateral controls. CD40L **(g)** and CD69 **(h)** acquisition expressed as fold change in vaccinated, vs unvaccinated population controls. (n=5)

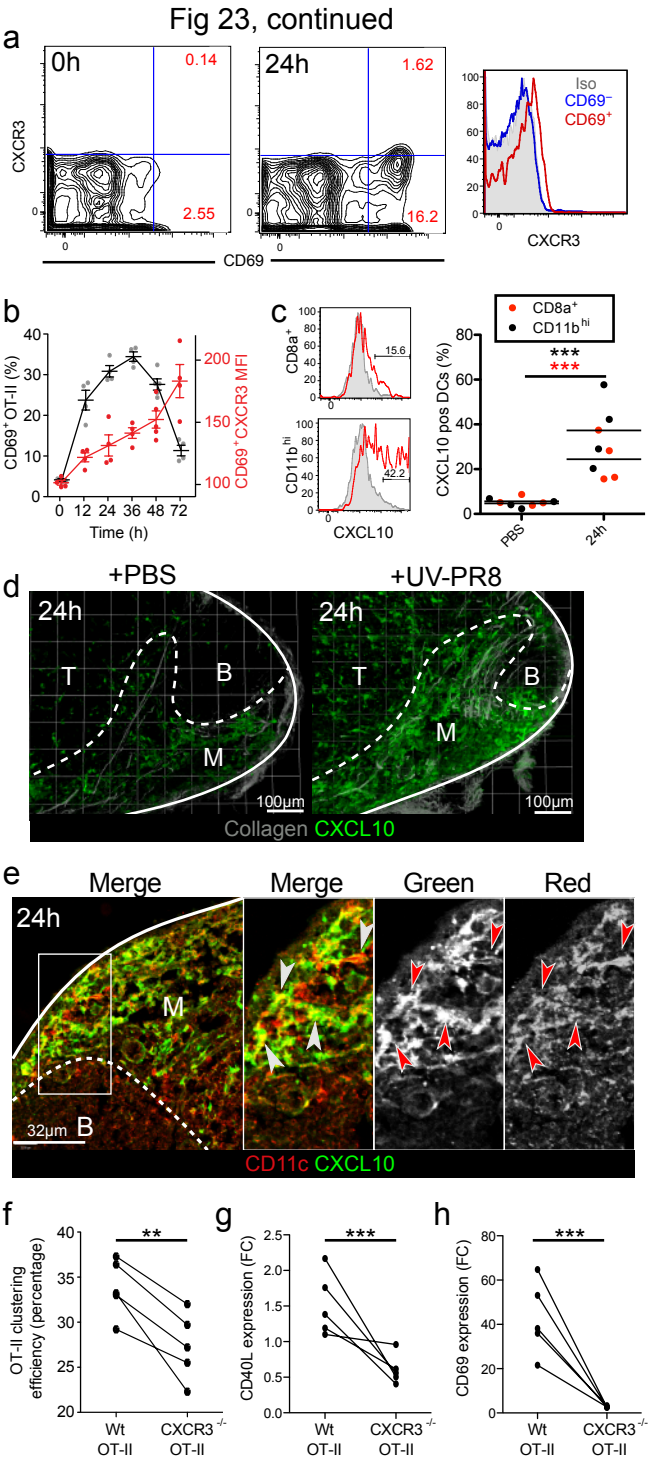

within the IFR could explain the extensive clustering of CD4+ T cells observed within the antigen rich IFRs. To test this possibility, CXCL9/10 reporter mice (REX3) (Groom et al., 2012) were vaccinated with UV-PR8, and LNs were harvested after 24h for analysis by flow cytometry and immuo-histochemistry (IHC). Flow analysis identified the expression of CXCL10 by both $CD11b^{hi}$ and $CD8a^{pos}$, LNDCs following vaccination (**Fig 23c**), although the $CD11b^{hi}$ population appeared more robustly responsive. Fluorescent reconstructions of vaccinated REX3 PLNs identified high CXCL10 expression on dendritic-looking cells within mIFRs following vaccination suggesting LNDC expression (**Fig 23d**). Confocal analysis positively identified these cells as DCs through CD11c expression, and confirmed clustering of CXCL10-positive DCs within IFRs by 24h following vaccination (**Fig 23e**). The timing of this event corresponded to both LNDC migration and formation of T cell clusters.

To confirm the importance of CXCL10 in attracting viral specific T cells to the IFRs, mice were adoptively transferred with differentially labeled CXCR3+/+ and CXCR3-/- OT-II T cells and subsequently immunized with UV-PR8 OTII virus. Characterization of the vaccinated recipients revealed a significant defect in the clustering of CXCR3-/- OT-II cells at 24 h post-vaccination, confirming the importance of CXCR3 in T cell migration (**Fig 23f**). Additionally, flow cytometric analysis of CXCR3-/- OT-II T cells displayed a profound deficiency in both CD69 activation, and CD40L expression (**Fig 23g,h**). These results replicate reports by Groom et. al. which described early activation defects, followed by a deficient Th1 response in the absence of CXCR3. Together, these data suggest a model whereby LNDC activation of CD4+ T cells at early time points leads to expression of CXCR3, and contributes to the efficient localization of cognate cells into medullary IFRs resulting in efficient early activation.

Chapter 3.7 – LNDC dependent T cell activation

While the activation of T cells within 6 hours of vaccination suggested a role for LNDCs in early activation of CD4+ T cell responses to UV-PR8, it remained unclear if skin resident mDCs were required to establish an enduring humoral response. Employing a system developed by Itano et. al., the contribution of the migrating DC population could be effectively removed through resection of the injection site within 30min post-immunization(Hickman et al., 2008; Itano et al., 2003; Lindquist et al., 2004; Kissenpfennig et al., 2005; Kastenmuller et al., 2013; Sung et al., 2012). By administering UV-PR8 intra-dermally (I.D.) in the ear and removing the ear shortly following administration, the relative contribution of migrating DC and LNDC populations could be evaluated in the auricular LN (ALN).

Using this approach, C57Bl/6 mice were vaccinated with PBS or UV-PR8 I.D., with half of the vaccinated group undergoing ear removal (here referred as the van Gogh, or vG group) within 30min following vaccine administration. Using REX3 reporter mice, expression of CXCL10 by both CD11b^{hi} and CD8a^{pos} in Wt, or vG vaccinated animals was assessed 24h following injection/resection. Interestingly, while CXCL10 expression was still robust in both LNDC populations suggesting normal responsiveness to vaccination despite a lack of mDCs in the vG group (**Fig 24a**), there was a small decrease in expression by the CD8a^{pos} subset, perhaps relating to its known reliance on incoming mDCs from the periphery(Gonzalez et al., 2010; Allan et al., 2006).

By transferring CFSE labeled naïve OT-II T cells into B6 recipients, and employing the vG vaccination system, potential deficiencies in T cell proliferation and activation could be assessed in the absence of mDCs from the injection site. Surprisingly, vG group OT-II T cells proliferated similarly to the Wt group (**Fig 24b**), and could be tracked through 7 divisions in 60h. Tracking T cell activation by division status, cells could be observed acquiring both CXCR3 and CD40L as they proliferated in both the Wt and vG groups (**Fig 24c,d**). Interestingly, while CD40L expression appeared identical in both groups, there was a slight delay in CXCR3 acquisition between the

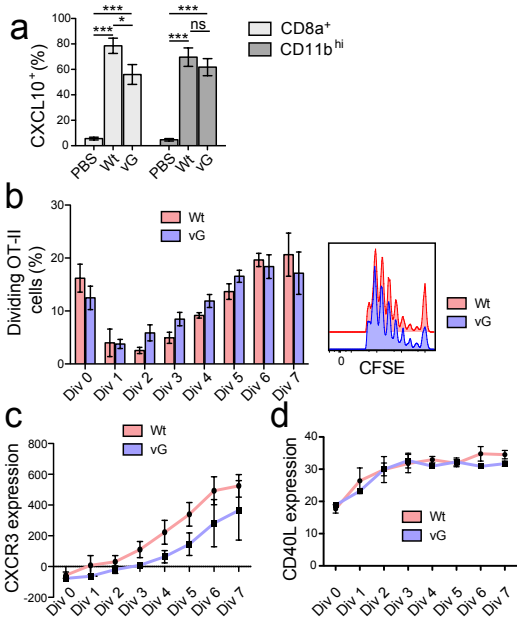

Figure 24. mDC independent LNDC/CD4+ T cell activation
Ear resection in the van Gogh (vG) model 30min following vaccination. **(a)** Percentage of CD8a+ (light gray), or CD11bhi (dark gray) cDCs in the ALN 24h following ear vaccination. PBS, Wt, and vG groups displayed. ANOVA (light gray) p<0.0001; ANOVA (dark gray) p<0.0001. (n=4) **(b)** CFSE labeled OT-II T cells were transferred into C57Bl/6 recipients. Recipients were vaccinated in the ear, and separated into Wt, and vG groups. ALNs were isolated at 60h post injection, and analyzed by flow cytometry. (left) Percent OT-II T cells by division number as assessed by CFSE dilution. ANOVA p>0.1. (right) Representative plot of CFSE dilution in Wt, and vG groups (n=4 mice/group). **(c,d)** adoptive transfers were established as in (c). OT-II T cell expression (MFI) of CXCR3 **(c)** and CD40L **(d)** was assessed by T cell generation to track acquisition over time. Two-way ANOVA (c) p<0.0001 overall, p<0.05 between groups. Two-way ANOVA (d) p<0.0001 overall, p>0.1 between groups. (n=4mice/group)

Wt, and vG group. These findings may also suggest collaboration with mDCs in reinforcing Th1 immunity development as they arrive from the periphery.

Chapter 3.8 – LNDC dependent B cell memory

As LNDC, and T cell activation appeared to be intact despite the absence of mDCs in the vG model, it was hypothesized that LNDCs may be sufficient to drive downstream protective humoral immunity despite the absence of mDCs. To test this hypothesis, the vG vaccination model was employed in C57Bl/6 mice alongside PBS vaccinated controls. ALNs were collected at d7 following vaccination, and germinal center staining appeared normal in both Wt, and vG groups confirming effective T cell help despite the absence of mDCs (**Fig 25a**). Ab titers collected at d10 following vaccination showed normal increases in IgM, IgG1, and IgG2b in vG, versus Wt vaccination groups in comparison to unvaccinated controls suggesting normal class switching and germinal center development(**Fig 25b**).

To test the functionality of this antibody response, vaccinated, or unvaccinated controls were challenged I.T. with a lethal dose of live PR8 on d21 following vaccination. Morbidity was monitored for 9 days post infection, at which point the unvaccinated control group was sacrificed due to excessive weight loss. Neither Wt, and vG groups experienced significant weight loss over the course of infection, indicating protective immunity had been generated with, or without mDC arrival from the injection site (**Fig 25c,d**). Finally, antibody titers were assessed at day 9, and compared to both unvaccinated, and uninfected controls. As expected, Ab titers showed extensive class switching in both Wt, and vG groups, and protective IgG2b responses were identical between groups. It is worth noting that while not required for protection, IgG1 Ab titers were slightly, but insignificantly decreased in the vG group providing additional evidence for LNDC/mDC collaboration in a vaccination setting. Altogether, these data demonstrate that LNDCs are capable of stimulating CD4+ Th1-dependent protective humoral responses to influenza vaccination.

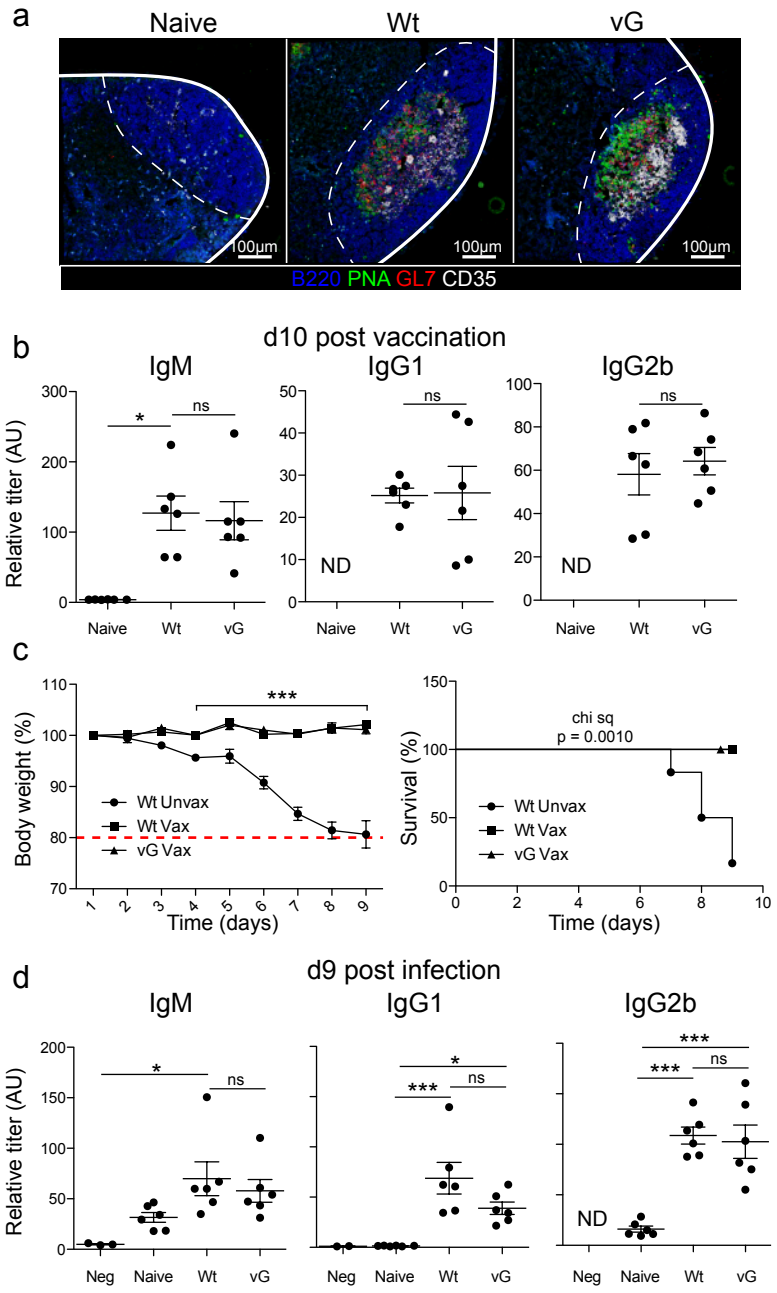

Figure 25. mDC independent protection from influenza
(a) Confocal imaging of ALN follicles at day 10 following UV-PR8 vaccination in Wt, and van Gogh (vG) mice. Dotted line: B cell follicle. Scale bars – 100μm. Representative of 2 independent trials; 5mice/group **(b)** ELISA analysis of PR8 specific serum antibodies at day 10 following UV-PR8 vaccination. Relative titers of PR8 specific IgM, IgG1, and IgG2b shown. Symbols represent individual animals **(c)** Unvaccinated, or vaccinated Wt, or vG groups were challenged with LD80 PR8 21 days following vaccination. Morbidity (left) and mortality (right) displayed as percent body weight, or percent survival respectively. 6 mice/group **(d)** ELISA analysis of PR8 specific serum antibodies at day 9 following PR8 challenge as in (c) compared to naive C57Bl/6 littermates. Relative titers of PR8 specific IgM, IgG1, and IgG2b shown. Symbols represent individual animals.

Chapter 3.9 – Discussion

Earlier studies identifying capture of lymph-borne inactive influenza virus by LNDC raised the question of the relative importance of this population in overall humoral immunity. To gain a broader understanding of LNDC in response to vaccination with inactive influenza, a whole-node imaging approach was developed and mice bearing a fluorescent reporter for DCs (CD11c+) were vaccinated with UV-PR8. Following sub-cutaneous vaccination, viral antigen was observed within the draining LN within minutes as expected. Surprisingly, however, the virus accumulated over the first six hours within specialized sites identified as medullary IFRs.

Using fluorescent reconstructions of full PLNs isolated at early time points following vaccination, we observed a major repositioning of LNDC from the T cell cortex to the medullary IFR where they acquired viral antigen and became activated. This was unexpected since LNDC are reported to be relatively sessile at steady state. The capture of virus by the resident DC was biologically relevant since they became positive for the chemokine CXCL10 and formed clusters with viral-specific CD4+T cells that became activated based on expression of CD69 , CD44 and CXCR3. Thus, three lines of evidence are presented that support a role for LNDCs in promoting a humoral response to inactive PR8 independent of migrating DCs: (i) activation of viral specific CD4+ T cells prior to expected arrival of skin migratory DC; (ii) activation of viral-specific CD4+ T cells within PLN in the absence of mDCs; and (iii) a normal humoral memory response despite surgical removal of the injection site within 30min of vaccination. Notably, while these findings clearly demonstrate sufficiency of the resident DC population in establishing humoral immunity, they do not address the requirement of migrating DCs under conditions where lymph borne antigen is not readily available.

While several groups have previously described resident DC populations in skin draining LNs(Grigorova et al., 2010; Lindquist et al., 2004), few have directly assessed their potential in presenting antigen acquired directly from the lymph. In one study, Itano et. al. describe a two step process of antigen presentation where resident DC in the LN were capable of acquisition

and presentation of soluble peptides, but skin resident mDCs were required for effective immunity. In another study, Allenspach et. al. found that in the case of soluble peptide administered with CFA, resident dendritic cells were similarly deficient in T cell presentation(León et al., 2012; Allenspach et al., 2008; Hickman et al., 2008; Sung et al., 2012). Our findings are not inconsistent with these results, as the robust activation/migration of resident dendritic cells cannot be identified following traditional adjuvant administration (alum or MF59). The profound differences in these responses also raises interesting questions about a potential gap between traditional vaccination approaches, and natural response to viral antigen. As medullary macrophages rapidly degrade protein antigen as a part of normal lymphatic filtration, it is important to understand how to maximize antigen exposure to efficient antigen presenters – especially when antigen concentration is highest immediately following vaccination. Data from this study suggest that LNDCs are capable of effectively utilizing antigen when appropriately stimulated, and could represent an efficient target for vaccination approaches.

An unexpected observation was the rapid kinetics of LNDC repositioning from the paracortical region to the medullary IFR in response to localization of viral antigen. While large deposits of LNDCs were observed in viral-loaded IFRs within hours of vaccination, individual LNDC morphological changes could be observed within 12 minutes of vaccination. The highly directional migration pattern of LNDC to the sites of viral accumulation suggests a response to chemotactic mediators released from a pre-stored source following innate sensing of viral antigen, although this source remains yet unclear.

Recent, studies have identified CXCR3 and its ligands CXCL9 and CXCL10 as required for migration of CD8 memory T cells into IFRs where they make contact with both antigen and APCs. While the distinction between medullary and cortical IFRs was not made in these studies, it is clear that this chemo-attractant is important in various conditions of immune response. In our study, formation of clusters of viral specific CD4+ T cells with LNDC was significantly reduced in CXCR3-/- OT-II T cells. Since CXCL10 expression is not restricted to LNDCs, this pathway might provide an efficient mechanism for collaboration between LNDCs and incoming

mDCs, whereby early activation of naïve CD4 T cells, and concomitant expression of CXCR3, allows activated T cells to more easily find mDCs from the injection site which also express CXCL10. Additionally, it is possible that mDCs might be able to locate hot spots of immune activation within the LN through their own expression of CXCR3.

In summary, using novel whole node imaging approaches, we observed a multistep system of immune activation whereby viral antigen, LNDCs, and cognate naïve CD4+ T cells rapidly assemble in highly organized environments within the draining LNs known to be relevant to vaccine design (Hickman et al., 2008; Liu et al., 2014). In addition to identifying an unexpected repositioning of LNDCs to specialized sites within the draining LN, these findings clarify the importance of CXCR3 in establishing immunostimulatory microenvironments in three dimensions, and establish LNDCs as biologically relevant cell populations – sufficient to drive humoral memory response to an influenza vaccine in the absence of migratory DCs.

Chapter 3.10 – Materials and Methods

Animals. Mice used in this study were bred and housed in standard conditions and used between 6-12 weeks of age. All experimental protocols approved through Harvard University's Institutional Animal Care and Use Committee.

In vivo labeling. *In vivo* labeling of the PLN subcapsular sinus and medulla was achieved through injection of alexa conjugated (A488, A568, A633) antibody targeting stromal (a-LYVE-1) or macrophage populations (a-CD169, a-SIGNR1, a-F4/80) S.C. in the footpad 4 hours prior to PLN imaging or tissue harvest.

PLN live imaging. PLN live imaging was carried out through surgical exposure of the PLN in anesthetized mice, and MPM. Temperature was monitored using a digital thermometer

embedded in the imaging chamber created around the PLN, and controlled using a closed-circuit water circulation system(Ertürk et al., 2012; Lindquist et al., 2004; Gonzalez et al., 2010).

Three-dimensional reconstruction. Collected organs were fixed in 4% PFA, embedded in OCT and serially cryosectioned (50um). PLN sections were serially imaged by MPM, and assembled using Imaris software to obtain 3D reconstructions. Final analysis was carried out using Volocity image analysis software.

Whole organ imaging. Lymph nodes were dissected and fixed overnight in 4% paraformaldehyde. The sample was then incubated in increasing concentrations of tetrahydrofurane followed by dichloromethane. Finally, the PLN was immersed in BABB (benzyl alcohol: benzyl benzoate-mix 1:2) for final clearing and imaging. (Liu et al., 2014; Lindquist et al., 2004; Ertürk et al., 2012).

Viral propogation/labeling. Influenza virus was grown in live chicken eggs, purified over sucrose gradients(Gray and Cyster, 2012; Gonzalez et al., 2010; Szretter et al., 2006), and labeled using standard alexa-labeling protocol (Invtrogen). 10-20µl sub-cutaneous injections were given in the footpad at $1x10^6$ pfu.

T cell isolation. LNs of OT-II mice were processed using Liberase DH (Sigma) digestion, and T cells isolated through MACS negative selection (CD11c, CD11b, NK1.1, B220, GR-1, CD69, CD8). T cells were labeled in 10um CMTMR for imaging, or 5uM CFSE for imaging and flow cytometric identification. 1 or 5x10^6 cells were adoptively transferred into naïve recipients for flow cytometric, or imaging experiments respectively.

3 dimensional image analysis. Images processed and analyzed using Volocity imaging software. Histocytometric analysis of reconstructions was performed with CellProfiler(Itano et

al., 2003; Grigorova et al., 2010; Carpenter et al., 2006), and CellProfiler Analyst(Thomas et al., 2006; León et al., 2012; Jones et al., 2008; Hickman et al., 2008). Analysis of reconstructions were carried out with individual XY imaging planes, which were representative of at least 400um of reconstructed LNs.

T cell clustering. CXCR3 -/- and Wt OT-II cells were isolated as above, differentially labeled, and adoptively transferred into C57BL6 recipients. PLNs were collected, processed and serially imaged 24h after vaccination with UV-PR8-OT2. T cell clusters were identified using a blinded approach, and the percentage of each population within these clusters was measured.

Ear resections. Ear removal carried out 30min following injection of 10ul PBS or UV-PR8 S.C. between the ear dermal layers. ELISA analysis of serum was carried out through immobilization of UV-PR8 on the plate, addition of serum, and probing for specific binding of IgM, IgG1, or IgG2b

Statistics. All statistics/graphical representations of collected data assembled through Prism. Mean, SEM displayed where applicable. Results from Student's T tests , or Tukey post-testing, indicated by asterisks in figure (*p<0.05, **p<0.005, ***p<0.001) . One-way, or Two-way ANOVA testing indicated in legend.

Chapter 3.11 – Author contributions

M.W., B.H., and C.H. performed all experiments and analysis described in text. J.G. and A.L. developed critical reagents for the completion of the study. M.W., S.T., and M.C. designed this study and developed the manuscript for publication.

Chapter 4

General discussion

Chapter 4.1 – Empiricism in vaccination

Chinese history suggests that by 1000 CE, vaccination was already being investigated as a viable tool for the control and prevention of infectious disease. As early western attempts to vaccinate against smallpox (largely credited to William Jenner in 1796) pre-dated the acceptance of germ theory by at least fifty years, vaccinology at its core is deeply rooted in empirical study. Despite a lack of mechanistic understanding surrounding vaccine development, human vaccination programs have been hugely impactful in reducing morbidity and mortality worldwide. The crown jewel of these programs, the successful worldwide eradication of variola virus, eliminated the leading cause of death among Europeans in the 18th century. Similar efforts are currently underway to eradicate polio from the human population, and incidence of serious diseases such as measles, mumps, yellow fever, and influenza has decreased markedly in areas with robust vaccination programs. It is the success of these programs that led then-US Secretary of Health and Human Services, Margaret Heckler, to announce in April of 1983 that the HIV virus had been discovered, and that a vaccine would be ready for testing within approximately two years.

In fairness, the first NIH approved vaccine trial for HIV was initiated in 1987, only four years after the announcement. That vaccine, however, demonstrated little to no efficacy in the prevention of HIV/AIDS(Controversial AIDS vaccine fails to delay disease., 1996). Similarly ambitious targets including malaria and dengue fever – both extremely deleterious to economically disadvantaged societies – have shown little progress in almost 40 years of research. This unexpected failure to achieve meaningful protection against some of humanities most notorious pathogens is seemingly at odds with the explosion of new technology currently being employed by the vaccination field. Recombinant DNA technology, reverse genetics, employment of nanomaterials, and even gene therapy have made gains in the prevention of human disease, but failed to adequately address these major health concerns. Somewhat surprisingly, the lack of success in these areas has had little impact on the empirical nature of

vaccine development, resulting in few resources spent developing basic understandings of the contextual requirements for vaccine efficacy.

In his landmark address to the Cold Spring Harbor symposium in 1989, Charles Janeway argued for a view of immunological activation where simple recognition of foreign antigen is not sufficient to drive robust immune response. In it, he asserted that the immune system must have a way to distinguish between pathogenic and non-pathogenic foreign antigen, and coined the term ‘pathogen associated molecular pattern’. Since that address, the field of innate immunity has undergone a renaissance in the discovery of a plethora of signals that the immune system uses to determine when, and how to respond to an incoming pathogen. From Toll-like receptors, to RIG-I like receptors, to inflammasomal signaling in response to danger associated molecular patterns, innate immunity has developed as a critical context for adaptive immune activation. However, even this context remains incomplete.

The lymph node even at rest is a chaotic, yet highly organized environment where the adaptive immune system rapidly scans the ‘antigen library’ from draining tissue for potential matches, before moving on to the next lymph node where it will repeat the process. These scanning functions are made possible by the underlying lymph node stroma, and are co-ordinated by the chemokine gradients that they produce. Normal filtration functions within the lymph node quietly sequester protein and cell-debris, and dendritic cells from the periphery periodically find their way into the environment to help promote peripheral tolerance. In the case of vaccination, however, this picture can change dramatically. The major objective of this study has been to understand the context of the hematopoietic system within the lymph node environment, and understand how changes within that context directly impact the quality and quantity of immune response to vaccination.

Chapter 4.2 – Stromal influence on vaccine success

The lymph node stroma serves as the basic cellular infrastructure of the lymph node environment. This study has described the dependency of the hematopoietic compartment on the FRC network, and previous studies have assessed the importance of other stromal cell types on immune function(Allen and Cyster, 2008; Malhotra et al., 2012a; Cohen et al., 2010). Further, disruption of these populations, either by infection or genetic modeling, results in profound deficiencies in immune function at steady state, as well as decreased vaccination efficacy(Wang et al., 2011; Estes, 2013). Despite this strong interconnection between the stromal and hematopoietic compartments, many basic questions about those interactions occur still exist.

An emerging theme in the stromal field is the concept of stromal flexibility. While the stroma in general has long been viewed as steady directors of lymph node organization and homeostasis, new data suggests that the stroma may actually be a dynamic environment(Wu et al., 2009; Jarjour et al., 2014). The discovery of functionally distinct LEC populations in the subcapsular sinus, defined by their attachment to the ceiling or the floor, suggests that these cells must be responding to signaling differences which exist within the span of only 10μm of sinus lumen(Ulvmar et al., 2014). The requirement for fluid flow for expression of CCL19 by FRCs in ev-vivo cultures raises the question of whether mechanoreceptor signaling may be a common theme in stromal population function and responsiveness(Tomei et al., 2009). Finally, this study describes functionally distinct subsets of FRCs, which seem to differ primarily by their geographic location within the lymph node. This brings up the question of how FRCs ‘know’ to express BAFF only in the context of the B cell follicle.

As previously described, subcapsular sinus macrophages perform extremely specialized functions in their ability to respond to viral infection, and serves as critical mediators of antigen hand off to underlying B cells(Carrasco and Batista, 2007; Junt et al., 2007; Martinez-Pomares and Gordon, 2012). Perhaps unsurprisingly, they can only be found in the subcapsular sinus

where this antigen hand off to B cells would be functionally useful. More unexpectedly, however, is the finding that these cells *require* B cells, and specifically LtB signaling, in order to acquire these specialized properties(Moseman et al., 2012). Interestingly, unpublished data surrounding FRC differentiation in vitro suggests that these stromal cells may also be responsive to LtB signaling, which offers a potential explanation for the restriction of BAFF expression by FRCs only in the B cell follicles. This sort of crosstalk between stromal and hematopoietic populations raises clear questions about how other stromal populations might be modifying their function depending on local hematopoietic signaling. Could responsiveness of LECs to LtB or other follicular signaling explain the difference between ceiling LECs and floor LECs? Are MRCs similarly responsive to their surrounding environment? Perhaps more importantly, could confusion surrounding cross expression surrounding 'MRC markers' on other stromal populations be clarified through the realization that expression of these markers are externally dependent?

While it may be interesting to speculate on how these populations interact at steady state, an even more intriguing question might be how stromal populations respond to the inflammation generated following vaccination. FRCs have already been described as responsive to signaling molecules required for effective immune response(Lukacs-Kornek et al., 2011), and the role of FDCs in the generation of germinal centers critical for humoral immunity has been well described(Allen and Cyster, 2008). Despite this, little data exist surrounding how stromal phenotypes are altered following various inflammatory stimuli (Malhotra et al., 2012b). With recent studies even suggesting that certain stromal populations might serve as antigen presenting cells(Cohen et al., 2010; 2014), the vaccination field can no longer afford to overlook the impact that the stroma has on the success or failure of specific vaccination approaches

Chapter 4.3 – Lymph flow and immune response

In addition to the cellular signals that the stroma provides, it is also responsible for the maintenance of the structural integrity of the lymph node through the production of the vast conduit network(Gretz et al., 1997; Mueller and Germain, 2010; Turley et al., 2010; Katakai et al., 2004). Often discussed in terms of antigen delivery, the collagen network also serves as the substrate for leukocyte migration within the node(Bajénoff et al., 2006; 2007), as well as a direct line of lymph flow through the paracortex(Gretz et al., 1997; 2000; Roozendaal et al., 2009). This lymph flow function of the conduit network, although not yet well understood, is particularly intriguing in the ability of the lymph node to respond to an upstream infected environment. Whether through the activation of mast cells at an infection site(Kunder et al., 2009), or the release of chemokine signals designed to draw in inflammatory monocytes(Palframan et al., 2001; Nakano et al., 2009), the conduit network might serve as a way to allow chemical signals to penetrate deep into the lymph node without sacrificing barrier integrity.

One of the most exciting phenotypes that have been identified in the current study is the activation, and rapid mobilization of the LNDC population following inactivated influenza vaccination. When injected into the footpad, inactivated influenza-A arrives in the PLN within 5 minutes under normal conditions. Once it has arrived, almost instantaneous changes in morphology can be seen in the LNDC population, and directional migration can be identified deep within the paracortex within 10 minutes of vaccine administration. Though neither the signal, nor the signaling cell have been identified to-date, the dramatic speed in which this response plays out suggests a number of features of the signaling cascade. First, the signal is likely to be pre-stored as the 5 minute window leaves little time for transcription or translation of a novel chemotactic agent. Second, the signaling cell is very likely responding directly to the virus prior to chemotactic release. As the TLR/RLR/DAMP signature of influenza is well established(McGill et al., 2009), one could reasonable hope to narrow down the molecular trigger, and use that information to identify potential cellular candidates capable of responding to

those signals in the lymph node. Finally, regardless of the kind of signal, it must be capable of penetrating deep into the paracortex where it can first stimulate LNDC populations.

The penetration of such rapid signaling from the medulla to the paracortex is difficult to explain without an efficient mechanism of signal transduction through the lymph node. While it is possible that simple diffusion through the parenchyma may play a role, it seems more likely that there is a path of lesser resistance than the packed lymph node environment. If the conduit network does indeed play an important role in carrying these signals through the node more efficiently, then the rate of fluid flow through the system might play an important role in the stimulation of immune response.

Although early studies looking at lymph flow and composition were able to establish basic parameters of how lymph flows through a node(Browse et al., 1984; Sainte-Marie et al., 1982), little work has been done on the effect of lymph flow on immune response. One of the earliest findings, that protein from the lymph is concentrated from afferent to efferent at the lymph node site(Knox and Pflug, 1983), has a potentially profound impact on the idea of antigen delivery within a vaccination model. These findings, in association with the idea that fluid flows 'downhill' into the lymph node vasculature(Gretz et al., 2000), suggests that small chemical signals may not only enter into the deep paracortex of the lymph node, but may even be able to stimulate the host organism systemically through the dissemination of soluble signals into the blood. This hypothesis may be difficult to reconcile at steady state, when the size cutoff of molecular entry into the vessels hovers around 2kD, but little is known about the effect of heavy inflammation on fluid dynamics in the lymph node. Could vasodilation in the lymph node lead to dissemination of activating signals into the blood? Could this help explain the mobilization of cells from the bone marrow in response to a segregated peripheral response?

Early collaborative studies based on these ideas have begun to identify an axis of fluid flow where flow direction from the vessels to the lymphatics (or vice versa) might hinge on relative fluid pressures from both inputs. Hopefully, as new imaging systems are able to capture these systems at higher detail, a greater understanding of how the flow environment might serves to

influence immune response will develop. Regardless, continued investigation into these sorts of basic physical systems, the conduit system in particular, should be considered a high priority in truly understanding the context of immune activation.

Chapter 4.4 – Dendritic cells in vaccine immunity

While the stromal and structural components of the lymph node have an important role in the induction of protective immunity, the hematopoietic system must still be considered the central player in immune response. The innate immune systems ability to differentially respond to external stimuli, and to create micro environments which are able to correctly activate and educate the adaptive system makes it clear that understanding exactly how, and under what circumstances these micro environments are created may be essential in guiding successful vaccination. This study lays out an example of this kind of microenvironment creation in the rapid mobilization of LNDCs, and the recruitment of $CD4^+$ T cells to antigen rich sites via the production of CXCL10. While this is an exciting first step in understanding the earliest responses to influenza vaccination, many questions still remain.

As previously discussed, early studies on LNDCs described a population that were relatively sessile, and had little ability to generate an effective downstream protective response(Itano et al., 2003; Lindquist et al., 2004). This view of these populations is in obvious conflict with the current study, however this conflict can be easily reconciled by assessing the methods used to initiate immunity. Although this study does not directly address the trigger signals for LNDC activation and migration, anecdotal evidence to date has suggested that this rapid response does not occur under all inflammatory situations. Even traditional adjuvants such as alum and MF59 do not seem to stimulate this population despite causing large scale inflammation and immune response. Although at face value this seems surprising, it is perhaps less so when considering the role of dendritic cells in the initiation of immunity.

Two defining roles of the dendritic cell population as a whole are their ability to present antigen, and their ability to educate adaptive immunity to shape an effective response. Both of these roles depend heavily on their ability to sense and respond to their surrounding environment, and relay that information appropriately. Careful studies across dendritic cell subsets have resulted in great variation of function, and the understanding that individual DCs populations have different capacities in response to the same stimuli(Desch et al., 2011; Jakubzick et al., 2008; Shklovskaya et al., 2008). Furthermore, variations in stimuli alter the way that individual DC populations will respond and present antigen(Stoitzner et al., 2005).

In this study, the responsiveness of LNDCs to influenza vaccination is assessed, and is shown to initiate Th1 immunity. While this finding is exciting, and suggests that these cells might be targeted for effective vaccination, it would be inappropriate to assume that this 'type' of activation is the only method of response that they are capable of, or even if it is an ideal outcome for long lasting immunity. While this system appears to stimulate a robust Th1 response, one could easily imagine a different scenario where these cells contribute to Th17, or even toleragenic responses depending on the associated PAMP or DAMP signatures. Likewise, migratory DC populations have similar plasticity, which has led to conflicting reports in the role of individual populations in stimulating adaptive immunity(Lutz and Schuler, 2002). Rather than attempting to pigeonhole these populations into immutable roles, it is perhaps more useful to think about the dendritic cell system as one where evolution has selected for multiple DC populations, all working in tandem, differentially responding and collaborating to shape a complete, well directed immune response. In this way, the question 'What do LNDCs do during vaccination?' is more appropriately replaced with 'How do LNDCs respond to selected stimuli, and how can those stimuli be used to shape immunity in the case of vaccination?'.

In summary, this study attempts to further understand the context in which immune response to vaccination occurs. Focusing on the collagen structure and conduit network, the foundation of how lymph flow, and thus signal transduction, might influence immune responses both locally and systemically might be laid. Looking to the stroma, understanding how FRCs

direct homeostasis of the adaptive immune system in secondary lymphoid organs, but also their indispensability for effective humoral immunity has been established. Finally, by addressing the role of LNDCs in response to influenza vaccination, a view of how the hematopoietic system generates stimulatory micro environments, even within the lymph node, for the generation of protective humoral has begun to emerge. Altogether, this work represents the early stages of the much broader question of how physical, stromal, and immune systems come together to generate immune response. Ultimately, the answer to those question might enable the manipulation of those systems, in the larger goal of generating and shaping immune responses against specific human pathogens.

Bibliography

Acton, S.E., J.L. Astarita, D. Malhotra, V. Lukacs-Kornek, B. Franz, P.R. Hess, Z. Jakus, M. Kuligowski, A.L. Fletcher, K.G. Elpek, A. Bellemare-Pelletier, L. Sceats, E.D. Reynoso, S.F. Gonzalez, D.B. Graham, J. Chang, A. Peters, M. Woodruff, Y.-A. Kim, W. Swat, T. Morita, V. Kuchroo, M.C. Carroll, M.L. Kahn, K.W. Wucherpfennig, and S.J. Turley. 2012. Podoplanin-Rich Stromal Networks Induce Dendritic Cell Motility via Activation of the C-type Lectin Receptor CLEC-2. *Immunity*. doi:10.1016/j.immuni.2012.05.022.

Alimzhanov, M.B., D.V. Kuprash, M.H. Kosco-Vilbois, A. Luz, R.L. Turetskaya, A. Tarakhovsky, K. Rajewsky, S.A. Nedospasov, and K. Pfeffer. 1997. Abnormal development of secondary lymphoid tissues in lymphotoxin β-deficient mice. *Proceedings of the …*.

Allan, R.S., J. Waithman, S. Bedoui, C.M. Jones, J.A. Villadangos, Y. Zhan, A.M. Lew, K. Shortman, W.R. Heath, and F.R. Carbone. 2006. Migratory dendritic cells transfer antigen to a lymph node-resident dendritic cell population for efficient CTL priming. *Immunity*. 25:153–162. doi:10.1016/j.immuni.2006.04.017.

Allen, C.D.C., and J.G. Cyster. 2008. Follicular dendritic cell networks of primary follicles and germinal centers: Phenotype and function. *Semin Immunol*. 20:14–25. doi:10.1016/j.smim.2007.12.001.

Allenspach, E.J., M.P. Lemos, P.M. Porrett, L.A. Turka, and T.M. Laufer. 2008. Migratory and lymphoid-resident dendritic cells cooperate to efficiently prime naive CD4 T cells. *Immunity*. 29:795–806. doi:10.1016/j.immuni.2008.08.013.

Alvarez, D., E.H. Vollmann, and U.H. von Andrian. 2008. Mechanisms and consequences of dendritic cell migration. *Immunity*. 29:325–342. doi:10.1016/j.immuni.2008.08.006.

Anderson, A.O., and N.D. Anderson. 1975. Studies on the structure and permeability of the microvasculature in normal rat lymph nodes. *Am J Pathol*. 80:387–418.

Anderson, A.O., and S. Shaw. 1993. T cell adhesion to endothelium: the FRC conduit system and other anatomic and molecular features which facilitate the adhesion cascade in lymph node. *Semin Immunol*. 5:271–282. doi:10.1006/smim.1993.1031.

Andrian, von, U.H., and T.R. Mempel. 2003. Homing and cellular traffic in lymph nodes. *Nat Rev Immunol*. 3:867–878. doi:10.1038/nri1222.

Ansel, K.M., V.N. Ngo, P.L. Hyman, S.A. Luther, R. Förster, J.D. Sedgwick, J.L. Browning, M. Lipp, and J.G. Cyster. 2000. A chemokine-driven positive feedback loop organizes lymphoid follicles. *Nature*. 406:309–314. doi:10.1038/35018581.

Arnason, J., and D. Avigan. 2012. Evolution of cellular immunotherapy: from allogeneic transplant to dendritic cell vaccination as treatment for multiple myeloma. *Immunotherapy*. 4:1043–1051. doi:10.2217/imt.12.118.

Austyn, J.M. 1996. New insights into the mobilization and phagocytic activity of dendritic cells. *J. Exp. Med.* 183:1287–1292.

Baekkevold, E.S., T. Yamanaka, R.T. Palframan, H.S. Carlsen, F.P. Reinholt, U.H. von Andrian, P. Brandtzaeg, and G. Haraldsen. 2001. The CCR7 ligand elc (CCL19) is transcytosed in high endothelial venules and mediates T cell recruitment. *J. Exp. Med.* 193:1105–1112.

Bajénoff, M., and R.N. Germain. 2009. B-cell follicle development remodels the conduit system and allows soluble antigen delivery to follicular dendritic cells. *Blood*. 114:4989–4997. doi:

10.1182/blood-2009-06-229567.

Bajénoff, M., J.G. Egen, H. Qi, A.Y.C. Huang, F. Castellino, and R.N. Germain. 2007. Highways, byways and breadcrumbs: directing lymphocyte traffic in the lymph node. *Trends Immunol.* 28:346–352. doi:10.1016/j.it.2007.06.005.

Bajénoff, M., J.G. Egen, L.Y. Koo, J.P. Laugier, F. Brau, N. Glaichenhaus, and R.N. Germain. 2006. Stromal cell networks regulate lymphocyte entry, migration, and territoriality in lymph nodes. *Immunity*. 25:989–1001. doi:10.1016/j.immuni.2006.10.011.

Baluk, P., J. Fuxe, H. Hashizume, T. Romano, E. Lashnits, S. Butz, D. Vestweber, M. Corada, C. Molendini, E. Dejana, and D.M. McDonald. 2007. Functionally specialized junctions between endothelial cells of lymphatic vessels. *J. Exp. Med.* 204:2349–2362. doi:10.1084/jem.20062596.

Berisio, R., L. Vitagliano, L. Mazzarella, and A. Zagari. 2002. Recent progress on collagen triple helix structure, stability and assembly. *Protein Pept. Lett.* 9:107–116.

Berney, C., S. Herren, C.A. Power, S. Gordon, L. Martinez-Pomares, and M.H. Kosco-Vilbois. 1999. A member of the dendritic cell family that enters B cell follicles and stimulates primary antibody responses identified by a mannose receptor fusion protein. *J. Exp. Med.* 190:851–860.

Boulianne, B., M.X. Le, L.A. Ward, L. Meng, D. Haddad, C. Li, A. Martin, and J.L. Gommerman. 2013. AID-Expressing Germinal Center B Cells Cluster Normally within Lymph Node Follicles in the Absence of FDC-M1+ CD35+ Follicular Dendritic Cells but Dissipate Prematurely. *J Immunol*. 191:4521–4530. doi:10.4049/jimmunol.1300769.

Braun, A., T. Worbs, G.L. Moschovakis, S. Halle, K. Hoffmann, J. Bölter, A. Münk, and R. Förster. 2011. Afferent lymph-derived T cells and DCs use different chemokine receptor CCR7-dependent routes for entry into the lymph node and intranodal migration. *Nat Immunol*. 12:879–887. doi:10.1038/ni.2085.

Breitfeld, D., L. Ohl, E. Kremmer, J. Ellwart, F. Sallusto, M. Lipp, and R. Förster. 2000. Follicular B helper T cells express CXC chemokine receptor 5, localize to B cell follicles, and support immunoglobulin production. *J. Exp. Med.* 192:1545–1552.

Browning, J.L., N. Allaire, A. Ngam-Ek, E. Notidis, J. Hunt, S. Perrin, and R.A. Fava. 2005. Lymphotoxin-beta receptor signaling is required for the homeostatic control of HEV differentiation and function. *Immunity*. 23:539–550. doi:10.1016/j.immuni.2005.10.002.

Browse, N.L., R.L. Doig, and D. Sizeland. 1984. The resistance of a lymph node to lymph flow. *Br J Surg*. 71:192–196.

Buch, T., F.L. Heppner, C. Tertilt, T.J.A.J. Heinen, M. Kremer, F.T. Wunderlich, S. Jung, and A. Waisman. 2005. A Cre-inducible diphtheria toxin receptor mediates cell lineage ablation after toxin administration. *Nat Meth*. 2:419–426. doi:10.1038/nmeth762.

Butcher, E.C. 1991. Leukocyte-endothelial cell recognition: three (or more) steps to specificity and diversity. *Cell*. 67:1033–1036.

Carpenter, A.E., T.R. Jones, M.R. Lamprecht, C. Clarke, I.H. Kang, O. Friman, D.A. Guertin, J.H. Chang, R.A. Lindquist, J. Moffat, P. Golland, and D.M. Sabatini. 2006. CellProfiler: image analysis software for identifying and quantifying cell phenotypes. *Genome Biol.*

7:R100. doi:10.1186/gb-2006-7-10-r100.

Carrasco, Y.R., and F.D. Batista. 2007. B cells acquire particulate antigen in a macrophage-rich area at the boundary between the follicle and the subcapsular sinus of the lymph node. *Immunity*. 27:160–171. doi:10.1016/j.immuni.2007.06.007.

Casley-Smith, J.R. 1985. The influence of tissue hydrostatic pressure and protein concentration on fluid and protein uptake by diaphragmatic initial lymphatics; effect of calcium dobesilate. *Microcirc Endothelium Lymphatics*. 2:385–415.

Chai, Q., L. Onder, E. Scandella, and C. Gil-Cruz. 2013. Maturation of Lymph Node Fibroblastic Reticular Cells from Myofibroblastic Precursors Is Critical for Antiviral Immunity. *Immunity*.

Chen, H., C. Griffin, L. Xia, and R.S. Srinivasan. 2014. Molecular and cellular mechanisms of lymphatic vascular maturation. *Microvasc. Res.* doi:10.1016/j.mvr.2014.06.002.

Chyou, S., E.H. Ekland, A.C. Carpenter, T.C.J. Tzeng, S. Tian, M. Michaud, J.A. Madri, and T.T. Lu. 2008. Fibroblast-Type Reticular Stromal Cells Regulate the Lymph Node Vasculature. *J Immunol*. 181:3887–3896. doi:10.4049/jimmunol.181.6.3887.

CLARK, S.L. 1962. The reticulum of lymph nodes in mice studied with the electron microscope. *Am. J. Anat.* 110:217–257. doi:10.1002/aja.1001100303.

Cliff, W. 1976. Blood Vessels. Cambridge University Press.

Cohen, J.N., C.J. Guidi, E.F. Tewalt, H. Qiao, S.J. Rouhani, A. Ruddell, A.G. Farr, K.S. Tung, and V.H. Engelhard. 2010. Lymph node-resident lymphatic endothelial cells mediate peripheral tolerance via Aire-independent direct antigen presentation. *Journal of Experimental Medicine*. 207:681–688. doi:10.1084/jem.20092465.

Cohen, J.N., E.F. Tewalt, S.J. Rouhani, E.L. Buonomo, A.N. Bruce, X. Xu, S. Bekiranov, Y.-X. Fu, and V.H. Engelhard. 2014. Tolerogenic properties of lymphatic endothelial cells are controlled by the lymph node microenvironment. *PLoS ONE*. 9:e87740. doi:10.1371/journal.pone.0087740.

Controversial AIDS vaccine fails to delay disease. 1996. Controversial AIDS vaccine fails to delay disease. *Nature*. 380:662. doi:10.1038/380662a0.

Cyster, J.G. 2010. B cell follicles and antigen encounters of the third kind. *Nat Immunol*. 11:989–996. doi:10.1038/ni.1946.

Cyster, J.G., K.M. Ansel, K. Reif, E.H. Ekland, P.L. Hyman, H.L. Tang, S.A. Luther, and V.N. Ngo. 2003. Follicular stromal cells and lymphocyte homing to follicles. *Immunol Rev*. 176:181–193. doi:10.1034/j.1600-065X.2000.00618.x.

Desch, A.N., G.J. Randolph, K. Murphy, E.L. Gautier, R.M. Kedl, M.H. Lahoud, I. Caminschi, K. Shortman, P.M. Henson, and C.V. Jakubzick. 2011. CD103+ pulmonary dendritic cells preferentially acquire and present apoptotic cell-associated antigen. *Journal of Experimental Medicine*. 208:1789–1797. doi:10.1084/jem.20110538.

Dieu, M.C., B. Vanbervliet, A. Vicari, J.M. Bridon, E. Oldham, S. Aït-Yahia, F. Brière, A. Zlotnik, S. Lebecque, and C. Caux. 1998. Selective recruitment of immature and mature dendritic cells by distinct chemokines expressed in different anatomic sites. *J. Exp. Med.* 188:373–386.

Dudziak, D., A.O. Kamphorst, G.F. Heidkamp, V.R. Buchholz, C. Trumpfheller, S. Yamazaki, C. Cheong, K. Liu, H.-W. Lee, C.G. Park, R.M. Steinman, and M.C. Nussenzweig. 2007. Differential antigen processing by dendritic cell subsets in vivo. *Science*. 315:107–111. doi: 10.1126/science.1136080.

Ertürk, A., C.P. Mauch, F. Hellal, F. Förstner, T. Keck, K. Becker, N. Jährling, H. Steffens, M. Richter, M. Hübener, E. Kramer, F. Kirchhoff, H.U. Dodt, and F. Bradke. 2012. Three-dimensional imaging of the unsectioned adult spinal cord to assess axon regeneration and glial responses after injury. *Nature Medicine*. 18:166–171. doi:10.1038/nm.2600.

Estes, J.D. 2013. Pathobiology of HIV/SIV-associated changes in secondary lymphoid tissues. *Immunol Rev*. 254:65–77. doi:10.1111/imr.12070.

Farr, A.G., Y. Cho, and P.P. De Bruyn. 1980. The structure of the sinus wall of the lymph node relative to its endocytic properties and transmural cell passage. *Am. J. Anat.* 157:265–284. doi:10.1002/aja.1001570304.

Fletcher, A.L., D. Malhotra, S.E. Acton, V. Lukacs-Kornek, A. Bellemare-Pelletier, M. Curry, M. Armant, and S.J. Turley. 2011. Reproducible isolation of lymph node stromal cells reveals site-dependent differences in fibroblastic reticular cells. *Frontiers in Immunology*. 2:35. doi: 10.3389/fimmu.2011.00035.

Fossum, S. 1980a. The architecture of rat lymph nodes. IV. Distribution of ferritin and colloidal carbon in the draining lymph nodes after foot-pad injection. *Scand. J. Immunol.* 12:433–441.

Fossum, S. 1980b. The architecture of rat lymph nodes. II. Lymph node compartments. *Scand. J. Immunol.* 12:411–420.

Fossum, S., and J.L. Vaaland. 1983. The architecture of rat lymph nodes. I. Combined light and electron microscopy of lymph node cell types. *Anat. Embryol.* 167:229–246.

Förster, R., A. Schubel, D. Breitfeld, E. Kremmer, I. Renner-Müller, E. Wolf, and M. Lipp. 1999. CCR7 coordinates the primary immune response by establishing functional microenvironments in secondary lymphoid organs. *Cell*. 99:23–33.

Förster, R., A.C. Davalos-Misslitz, and A. Rot. 2008. CCR7 and its ligands: balancing immunity and tolerance. *Nat Rev Immunol*. 8:362–371. doi:10.1038/nri2297.

Garin, A., M. Meyer-Hermann, M. Contie, and M.T. Figge. 2010. Toll-like Receptor 4 Signaling by Follicular Dendritic Cells Is Pivotal for Germinal Center Onset and Affinity Maturation. *Immunity*.

Gerner, M.Y., W. Kastenmuller, I. Ifrim, J. Kabat, and R.N. Germain. 2012. Histo-cytometry: a method for highly multiplex quantitative tissue imaging analysis applied to dendritic cell subset microanatomy in lymph nodes. *Immunity*. 37:364–376. doi:10.1016/j.immuni. 2012.07.011.

Girard, J.P., and T.A. Springer. 1995. High endothelial venules (HEVs): specialized endothelium for lymphocyte migration. *Immunol. Today*. 16:449–457.

Gonzalez, S.F., S.E. Degn, L.A. Pitcher, M. Woodruff, B.A. Heesters, and M.C. Carroll. 2011. Trafficking of B cell antigen in lymph nodes. *http://dx.doi.org.ezp-prod1.hul.harvard.edu/10.1146/annurev-immunol-031210-101255*. 29:215–233. doi:10.1146/annurev-immunol-031210-101255.

Gonzalez, S.F., V. Lukacs-Kornek, M.P. Kuligowski, L.A. Pitcher, S.E. Degn, Y.-A. Kim, M.J. Cloninger, L. Martinez-Pomares, S. Gordon, S.J. Turley, and M.C. Carroll. 2010. Capture of influenza by medullary dendritic cells via SIGN-R1 is essential for humoral immunity in draining lymph nodes. *Nat Immunol*. doi:10.1038/ni.1856.

Gorelik, L., K. Gilbride, M. Dobles, S.L. Kalled, D. Zandman, and M.L. Scott. 2003. Normal B cell homeostasis requires B cell activation factor production by radiation-resistant cells. *J. Exp. Med.* 198:937–945. doi:10.1084/jem.20030789.

Gray, E.E., and J.G. Cyster. 2012. Lymph node macrophages. *J Innate Immun*. 4:424–436. doi: 10.1159/000337007.

Gretz, J.E., A.O. Anderson, and S. Shaw. 1997. Cords, channels, corridors and conduits: critical architectural elements facilitating cell interactions in the lymph node cortex. *Immunol Rev*. 156:11–24.

Gretz, J.E., C.C. Norbury, A.O. Anderson, A.E. Proudfoot, and S. Shaw. 2000. Lymph-borne chemokines and other low molecular weight molecules reach high endothelial venules via specialized conduits while a functional barrier limits access to the lymphocyte microenvironments in lymph node cortex. *J. Exp. Med.* 192:1425–1440.

Grigorova, I.L., M. Panteleev, and J.G. Cyster. 2010. Lymph node cortical sinus organization and relationship to lymphocyte egress dynamics and antigen exposure. *Proc Natl Acad Sci USA*. 107:20447–20452. doi:10.1073/pnas.1009968107.

Groom, J.R., J. Richmond, T.T. Murooka, E.W. Sorensen, J.H. Sung, K. Bankert, U.H. von Andrian, J.J. Moon, T.R. Mempel, and A.D. Luster. 2012. CXCR3 chemokine receptor-ligand interactions in the lymph node optimize CD4+ T helper 1 cell differentiation. *Immunity*. 37:1091–1103. doi:10.1016/j.immuni.2012.08.016.

Gunn, M.D., K. Tangemann, C. Tam, J.G. Cyster, S.D. Rosen, and L.T. Williams. 1998. A chemokine expressed in lymphoid high endothelial venules promotes the adhesion and chemotaxis of naive T lymphocytes. *Proc Natl Acad Sci USA*. 95:258–263.

Hawiger, D., K. Inaba, Y. Dorsett, M. Guo, K. Mahnke, M. Rivera, J.V. Ravetch, R.M. Steinman, and M.C. Nussenzweig. 2001. Dendritic cells induce peripheral T cell unresponsiveness under steady state conditions in vivo. *J. Exp. Med.* 194:769–779.

Heath, T.J., R.L. Kerlin, and H.J. Spalding. 1986. Afferent pathways of lymph flow within the popliteal node in sheep. *J. Anat.* 149:65–75.

Heath, W.R., and F.R. Carbone. 2009. Dendritic cell subsets in primary and secondary T cell responses at body surfaces. *Nat Immunol*. 10:1237–1244. doi:10.1038/ni.1822.

Heesters, B.A., R.C. Myers, and M.C. Carroll. 2014. Follicular dendritic cells: dynamic antigen libraries. *Nat Rev Immunol*. 14:495–504. doi:10.1038/nri3689.

Helft, J., F. Ginhoux, M. Bogunovic, and M. Merad. 2010. Origin and functional heterogeneity of non-lymphoid tissue dendritic cells in mice. *Immunol Rev*. 234:55–75. doi:10.1111/j. 0105-2896.2009.00885.x.

Hickman, H.D., K. Takeda, C.N. Skon, F.R. Murray, S.E. Hensley, J. Loomis, G.N. Barber, J.R. Bennink, and J.W. Yewdell. 2008. Direct priming of antiviral CD8+ T cells in the peripheral interfollicular region of lymph nodes. *Nat Immunol*. 9:155–165. doi:10.1038/ni1557.

Hill, M., M. Segovia, and M.C. Cuturi. 2011. What is the role of antigen-processing mechanisms in autologous tolerogenic dendritic cell therapy in organ transplantation? *Immunotherapy*. 3:12–14. doi:10.2217/imt.11.40.

Hudack, S., and P.D. McMaster. 1932. I. THE PERMEABILITY OF THE WALL OF THE LYMPHATIC CAPILLARY. *J. Exp. Med.* 56:223–238.

Iannacone, M., E.A. Moseman, E. Tonti, L. Bosurgi, T. Junt, S.E. Henrickson, S.P. Whelan, L.G. Guidotti, and U.H. von Andrian. 2010. Subcapsular sinus macrophages prevent CNS invasion on peripheral infection with a neurotropic virus. *Nature*. 465:1079–1083. doi: 10.1038/nature09118.

Igyártó, B.Z., K. Haley, D. Ortner, A. Bobr, M. Gerami-Nejad, B.T. Edelson, S.M. Zurawski, B. Malissen, G. Zurawski, J. Berman, and D.H. Kaplan. 2011. Skin-resident murine dendritic cell subsets promote distinct and opposing antigen-specific T helper cell responses. *Immunity*. 35:260–272. doi:10.1016/j.immuni.2011.06.005.

Itano, A.A., S.J. McSorley, R.L. Reinhardt, B.D. Ehst, E. Ingulli, A.Y. Rudensky, and M.K. Jenkins. 2003. Distinct dendritic cell populations sequentially present antigen to CD4 T cells and stimulate different aspects of cell-mediated immunity. *Immunity*. 19:47–57.

Jakubzick, C., J. Helft, T.J. Kaplan, and G.J. Randolph. 2008. Optimization of methods to study pulmonary dendritic cell migration reveals distinct capacities of DC subsets to acquire soluble versus particulate antigen. *J Immunol Methods*. 337:121–131. doi:10.1016/j.jim. 2008.07.005.

Jarjour, M., A. Jorquera, I. Mondor, S. Wienert, P. Narang, M.C. Coles, F. Klauschen, and M. Bajénoff. 2014. Fate mapping reveals origin and dynamics of lymph node follicular dendritic cells. *Journal of Experimental Medicine*. 211:1109–1122. doi:10.1084/jem.20132409.

Jillian L Astarita, S.E.A.S.J.T. 2012. Podoplanin: emerging functions in development, the immune system, and cancer. *Frontiers in Immunology*. 3. doi:10.3389/fimmu.2012.00283.

Jones, T.R., I.H. Kang, D.B. Wheeler, R.A. Lindquist, A. Papallo, D.M. Sabatini, P. Golland, and A.E. Carpenter. 2008. CellProfiler Analyst: data exploration and analysis software for complex image-based screens. *BMC Bioinformatics*. 9:482. doi:10.1186/1471-2105-9-482.

Junt, T., E. Scandella, and B. Ludewig. 2008. Form follows function: lymphoid tissue microarchitecture in antimicrobial immune defence. *Nat Rev Immunol*. 8:764–775. doi: 10.1038/nri2414.

Junt, T., E.A. Moseman, M. Iannacone, S. Massberg, P.A. Lang, M. Boes, K. Fink, S.E. Henrickson, D.M. Shayakhmetov, N.C. Di Paolo, N. van Rooijen, T.R. Mempel, S.P. Whelan, and U.H. von Andrian. 2007. Subcapsular sinus macrophages in lymph nodes clear lymph-borne viruses and present them to antiviral B cells. *Nature*. 450:110–114. doi:10.1038/ nature06287.

Kaldjian, E.P., J.E. Gretz, A.O. Anderson, Y. Shi, and S. Shaw. 2001. Spatial and molecular organization of lymph node T cell cortex: a labyrinthine cavity bounded by an epithelium-like monolayer of fibroblastic reticular cells anchored to basement membrane-like extracellular matrix. *International Immunology*. 13:1243–1253.

Kastenmuller, W., M. Brandes, Z. Wang, J. Herz, J.G. Egen, and R.N. Germain. 2013. Peripheral Prepositioning and Local CXCL9 Chemokine-Mediated Guidance Orchestrate

Rapid Memory CD8(+) T Cell Responses in the Lymph Node. *Immunity*. 38:502–513. doi: 10.1016/j.immuni.2012.11.012.

Katakai, T. 2012. Marginal reticular cells: a stromal subset directly descended from the lymphoid tissue organizer. *Frontiers in Immunology*. 3:200. doi:10.3389/fimmu.2012.00200.

Katakai, T., H. Suto, M. Sugai, H. Gonda, A. Togawa, S. Suematsu, Y. Ebisuno, K. Katagiri, T. Kinashi, and A. Shimizu. 2008. Organizer-like reticular stromal cell layer common to adult secondary lymphoid organs. *J Immunol*. 181:6189–6200.

Katakai, T., T. Hara, J.-H. Lee, H. Gonda, M. Sugai, and A. Shimizu. 2004. A novel reticular stromal structure in lymph node cortex: an immuno-platform for interactions among dendritic cells, T cells and B cells. *International Immunology*. 16:1133–1142. doi:10.1093/intimm/dxh113.

Kelsoe, G. 1996. Life and death in germinal centers (redux). *Immunity*. 4:107–111.

Khan, O., M. Headley, A. Gerard, W. Wei, L. Liu, and M.F. Krummel. 2011. Regulation of T cell priming by lymphoid stroma. *PLoS ONE*. 6:e26138. doi:10.1371/journal.pone.0026138.

Kim, C.H., L.S. Rott, I. Clark-Lewis, D.J. Campbell, L. Wu, and E.C. Butcher. 2001. Subspecialization of CXCR5+ T cells: B helper activity is focused in a germinal center-localized subset of CXCR5+ T cells. *J. Exp. Med.* 193:1373–1381.

Kissenpfennig, A., S. Henri, B. Dubois, C. Laplace-Builhé, P. Perrin, N. Romani, C.H. Tripp, P. Douillard, L. Leserman, D. Kaiserlian, S. Saeland, J. Davoust, and B. Malissen. 2005. Dynamics and function of Langerhans cells in vivo: dermal dendritic cells colonize lymph node areas distinct from slower migrating Langerhans cells. *Immunity*. 22:643–654. doi: 10.1016/j.immuni.2005.04.004.

Knox, P., and J.J. Pflug. 1983. The effect of the canine popliteal node on the composition of lymph. *J. Physiol. (Lond.)*. 345:1–14.

Koni, P.A., R. Sacca, P. Lawton, J.L. Browning, N.H. Ruddle, and R.A. Flavell. 1997. Distinct roles in lymphoid organogenesis for lymphotoxins alpha and beta revealed in lymphotoxin beta-deficient mice. *Immunity*. 6:491–500.

Koning, J.J., and R.E. Mebius. 2012. Interdependence of stromal and immune cells for lymph node function. 33:264–270. doi:10.1016/j.it.2011.10.006.

Kunder, C.A., A.L. St John, G. Li, K.W. Leong, B. Berwin, H.F. Staats, and S.N. Abraham. 2009. Mast cell-derived particles deliver peripheral signals to remote lymph nodes. *Journal of Experimental Medicine*. 206:2455–2467. doi:10.1084/jem.20090805.

Larsen, C.P., R.M. Steinman, M. Witmer-Pack, D.F. Hankins, P.J. Morris, and J.M. Austyn. 1990. Migration and maturation of Langerhans cells in skin transplants and explants. *J. Exp. Med.* 172:1483–1493.

Lämmermann, T., and M. Sixt. 2008. The microanatomy of T-cell responses. *Immunol Rev*. 221:26–43. doi:10.1111/j.1600-065X.2008.00592.x.

Lämmermann, T., B.L. Bader, S.J. Monkley, T. Worbs, R. Wedlich-Söldner, K. Hirsch, M. Keller, R. Förster, D.R. Critchley, R. Fässler, and M. Sixt. 2008. Rapid leukocyte migration by integrin-independent flowing and squeezing. *Nature*. 453:51–55. doi:10.1038/nature06887.

León, B., A. Ballesteros-Tato, J.L. Browning, R. Dunn, T.D. Randall, and F.E. Lund. 2012. Regulation of T(H)2 development by CXCR5(+) dendritic cells and lymphotoxin-expressing B cells. *Nat Immunol*. 13:681–690. doi:10.1038/ni.2309.

Lindquist, R.L., G. Shakhar, D. Dudziak, H. Wardemann, T. Eisenreich, M.L. Dustin, and M.C. Nussenzweig. 2004. Visualizing dendritic cell networks in vivo. *Nat Immunol*. 5:1243–1250. doi:10.1038/ni1139.

Link, A., T.K. Vogt, S. Favre, M.R. Britschgi, H. Acha-Orbea, B. Hinz, J.G. Cyster, and S.A. Luther. 2007. Fibroblastic reticular cells in lymph nodes regulate the homeostasis of naive T cells. *Nat Immunol*. 8:1255–1265. doi:10.1038/ni1513.

Liu, H., K.D. Moynihan, Y. Zheng, G.L. Szeto, A.V. Li, B. Huang, D.S. Van Egeren, C. Park, and D.J. Irvine. 2014. Structure-based programming of lymph-node targeting in molecular vaccines. *Nature*. 507:519–522. doi:10.1038/nature12978.

Llanos, C., L.J. Carreño, and A.M. Kalergis. 2011. Contribution of dendritic cell/T cell interactions to triggering and maintaining autoimmunity. *Biol. Res.* 44:53–61.

Lukacs-Kornek, V., D. Malhotra, A.L. Fletcher, S.E. Acton, K.G. Elpek, P. Tayalia, A.-R. Collier, and S.J. Turley. 2011. Regulated release of nitric oxide by nonhematopoietic stroma controls expansion of the activated T cell pool in lymph nodes. *Nat Immunol*. 12:1096–1104. doi:10.1038/ni.2112.

Luther, S.A., H.L. Tang, P.L. Hyman, A.G. Farr, and J.G. Cyster. 2000. Coexpression of the chemokines ELC and SLC by T zone stromal cells and deletion of the ELC gene in the plt/plt mouse. *Proc Natl Acad Sci USA*. 97:12694–12699. doi:10.1073/pnas.97.23.12694.

Lutz, M.B., and G. Schuler. 2002. Immature, semi-mature and fully mature dendritic cells: which signals induce tolerance or immunity? *Trends Immunol.* 23:445–449.

Mackay, F., and J.L. Browning. 2002. BAFF: A fundamental survival factor for B cells. *Nat Rev Immunol*. 2:465–475. doi:10.1038/nri844.

MacLennan, I.C. 1994. Germinal centers. *Annu Rev Immunol*. 12:117–139. doi:10.1146/annurev.iy.12.040194.001001.

Malhotra, D., A.L. Fletcher, and S.J. Turley. 2012a. Stromal and hematopoietic cells in secondary lymphoid organs: partners in immunity. *Immunol Rev*. 251:160–176. doi:10.1111/imr.12023.

Malhotra, D., A.L. Fletcher, J. Astarita, V. Lukacs-Kornek, P. Tayalia, S.F. Gonzalez, K.G. Elpek, S.K. Chang, K. Knoblich, M.E. Hemler, M.B. Brenner, M.C. Carroll, D.J. Mooney, S.J. Turley, Y. Zhou, S.A. Shinton, R.R. Hardy, N.A. Bezman, J.C. Sun, C.C. Kim, L.L. Lanier, J. Miller, B. Brown, M. Merad, A.L. Fletcher, K.G. Elpek, A. Bellemare-Pelletier, D. Malhotra, S.J. Turley, K. Narayan, K. Sylvia, J. Kang, R. Gazit, B. Garrison, D.J. Rossi, V. Jojic, D. Koller, R. Jianu, D. Laidlaw, J. Costello, J. Collins, N. Cohen, P. Brennan, M.B. Brenner, T. Shay, A. Regev, F. Kim, T.N. Rao, A. Wagers, E.L. Gautier, C. Jakubzick, G.J. Randolph, P. Monach, A.J. Best, J. Knell, A. Goldrath, T. Heng, T. Kreslavsky, M. Painter, D. Mathis, and C. Benoist. 2012b. Transcriptional profiling of stroma from inflamed and resting lymph nodes defines immunological hallmarks. *Nat Immunol*. 13:499–510. doi:10.1038/ni.2262.

Mandel, T.E., R.P. Phipps, A. Abbot, and J.G. Tew. 1980. The follicular dendritic cell: long term antigen retention during immunity. *Immunol Rev*. 53:29–59.

Martinez-Pomares, L., and S. Gordon. 2012. CD169+ macrophages at the crossroads of antigen presentation. *Trends Immunol.* 33:66–70. doi:10.1016/j.it.2011.11.001.

Martinez-Pomares, L., M. Kosco-Vilbois, E. Darley, P. Tree, S. Herren, J.Y. Bonnefoy, and S. Gordon. 1996. Fc chimeric protein containing the cysteine-rich domain of the murine mannose receptor binds to macrophages from splenic marginal zone and lymph node subcapsular sinus and to germinal centers. *J. Exp. Med.* 184:1927–1937.

McGill, J., J.W. Heusel, and K.L. Legge. 2009. Innate immune control and regulation of influenza virus infections. *Journal of Leukocyte Biology*. 86:803–812. doi:10.1189/jlb.0509368.

Mebius, R.E. 2003. Organogenesis of lymphoid tissues. *Nat Rev Immunol*. 3:292–303. doi:10.1038/nri1054.

Mendoza, E., and G.W. Schmid-Schönbein. 2003. A model for mechanics of primary lymphatic valves. *J Biomech Eng*. 125:407–414.

Moodycliffe, A.M., I. Kimber, and M. Norval. 1994. Role of tumour necrosis factor-alpha in ultraviolet B light-induced dendritic cell migration and suppression of contact hypersensitivity. *Immunology*. 81:79–84.

Moseman, E.A., M. Iannacone, L. Bosurgi, E. Tonti, N. Chevrier, A. Tumanov, Y.-X. Fu, N. Hacohen, and U.H. von Andrian. 2012. B cell maintenance of subcapsular sinus macrophages protects against a fatal viral infection independent of adaptive immunity. *Immunity*. 36:415–426. doi:10.1016/j.immuni.2012.01.013.

Mueller, S.N., and R.N. Germain. 2010. Stromal cell contributions to the homeostasis and functionality of the immune system. *Nat Rev Immunol*. doi:10.1038/nri2588.

Nakano, H., K.L. Lin, M. Yanagita, C. Charbonneau, D.N. Cook, T. Kakiuchi, and M.D. Gunn. 2009. Blood-derived inflammatory dendritic cells in lymph nodes stimulate acute T helper type 1 immune responses. *Nat Immunol*. 10:394–402. doi:10.1038/ni.1707.

Nossal, G.J., G.L. Ada, C.M. Austin, and J. Pye. 1965. Antigens in immunity. 8. Localization of 125-I-labelled antigens in the secondary response. *Immunology*. 9:349–357.

Nurieva, R.I., and Y. Chung. 2010. Understanding the development and function of T follicular helper cells. *Cell Mol Immunol*. 7:190–197. doi:10.1038/cmi.2010.24.

Ohl, L., M. Mohaupt, N. Czeloth, G. Hintzen, Z. Kiafard, J. Zwirner, T. Blankenstein, G. Henning, and R. Förster. 2004. CCR7 governs skin dendritic cell migration under inflammatory and steady-state conditions. *Immunity*. 21:279–288. doi:10.1016/j.immuni.2004.06.014.

Ohtani, O., and Y. Ohtani. 2008. Structure and function of rat lymph nodes. *Arch. Histol. Cytol.* 71:69–76.

Okada, T., and J.G. Cyster. 2006. B cell migration and interactions in the early phase of antibody responses. *Curr Opin Immunol*. 18:278–285. doi:10.1016/j.coi.2006.02.005.

Okada, T., V.N. Ngo, E.H. Ekland, R. Förster, M. Lipp, D.R. Littman, and J.G. Cyster. 2002. Chemokine requirements for B cell entry to lymph nodes and Peyer's patches. *J. Exp. Med.* 196:65–75.

Okuyama, K. 2008. Revisiting the molecular structure of collagen. *Connect. Tissue Res.* 49:299–310. doi:10.1080/03008200802325110.

Palframan, R.T., S. Jung, G. Cheng, W. Weninger, Y. Luo, M. Dorf, D.R. Littman, B.J. Rollins, H. Zweerink, A. Rot, and U.H. von Andrian. 2001. Inflammatory chemokine transport and presentation in HEV: a remote control mechanism for monocyte recruitment to lymph nodes in inflamed tissues. *J. Exp. Med.* 194:1361–1373.

Pellegrini, M., T. Calzascia, J.G. Toe, S.P. Preston, A.E. Lin, A.R. Elford, A. Shahinian, P.A. Lang, K.S. Lang, M. Morre, B. Assouline, K. Lahl, T. Sparwasser, T.F. Tedder, J.-H. Paik, R.A. DePinho, S. Basta, P.S. Ohashi, and T.W. Mak. 2011. IL-7 engages multiple mechanisms to overcome chronic viral infection and limit organ pathology. *Cell*. 144:601–613. doi:10.1016/j.cell.2011.01.011.

Pereira, J.P., L.M. Kelly, and J.G. Cyster. 2010. Finding the right niche: B-cell migration in the early phases of T-dependent antibody responses. *International Immunology*. 22:413–419. doi:10.1093/intimm/dxq047.

Perez-Shibayama, C., C. Gil-Cruz, M. Nussbacher, E. Allgäuer, L. Cervantes-Barragan, R. Züst, and B. Ludewig. 2013. Dendritic cell-specific delivery of Flt3L by coronavirus vectors secures induction of therapeutic antitumor immunity. *PLoS ONE*. 8:e81442. doi:10.1371/journal.pone.0081442.

Phan, T.G., I. Grigorova, T. Okada, and J.G. Cyster. 2007. Subcapsular encounter and complement-dependent transport of immune complexes by lymph node B cells. *Nat Immunol*. 8:992–1000. doi:10.1038/ni1494.

Platt, A.M., and G.J. Randolph. 2013. Dendritic cell migration through the lymphatic vasculature to lymph nodes. *Adv. Immunol.* 120:51–68. doi:10.1016/B978-0-12-417028-5.00002-8.

Poudrier, J., J. Chagnon-Choquet, and M. Roger. 2012. Influence of dendritic cells on B-cell responses during HIV infection. *Clin. Dev. Immunol.* 2012:592187. doi:10.1155/2012/592187.

Qi, H., J.G. Egen, A.Y.C. Huang, and R.N. Germain. 2006. Extrafollicular activation of lymph node B cells by antigen-bearing dendritic cells. *Science*. 312:1672–1676. doi:10.1126/science.1125703.

Randolph, G.J., V. Angeli, and M.A. Swartz. 2005. Dendritic-cell trafficking to lymph nodes through lymphatic vessels. *Nat Rev Immunol*. 5:617–628. doi:10.1038/nri1670.

Rescigno, M., C. Winzler, D. Delia, C. Mutini, M. Lutz, and P. Ricciardi-Castagnoli. 1997. Dendritic cell maturation is required for initiation of the immune response. *Journal of Leukocyte Biology*. 61:415–421.

Rollins, B.J. 1997. Chemokines. *Blood*. 90:909–928.

Roozendaal, R., and M.C. Carroll. 2007. Complement receptors CD21 and CD35 in humoral immunity. *Immunol Rev*. 219:157–166. doi:10.1111/j.1600-065X.2007.00556.x.

Roozendaal, R., T.R. Mempel, L.A. Pitcher, S.F. Gonzalez, A. Verschoor, R.E. Mebius, U.H. von Andrian, and M.C. Carroll. 2009. Conduits Mediate Transport of Low-Molecular-Weight Antigen to Lymph Node Follicles. *Immunity*. 30:264–276. doi:10.1016/j.immuni.2008.12.014.

Saini, M., C. Pearson, and B. Seddon. 2009. Regulation of T cell-dendritic cell interactions by IL-7 governs T-cell activation and homeostasis. *Blood*. 113:5793–5800. doi:10.1182/blood-2008-12-192252.

Sainte-Marie, G., F.S. Peng, and C. Bélisle. 1982. Overall architecture and pattern of lymph flow in the rat lymph node. *Am. J. Anat.* 164:275–309. doi:10.1002/aja.1001640402.

Scandella, E., B. Bolinger, E. Lattmann, S. Miller, S. Favre, D.R. Littman, D. Finke, S.A. Luther, T. Junt, and B. Ludewig. 2008. Restoration of lymphoid organ integrity through the interaction of lymphoid tissue–inducer cells with stroma of the T cell zone. *Nat Immunol*. 9:667–675. doi:10.1038/ni.1605.

Schmid-Schönbein, G.W. 2003. The second valve system in lymphatics. *Lymphat Res Biol*. 1:25–9– discussion 29–31.

Schmidt, S., and P. Friedl. 2010. Interstitial cell migration: integrin-dependent and alternative adhesion mechanisms. *Cell Tissue Res.* 339:83–92. doi:10.1007/s00441-009-0892-9.

Shklovskaya, E., B. Roediger, and B. Fazekas de St Groth. 2008. Epidermal and dermal dendritic cells display differential activation and migratory behavior while sharing the ability to stimulate CD4+ T cell proliferation in vivo. *J Immunol*. 181:418–430.

Shortman, K., and W.R. Heath. 2010. The CD8+ dendritic cell subset. *Immunol Rev*. 234:18–31. doi:10.1111/j.0105-2896.2009.00870.x.

Shoulders, M.D., and R.T. Raines. 2009. Collagen structure and stability. *Annu Rev Biochem*. 78:929–958. doi:10.1146/annurev.biochem.77.032207.120833.

Siegert, S., H.-Y. Huang, C.-Y. Yang, L. Scarpellino, L. Carrie, S. Essex, P.J. Nelson, M. Heikenwalder, H. Acha-Orbea, C.D. Buckley, B.J. Marsland, D. Zehn, and S.A. Luther. 2011. Fibroblastic Reticular Cells From Lymph Nodes Attenuate T Cell Expansion by Producing Nitric Oxide. *PLoS ONE*. 6:e27618. doi:10.1371/journal.pone.0027618.

Sixt, M., N. Kanazawa, M. Selg, T. Samson, G. Roos, D.P. Reinhardt, R. Pabst, M.B. Lutz, and L. Sorokin. 2005. The conduit system transports soluble antigens from the afferent lymph to resident dendritic cells in the T cell area of the lymph node. *Immunity*. 22:19–29. doi:10.1016/j.immuni.2004.11.013.

Springer, T.A. 1994. Traffic signals for lymphocyte recirculation and leukocyte emigration: the multistep paradigm. *Cell*. 76:301–314.

Springer, T.A. 1995. Traffic signals on endothelium for lymphocyte recirculation and leukocyte emigration. *Annu. Rev. Physiol.* 57:827–872. doi:10.1146/annurev.ph.57.030195.004143.

Steer, H.W., and R.A. Foot. 1987. Changes in the medulla of the parathymic lymph nodes of the rat during acute gastro-intestinal inflammation. *J. Anat.* 152:23–36.

Stein, J.V., A. Rot, Y. Luo, M. Narasimhaswamy, H. Nakano, M.D. Gunn, A. Matsuzawa, E.J. Quackenbush, M.E. Dorf, and U.H. von Andrian. 2000. The CC chemokine thymus-derived chemotactic agent 4 (TCA-4, secondary lymphoid tissue chemokine, 6Ckine, exodus-2) triggers lymphocyte function-associated antigen 1-mediated arrest of rolling T lymphocytes in peripheral lymph node high endothelial venules. *J. Exp. Med.* 191:61–76.

Steinman, R.M. 1991. The dendritic cell system and its role in immunogenicity. *Annu Rev*

Immunol. 9:271–296. doi:10.1146/annurev.iy.09.040191.001415.

Steinman, R.M., M. Pack, and K. Inaba. 1997. Dendritic cells in the T-cell areas of lymphoid organs. *Immunol Rev*. 156:25–37.

Stoitzner, P., C.H. Tripp, P. Douillard, S. Saeland, and N. Romani. 2005. Migratory Langerhans cells in mouse lymph nodes in steady state and inflammation. *J Invest Dermatol*. 125:116–125. doi:10.1111/j.0022-202X.2005.23757.x.

Sung, J.H., H. Zhang, E.A. Moseman, D. Alvarez, M. Iannacone, S.E. Henrickson, J.C. de la Torre, J.R. Groom, A.D. Luster, and U.H. von Andrian. 2012. Chemokine guidance of central memory T cells is critical for antiviral recall responses in lymph nodes. *Cell*. 150:1249–1263. doi:10.1016/j.cell.2012.08.015.

Szakal, A.K., K.L. Holmes, and J.G. Tew. 1983. Transport of immune complexes from the subcapsular sinus to lymph node follicles on the surface of nonphagocytic cells, including cells with dendritic morphology. *J Immunol*. 131:1714–1727.

Szretter, K.J., A.L. Balish, and J.M. Katz. 2006. Influenza: propagation, quantification, and storage. *Curr Protoc Microbiol*. Chapter 15:Unit 15G.1. doi: 10.1002/0471729256.mc15g01s3.

Takahashi, K., M.J. Donovan, R.A. Rogers, and R.A. Ezekowitz. 1998. Distribution of murine mannose receptor expression from early embryogenesis through to adulthood. *Cell Tissue Res.* 292:311–323.

Tal, O., H.Y. Lim, I. Gurevich, I. Milo, Z. Shipony, L.G. Ng, V. Angeli, and G. Shakhar. 2011. DC mobilization from the skin requires docking to immobilized CCL21 on lymphatic endothelium and intralymphatic crawling. *J. Exp. Med.* 208:2141–2153. doi:10.1084/jem.20102392.

Tew, J.G., M.H. Kosco, G.F. Burton, and A.K. Szakal. 1990. Follicular dendritic cells as accessory cells. *Immunol Rev*. 117:185–211.

Thomas, P.G., S.A. Brown, W. Yue, J. So, R.J. Webby, and P.C. Doherty. 2006. An unexpected antibody response to an engineered influenza virus modifies CD8+ T cell responses. *Proc Natl Acad Sci USA*. 103:2764–2769. doi:10.1073/pnas.0511185103.

Tomei, A.A., S. Siegert, M.R. Britschgi, S.A. Luther, and M.A. Swartz. 2009. Fluid flow regulates stromal cell organization and CCL21 expression in a tissue-engineered lymph node microenvironment. *J Immunol*. 183:4273–4283. doi:10.4049/jimmunol.0900835.

Traub, W., A. Yonath, and D.M. Segal. 1969. On the molecular structure of collagen. *Nature*. 221:914–917.

Trzewik, J., S.K. Mallipattu, G.M. Artmann, F.A. Delano, and G.W. Schmid-Schönbein. 2001. Evidence for a second valve system in lymphatics: endothelial microvalves. *FASEB J.* 15:1711–1717.

Turley, S.J., A.L. Fletcher, and K.G. Elpek. 2010. The stromal and haematopoietic antigen-presenting cells that reside in secondary lymphoid organs. *Nat Rev Immunol*. 10:813–825. doi:10.1038/nri2886.

Ulvmar, M.H., K. Werth, A. Braun, P. Kelay, E. Hub, K. Eller, L. Chan, B. Lucas, I. Novitzky-Basso, K. Nakamura, T. Rülicke, R.J.B. Nibbs, T. Worbs, R. Förster, and A. Rot. 2014. The

atypical chemokine receptor CCRL1 shapes functional CCL21 gradients in lymph nodes. *Nat Immunol*. 15:623–630. doi:10.1038/ni.2889.

Villadangos, J.A., and P. Schnorrer. 2007. Intrinsic and cooperative antigen-presenting functions of dendritic-cell subsets in vivo. *Nat Rev Immunol*. 7:543–555. doi:10.1038/nri2103.

Wang, X., B. Cho, K. Suzuki, Y. Xu, J.A. Green, J. An, and J.G. Cyster. 2011. Follicular dendritic cells help establish follicle identity and promote B cell retention in germinal centers. *The Journal of …*.

Weber, M., R. Hauschild, J. Schwarz, C. Moussion, I. de Vries, D.F. Legler, S.A. Luther, T. Bollenbach, and M. Sixt. 2013. Interstitial dendritic cell guidance by haptotactic chemokine gradients. *Science*. 339:328–332. doi:10.1126/science.1228456.

Wess, T.J., A.P. Hammersley, L. Wess, and A. Miller. 1998. A consensus model for molecular packing of type I collagen. *J. Struct. Biol.* 122:92–100. doi:10.1006/jsbi.1998.3991.

Wu, Y., M.E.M. El Shikh, R.M. El Sayed, A.M. Best, A.K. Szakal, and J.G. Tew. 2009. IL-6 produced by immune complex-activated follicular dendritic cells promotes germinal center reactions, IgG responses and somatic hypermutation. *International Immunology*. 21:745–756. doi:10.1093/intimm/dxp041.

Yang, C.-Y., T.K. Vogt, S. Favre, L. Scarpellino, H.-Y. Huang, F. Tacchini-Cottier, and S.A. Luther. 2014. Trapping of naive lymphocytes triggers rapid growth and remodeling of the fibroblast network in reactive murine lymph nodes. *Proc Natl Acad Sci USA*. 111:E109–18. doi: 10.1073/pnas.1312585111.

Yen, J.-H., T. Khayrullina, and D. Ganea. 2008. PGE2-induced metalloproteinase-9 is essential for dendritic cell migration. *Blood*. 111:260–270. doi:10.1182/blood-2007-05-090613.